12-2017

Development of an Internal Camera-Based Volume Determination System for Triaxial Testing

Sean Elliott Salazar
University of Arkansas, Fayetteville

Development of an Internal Camera-Based Volume Determination System for Triaxial Testing

A thesis submitted in partial fulfillment
of the requirements for the degree of
Master of Science in Civil Engineering

by

Sean Elliott Salazar
University of Arkansas
Bachelor of Science in Civil Engineering, 2013

December 2017
University of Arkansas

This thesis is approved for recommendation to the Graduate Council.

_____

Dr. Richard Coffman
Thesis Director

_____

Dr. Michelle Bernhardt-Barry
Committee Member

_____

Dr. Thomas Oommen
Committee Member

ABSTRACT

Accurate measurement of axial, radial, and volumetric strain parameters are critical to the understanding of phase relationships and the constitutive behavior for saturated and unsaturated soils. The use of photographic monitoring techniques for laboratory-based measurement of these parameters have become common. A novel technique that utilized camera instrumentation located within the triaxial testing cell was developed and validated. By placing the instrumentation inside of the cell, instead of the instrumentation being located outside of the cell, the technique eliminated cumbersome corrections required to account for optical distortions due to 1) the refraction of light at the confining fluid-cell wall-atmosphere interfaces, 2) the curvature of the cylindrical cell wall, and 3) the deformation of the cell wall induced by changes in cell pressure. Digital images of various soil and analog (brass, acrylic) specimens were captured within the triaxial apparatus during testing. The images were processed using the principles of close-range photogrammetry to construct three-dimensional models of the specimens. The models were analysed to determine surface deformation and total volume of the specimens. Additionally, the models obtained from triaxial tests performed on the soil samples were compared to quantify deformation and volume of the sample as a function of axial strain.

Sensitivity studies and evaluation of measurement accuracy for the internal, close-range photogrammetry approach are documented herein. Specimen volume, as obtained using the approach, was compared with volume obtained from four other techniques, including: DSLR camera photogrammetry, 3D structured light scanning, manual measurements (caliper and pi tape), and water displacement. A relative error of 0.13 percent was assessed for the internal photogrammetry technique. The viability of determining total and local strains, volumetric changes, and total volume at any stage of triaxial testing was demonstrated through undrained

triaxial compression and extension tests. Results from all tests are presented herein. The use of the internal, close-range photogrammetry technique is recommended.

ACKNOWLEDGEMENTS

A portion of this material is based upon work supported by the National Science Foundation Graduate Research Fellowship Program under Grant No. DGE-1450079, as awarded to Sean Salazar. Any opinions, findings, and conclusions or recommendations expressed in this material are those of the author and do not necessarily reflect the views of the National Science Foundation. The author would also like to acknowledge 1) support from the University of Arkansas Provost Collaborative Research Grant, awarded to Richard Coffman (PI), Michelle Bernhardt (Co-PI) and Adam Barnes (Co-PI), and 2) undergraduate student support from the United States Department of Transportation (USDOT) Office of the Assistant Secretary for Research and Technology (OST-R) under Research and Innovation Technology Administration (RITA) Cooperative Agreement Award No. OASRTRS-14-H-UARK, awarded to Richard Coffman (PI) and Thomas Oommen (Co-PI).

DEDICATION

I would like to dedicate this thesis to my mother, Betty, to my father, John, to my grandfather, (Grandpop) Joe, to my brother, Eric, to my sister, Rachel, and to my wife, Alexandra. Without their love, strength, and unending support, I could not have completed this work. I would also like to acknowledge the guidance, encouragement, and leadership, of my advisor, Dr. Richard Coffman. Finally, I would like to thank those colleagues and friends that helped me along the way, in no particular order, Adam Barnes, Johnathan Blanchard, Cyrus Garner, Mark Kuss, Nabeel Mahmood, Leah Miramontes, Guilherme Pontes, Morgan Race, Andrew Schriver, and Brendan Yarborough.

TABLE OF CONTENTS

LIST OF FIGURES

LIST OF TABLES

LIST OF SYMBOLS AND ACRONYMS

Symbol	Definition
3D	Three-dimensional
A_c	Corrected area
A_f	Area of failure plane
BCPA	Board Camera with Pinhole Aperture
CCD	Charge-Coupled Device
cm	Centimeter
CMOS	Complementary Metal Oxide Semiconductor
CTC	Conventional Triaxial Compression
DIA	Digital Image Analysis
DIC	Digital Image Correlation
DSLR	Digital Single Lens Reflex
d	Diameter
d_0	Initial diameter
f	Focal length
h_0	Initial height
K_0	Coefficient of lateral earth pressure at-rest
K_1, K_2, K_3	Dimensionless coefficients of radial distortion
kPa	Kilopascal
LoHR	Lines of Horizontal Resolution
m	Mass
mm	Millimeter
MVS	Multi-View Stereo
n_1	Refractive index of lens material
n_2	Refractive index of surrounding medium
OCR	Overconsolidation Ratio
p'	Mean stress
P_1, P_2	Dimensionless coefficients of decentering distortion
PIV	Particle Image Velocimetry
psi	Pounds per square inch
q	Deviatoric stress
r	Radius of the pinhole opening (aperture)
r_1	Radius of curvature of front surface of lens
r_2	Radius of curvature of back surface of lens
RAD	Ringed Automatically Detected
RTE	Reduced Triaxial Extension
SfM	Structure from Motion
UC	Unconfined Compression
V	Volume
V_0	Initial volume
V_T	Total volume
w	Water content
w_c	Water content
Δd	Change in diameter

Δh	Change in height
Δu	Excess pore pressure
ΔV	Change in volume
ε_a	Axial strain
ε_r	Radial strain
ε_v	Volumetric strain
λ	Design wavelength
μm	Micrometer
σ_1	Major principal stress
σ_3	Confining stress
^{o}	Degree
%	Percent

LIST OF PUBLISHED OR SUBMITTED PAPERS

Chapter 3: Consideration of Internal Board Camera Optics for Triaxial Testing Applications. Published as: *Salazar, S.E., Coffman, R.A. (2015). "Consideration of Internal Board Camera Optics for Triaxial Testing Applications." Geotechnical Testing Journal, Vol. 38, No. 1, pp. 40-49. doi:10.1520/GTJ20140163.*

Chapter 4: Development of an Internal Camera-Based Volume Determination System for Triaxial Testing. Published as: *Salazar, S.E., Barnes, A., Coffman, R.A. (2015). "Development of an Internal Camera-Based Volume Determination System for Triaxial Testing." Geotechnical Testing Journal, Vol. 38, No. 4, pp. 549-555. doi:10.1520/GTJ20140249.*

Chapter 5: Discussion of "A Photogrammetry-based Method to Measure Total and Local Volume Changes of Unsaturated Soils During Triaxial Testing" by Zhang et al., 2015. Published as: *Salazar, S.E., Coffman, R.A. (2015). "Discussion of 'A Photogrammetry-based Method to Measure Total and Local Volume Changes of Unsaturated Soils During Triaxial Testing' by Zhang et al." Acta Geotechnica, Vol. 10, No. 5, pp. 693-696. doi:10.1007/s11440-015-0380-1.*

Chapter 6: Closure to "Discussion of 'Development of an Internal Camera-Based Volume Determination System for Triaxial Testing' by S. E. Salazar, A. Barnes, and R. A. Coffman" by Mehdizadeh et al., 2016. Published as: *Salazar, S.E., Barnes, A., Coffman, R.A. (2017). "Closure to "Discussion of 'Development of an Internal Camera-Based Volume Determination System for Triaxial Testing' S.E. Salazar, A. Barnes, and R.A. Coffman" by A. Mehdizadeh, M.M. Disfani, R. Evans, A. Arulrajah and D.E.L. Ong." Geotechnical Testing Journal. Vol. 40, No. 1, pp. 47-51. doi:10.1520/GTJ20160154.*

Chapter 7: Verification of an Internal Close-Range Photogrammetry Approach for Volume Determination During Triaxial Testing. Submitted as: *Salazar, S.E., Miramontes, L.D., Barnes, A.R., Bernhardt, M.L., Coffman, R.A. (2017). "Verification of an Internal Close-Range Photogrammetry Approach for Volume Determination During Triaxial Testing." Geotechnical Testing Journal. Submitted for Review. Manuscript Number: GTJ-2017-0125.R2.*

CHAPTER 1: INTRODUCTION

1.1. Chapter Overview

The development of an internal camera-based volume determination system for triaxial testing is described in this document. The system was used in conjunction with a close-range photogrammetry technique to 1) capture digital images, 2) photogrammetrically construct three-dimensional models, and 3) calculate the volume and deformation for soil specimens during all stages of triaxial compression and triaxial extension tests. This chapter is subdivided into four sections. A brief overview of the work that is described in this document is contained in Section 1.2. The motivation for conducting this research is described in Section 1.3. An overview of the entire document is presented in Section 1.4.

1.2. Description of the Work

The development of the internal camera-based instrumentation for triaxial cell photogrammetry and the associated data collection and processing techniques are described in this document. The development is also briefly described in this section. A set of ten small board cameras was designed and incorporated into two, diametrically opposed, camera towers. Each tower, with five camera devices, was mounted to a rotational track within the cell; the towers were free to rotate about the soil specimen during triaxial testing. At any desired stage during the triaxial test (e.g. at a given axial strain level during shearing), the test was paused and the camera towers were rotated incrementally about the specimen while capturing images of the specimen. To facilitate measurements during the triaxial test, the entire system was designed to be incorporated into the triaxial cell to be in direct contact with the confining fluid. A rendering of the camera instrumentation, as mounted inside of the triaxial cell, is presented as Figure 1.1.

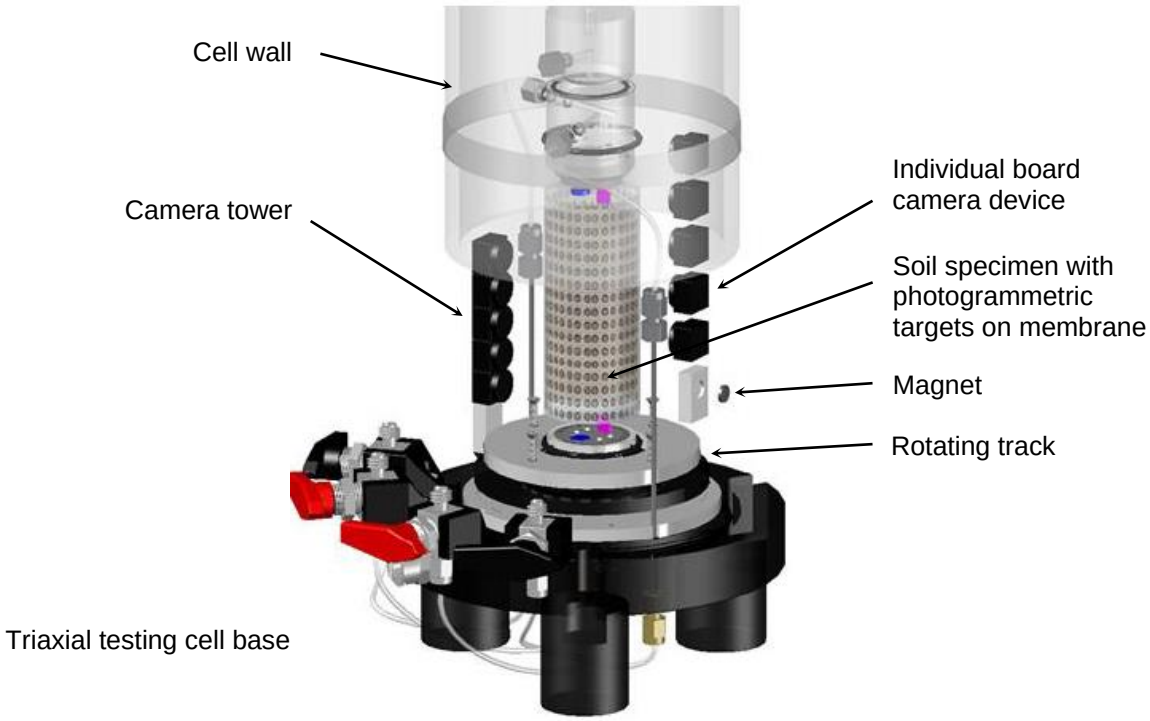

Figure 1.1. Exploded, transparent view of the major components of the internal camera-based photogrammetry system (note: shown with piezoelectric transducer end caps).

The images that were collected with the system were processed using a close-range photogrammetry technique to 1) construct the digital surface of the specimen, and 2) determine the total volume of the specimen. To demonstrate the viability of the technique for triaxial tests, one conventional triaxial compression test and one reduced triaxial extension test was performed. During each test, images of the specimen were captured for various levels of axial strain and a three-dimensional model was created for each of the various axial strain levels. To evaluate the accuracy of the internal photogrammetry technique, several validation tests were performed. Specifically, the technique was evaluated using analog specimens (one brass and two acrylic specimens). The effect of the number of images on the reconstruction of a specimen (ranging from 40 to 320 images) was examined and the total volume of the specimens that were obtained

were compared with volumes measured using four other methods. An overview of the evaluation steps is presented as Figure 1.2.

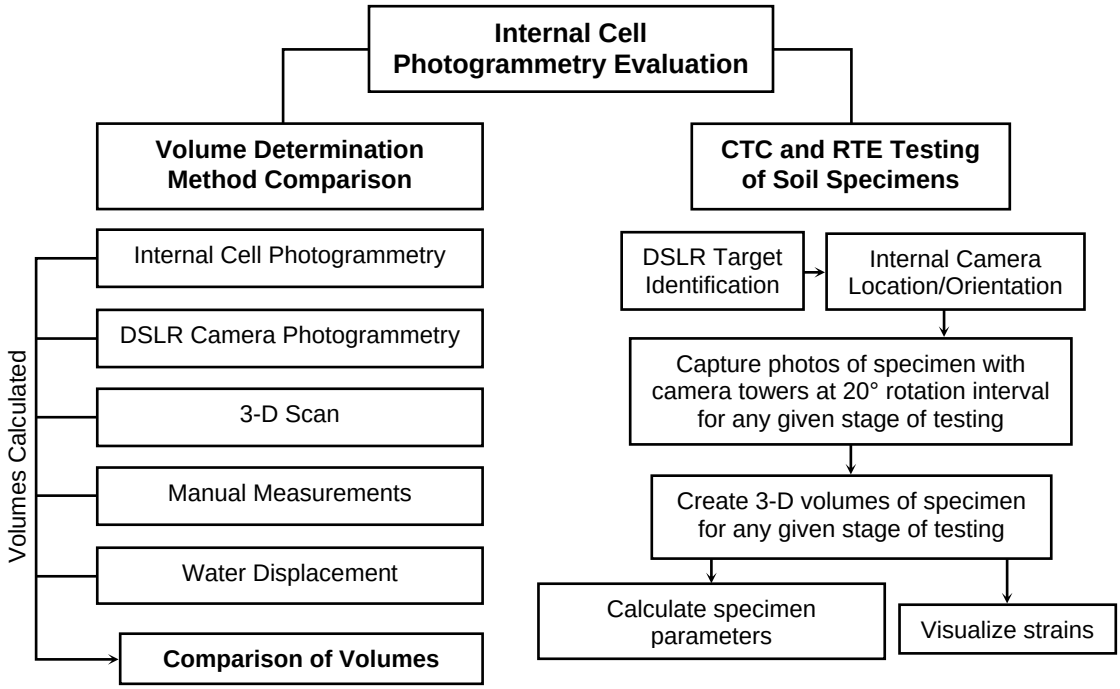

Figure 1.2. Overview of the evaluation process for the internal cell photogrammetry technique presented in this document (modified from Salazar et al. 2017b).

1.3. Motivation

The motivation for the research conducted for this work is presented in this section. The limitations of the techniques that are currently employed in the laboratory to monitor triaxial specimens during testing are discussed in Section 1.3.1. The contribution of the work to the field of geotechnical engineering is discussed in Section 1.3.2.

1.3.1. *Limitations of Current Techniques*

Various methods have been employed by researchers to monitor soil specimens during triaxial tests. These monitoring efforts have enabled one or more of the following: 1) measurement of axial and/or radial dimensions and deformations during testing, 2) measurement

of local and/or total volume, 3) calculation of axial, radial, and/or volumetric strains, and 4) characterization of shear banding behavior. Techniques that have been described in the literature include double-wall cell systems (e.g. Bishop and Donald 1961), differential pressure transducers (e.g. Ng et al. 2002), measurements of air and water volume changes (e.g. Leong et al. 2004), displacement and strain sensors (e.g. Scholey et al. 1995), non-contact proximity sensors (e.g. Clayton et al. 1989), laser scanners (e.g. Messerklinger and Springman 2007), digital image analysis (e.g. Bhandari et al. 2012), x-ray computed tomography (e.g. Viggiani et al. 2004), and photogrammetry (e.g. Zhang et al. 2015). Broadly speaking, these techniques can be divided into photograph-based and non-photograph-based categories.

In recent years, photograph-based methods have achieved prominence due to their practicality, cost-effectiveness, and versatility. Furthermore, many of the non-photograph-based techniques suffered from poor data resolution, relied heavily on geometric assumptions, and often required installation of complex and expensive instrumentation. However, even the photograph-based techniques have been limited by poor resolution, and the need to perform computationally intensive corrections to overcome distortions caused by the confining fluid and the cell wall surrounding the soil specimen. The limitations of the photograph-based and non-photograph-based approaches were discussed in detail in Salazar and Coffman (2015a, 2015b) and Salazar et al. (2015, 2017a, 2017b). Based on a review of the existing literature, there was a need for a better photogrammetry technique that relied upon cameras internal to the cell.

1.3.2. *Contribution to Geotechnical Engineering*

Testing of the novel Salazar and Coffman (2016) device, in conjunction with the close-range photogrammetry technique detailed in Salazar et al. (2017b), was shown to be a viable alternative to other photograph-based techniques. Moreover, the technique allowed for direct

observation and coverage of the entire radial surface of a specimen. This coverage resulted in highly detailed construction of the three-dimensional surface of the specimen. Moreover, the measurements were independent of any assumptions of initial dimensions or deformation behavior. The technique simplified the computations required by other photogrammetric methods, such as the method presented by Zhang et al. (2015). The potential for obtaining more information about a given soil specimen, such as axial, radial, and volumetric strains during a triaxial test is demonstrated by the technique that is presented in this document. This information can be used together with the other soil parameters to improve the development of constitutive models of soil. With continued improvements to the device and to the processing workflow, the potential for less time-consuming data collection and data reduction is envisioned.

1.4. Document Overview

This document is comprised of nine chapters. In this chapter (Chapter 1), an overview of the work contained within the document and the contribution of the work to the field of geotechnical engineering were provided. The background for the work is presented in the form of a literature review in Chapter 2. Five subsequent archival journal publications, on the subject of this work, are presented in Chapters 3 through 7, in the order in which the manuscripts were conceived and published. The process of developing suitable cameras for the internal photogrammetry system is described in Chapter 3. The development of the mechanical, electrical, and photogrammetric components of the system is described in Chapter 4. A discussion of the paper by Zhang et al. (2015), on the topic of photogrammetry for triaxial testing, is included as Chapter 5. A closure to a discussion paper written by Mehdizadeh et al. (2016) on the Salazar et al. (2015) publication is included as Chapter 6. The validation of the internal, close-range photogrammetry approach for triaxial testing is described in Chapter 7.

Conclusions drawn from the work presented in Chapter 3 through Chapter 7 are discussed in Chapter 8. Finally, a comprehensive list of works cited in this document is included as Chapter 9.

1.5. References

Bhandari, A. R., Powrie, W., and Harkness, R. M., 2012, "A Digital Image-Based Deformation Measurement System for Triaxial Tests," *Geotech. Test. J.*, Vol. 35, No. 2, pp. 1-18.

Bishop, A. W. and Donald, I. B., 1961, "The Experimental Study of Partly Saturated Soil in Triaxial Apparatus," *Proceedings of the Fifth International Conference on Soil Mechanics and Foundation Engineering*, Vols. 1/3, Paris, July 17–22, Institution of Civil Engineers, London, pp. 13–21.

Clayton, C. R. I., Khatrush, S. A., Adriano, V. D. B., and Siddique, A., 1989, "The Use of Hall Effect Semiconductors in Geotechnical Instrumentation," *Geotech. Test. J.*, Vol. 12, No. 1, pp. 69-76.

Kikkawa, N., Nakata, Y., Hyodo, M., Murata, H., and Nishio, S., 2006, "Three-Dimensional Measurement of Local Strain Using Digital Stereo Photogrammetry in the Triaxial Test," *Geomechanics and Geotechnics of Particulate Media*, M. Hyodo, H. Murata, and Y. Nakata, Eds., Taylor and Francis, London, pp. 61-67.

Leong, E.C., Agus, S.S., and Rahardjo, H., 2004, "Volume Change Measurement of Soil Specimen in Triaxial Test," *Geotech. Test. J.*, Vol. 27, No. 1, pp. 47-56.

Mehdizadeh, A., Disfani, M. M., Evans, R., Arulrajah, A., and Ong, D. E. L., 2016, "Discussion of 'Development of an Internal Camera-Based Volume Determination System for Triaxial Testing' by S. E. Salazar, A. Barnes and R. A. Coffman (doi:10.1520/GTJ20140249)." *Geotech. Test J.*, Vol. 39, No. 1, pp. 165-168. doi:10.1520/GTJ20150153.

Messerklinger, S. and Springman, S. M., 2007, "Local Radial Displacement Measurements of Soil Specimens in a Triaxial Test Apparatus Using Laser Transducers," *Geotech. Test. J.*, Vol. 30, No. 6, pp. 1-12.

Ng, C. W. W., Zhan L. T., and Cui Y. J., 2002, "A New Simple System for Measuring Volume Changes in Unsaturated Soils," *Can. Geotech. J.*, Vol. 39, No. 3, pp. 757-764.

Salazar, S. E., Barnes, A., and Coffman, R. A., 2015, "Development of an Internal Camera Based Volume Determination System for Triaxial Testing," *Geotech. Test. J.*, Vol. 38, No. 4, pp. 549-555. doi:10.1520/GTJ20140249.

Salazar, S. E., Barnes, A., and Coffman, R. A., 2017a, "Closure to "Discussion of 'Development of an Internal Camera-Based Volume Determination System for Triaxial Testing' S. E. Salazar, A. Barnes and R. A. Coffman" by A. Mehdizadeh, M. M. Disfani, R. Evans, A. Arulrajah and D. E. L. Ong," *Geotech. Test. J.*, Vol. 40, No. 1, pp. 47-51. doi:10.1520/GTJ20160154.

Salazar, S. E. and Coffman, R. A., 2015a, "Consideration of Internal Board Camera Optics for Triaxial Testing Applications," *Geotech. Test. J.*, Vol. 38, No. 1, pp. 40-49. doi:10.1520/GTJ20140163.

Salazar, S. E. and Coffman, R. A., 2015b, "Discussion of "A Photogrammetry-Based Method to Measure Total and Local Volume Changes of Unsaturated Soils During Triaxial Testing" by Zhang et al. (doi:10.1007/s11440-014-0346-8)" *Acta Geotech.*, Vol. 10, No. 5, pp. 693-696. doi:10.1007/s11440-015-0380-1.

Salazar, S. E. and Coffman, R. A., 2016, "Pressurized Fluid-Submerged, Internal, Close-Range Photogrammetry System for Laboratory Testing," U.S. Patent and Trademark Office. Patent 15/360,820. Filed November, 2016.

Salazar, S. E., Miramontes, L. D., Barnes, A., Bernhardt, M. L., and Coffman, R. A., 2017b, "Verification of an Internal Close-Range Photogrammetry Approach for Volume Determination During Triaxial Testing," *Geotech. Test. J.* Submitted for Review. Manuscript Number: GTJ-2017-0125.R2.

Scholey, G. K., Frost, J. D., Lo Presti, C. F., and Jamiolkowski, M., 1995, "A Review of Instrumentation for Measuring Small Strains During Triaxial Testing of Soil Specimens," *Geotech. Test. J.*, Vol. 18, No. 2, pp. 137–156.

Viggiani, G., Lenoir, N., Bésuelle, P., Di Michiel, M., Marello, S., Desrues, J., and Kretzschmer, M., 2004, "X-ray Microtomography for Studying Localized Deformation in Fine-Grained Geomaterials Under Triaxial Compression," *Cr Acad Sci II B-Mec*, Vol. 332, pp. 819-826.

Zhang, X., Li, L., Chen, G., and Lytton, R., 2015, "A Photogrammetry-Based Method to Measure Total and Local Volume Changes of Unsaturated Soils During Triaxial Testing," *Acta Geotechnica*, Vol. 10, No. 1, pp. 55-82. doi:10.1007/s11440-014-0346-8.

CHAPTER 2: BACKGROUND

2.1. Chapter Overview

A review of the relevant literature is contained within this chapter. The parameters of interest for triaxial testing of saturated and unsaturated soils are presented in Section 2.2. An overview of non-photograph-based soil specimen monitoring methods, with a focus on triaxial testing, is provided in Section 2.3. A summary of the literature related to photograph-based soil specimen monitoring, with a focus on triaxial testing, is presented in Section 2.4. Subsections for digital image analysis techniques (Section 2.4.1) and photogrammetric techniques (Section 2.4.2) are contained within Section 2.4.

2.2. Parameters of Interest for Triaxial Testing of Soils

Numerous techniques have been applied to study the volume and strain evolutions for saturated and unsaturated soil specimens during triaxial tests. The practice of measuring changes in volume during a test has become routine for many laboratories and is critical for triaxial testing of unsaturated soils. The parameters of interest for a given triaxial test typically include: 1) total and local volume changes, and 2) axial, radial, and volumetric strains. Although there are several methods for indirectly obtaining or calculating these parameters, assumptions of elastic and uniform deformation behaviors to estimate shape are typically associated with this approach. An example of one set of calculations for obtaining axial, radial, and volumetric strains during an undrained triaxial test is presented in Equations 2.1, 2.2, and 2.3, respectively. This method relies on a geometric estimation of specimen shape after deformation and relies on relative changes in specimen dimensions. Ehrgott (1971) presented five additional variations of the equations used to calculate the strains, but all of the variations suffer from fundamentally flawed assumptions regarding the specimen shape.

$$\varepsilon_a = \frac{\Delta h}{h_0}$$ (modified from Ehrgott 1971) Equation 2.1

$$\varepsilon_r = \frac{\Delta d}{d_0}$$ (modified from Ehrgott 1971) Equation 2.2

$$\varepsilon_v = \frac{\Delta V}{V_0} = \varepsilon_a + \varepsilon_r - \varepsilon_r \varepsilon_a + \frac{\varepsilon_r^2}{3}(\varepsilon_a - 1)$$ (modified from Ehrgott 1971) Equation 2.3

Where ε_a is axial strain, Δh and h_0 are change in height and initial height of a test specimen, respectively, ε_r is radial strain, Δd and d_0 are change in diameter and initial diameter of a test specimen, respectively, ε_v is volumetric strain, and ΔV and V_0 are change in volume and initial volume of a test specimen, respectively.

To further illustrate an example of the assumptions that are typically made regarding the specimen deformation behavior during a triaxial test, the five testing stages of a reduced triaxial extension test are illustrated in Figure 2.1. It is commonly assumed that the specimen deforms as a perfect, right, circular cylinder (ASTM D4767, 2011). Therefore, this technique is not suitable for obtaining the correct area of the failure plane and the resulting shear strength calculations for the specimen are inaccurate. Due to these inaccuracies, researchers have turned to a variety of techniques to directly measure the parameters of interest during triaxial testing.

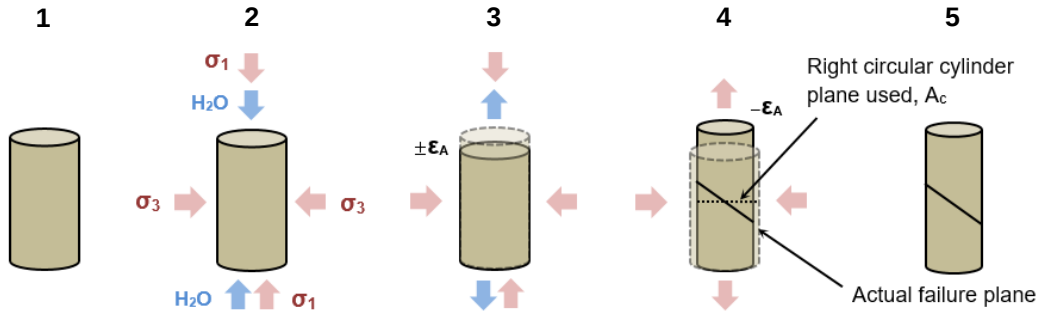

1. *Pre-test:* Mass (m) and water content (*w*), measured; Volume (V) calculated using caliper measurements.
2. *Back-pressure saturation:* Drain lines filled. Total volume change (ΔV) from pore pump measurements. This volume change includes air *1)* purged from lines, and *2)* going into suspension.
3. K_0 *Consolidation:* Sample ΔV from pore pump measurements.
4. *Shearing*: m, *w*, and V assumed to be equal to post-test m, *w*, and V (if undrained); calculated from pore pump measurements (if drained).
5. *Post-test:* m and *w*, measured. Shear strength determined based on corrected area (A_c).

Figure 2.1. Typical measurements and calculations required to determine the phase diagram of the soil specimen during a reduced triaxial extension test (modified from Salazar et al. 2017b).

2.3. Non-Photograph-Based Soil Specimen Monitoring Methods

Historically, changes in confining fluid or pore fluid volume have been directly correlated with changes in specimen volume. However, volume measurements have been influenced by temperature- and pressure-induced flexure of the cell wall and drain lines. Bishop and Donald (1961) modified a standard triaxial testing apparatus to include a second, inner cell that was filled with mercury to measure total changes in volume of a specimen. Other double-cell techniques that relied on measuring the changes in volume of the confining fluid (water and/or air) within the pressurized cell were introduced by Wheeler (1986), Cui and Delage (1996), Toyota et al. (2001), Aversa and Nicotera (2002), and Ng et al. (2002). A review of these volume measurement techniques was provided in Leong et al. (2004), which also contained a method for correcting for the expansion of the confining fluid due to temperature fluctuations. An example of a double-cell triaxial apparatus is presented as Figure 2.2.

To complement volume measurements, axial deformation measurements have also been collected during testing. Changes in axial deformation have been used to calculate average specimen dimensions by adding or subtracting deformation measurements from initial dimensions, with the initial dimensions having been established prior to testing (typically by means of caliper and pi tape measurements). Therefore, known or assumed specimen dimensions were used to calculate axial, radial, or volumetric strains, as described in Section 2.2. However, conventional axial (Scholey et al. 1995, Cuccovillo and Coop 1997, Ng and Chiu 2001) and lateral or radial (Khan and Hoag 1979, Bésuelle and Desrues 2001) displacement transducer measurements have relied on averaging methods and total volumetric changes that did not accurately account for irregular deformation behavior, such as shear banding, bulging bifurcation, or necking.

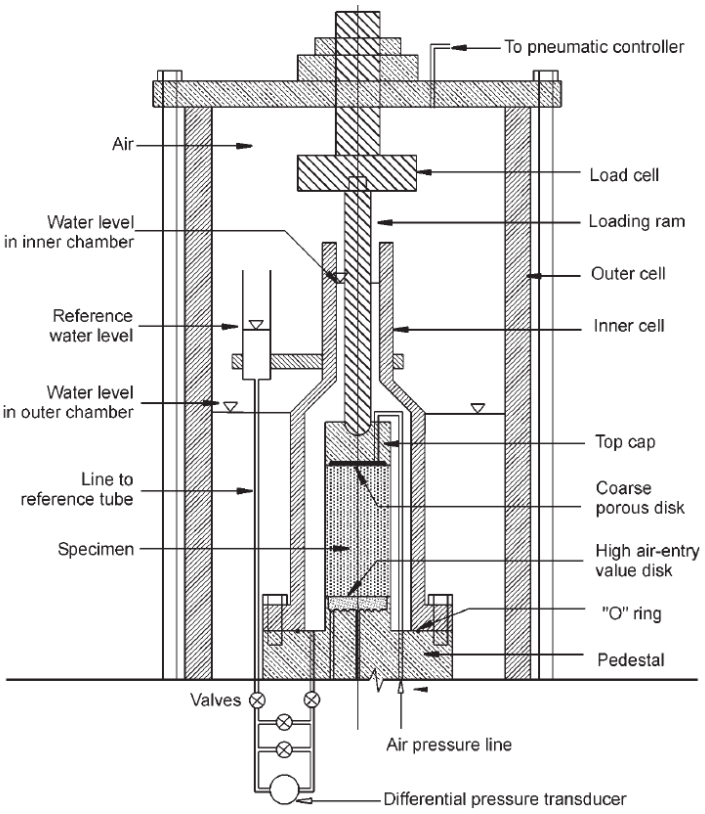

Figure 2.2. Schematic of a double-cell volume measuring system for triaxial testing of unsaturated soils (from Ng et al. 2002).

Other measurement techniques have been employed to measure soil specimen parameters. Clayton and Khatrush (1986) and Clayton et al. (1989) introduced a non-contact proximity sensor technique to measure local radial and axial strains during triaxial testing. Romero et al. (1997), Messerklinger and Springman (2007), and Jain et al. (2015) employed laser-scanning devices. The aforementioned Romero et al. (1997) device was incorporated into a suction- and temperature-controlled triaxial apparatus for the testing of unsaturated soils. Two externally mounted, diametrically opposed lasers were utilized to measure the radial deformation profile along the length of the specimen at two locations. Similarly, the Messerklinger and Springman (2007) device was utilized to measure radial displacements for three vertical profiles around the circumference of the specimen during triaxial testing (Figure 2.3). In both techniques, the radial displacements between the measured profiles were inferred. Although the Jain et al. (2015) device was not employed during triaxial tests, the technique utilized a fixed laser pointed at a soil specimen placed on a rotating turntable. This allowed for continuous measurements of the entire specimen surface at desired intervals during a shrinkage test and subsequent calculation of specimen volume. Desrues et al. (1996) and Viggiani et al. (2004) utilized x-ray computed tomography to study the triaxial soil specimens.

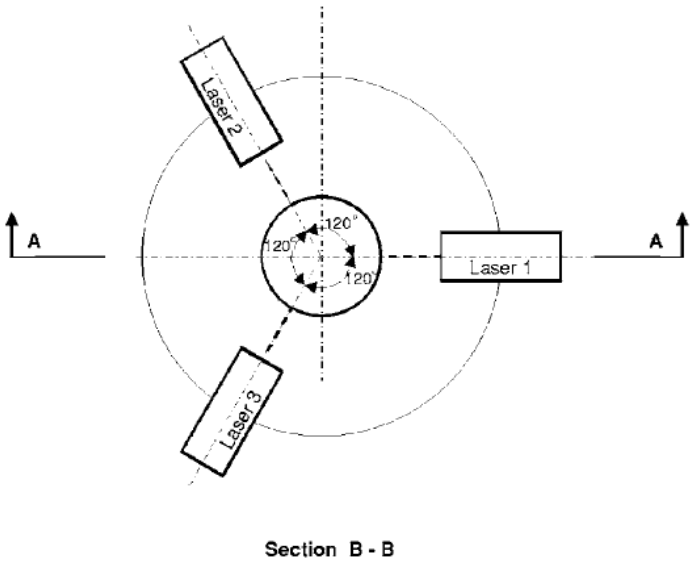

Figure 2.3. Plan view schematic of laser scanning device for triaxial testing (from Messerklinger and Springman 2007).

2.4. Photograph-Based Soil Specimen Monitoring Methods

To overcome the limitations of the previously discussed techniques in Section 2.3, digital imaging techniques have increasingly been employed to monitor soil specimens. Specifically, these techniques have been used to 1) calculate the total volume and volumetric strain of soil specimens and/or to 2) monitor the evolution of shear bands and local strains. The photograph-based techniques have been shown to be robust alternatives to conventional measurement techniques for obtaining measurements during triaxial testing. The photograph-based techniques in the literature fall under one or more of the following classifications: Digital Image Analysis (DIA), Digital Image Correlation (DIC), Particle Image Velocimetry (PIV), or photogrammetry. For the purposes of this discussion, DIA, DIC, and PIV techniques have all been grouped under the digital image analysis category, while photogrammetry technique is treated separately.

2.4.1. *Digital Image Analysis Techniques*

Throughout the literature, the terms DIA and DIC have sometimes been used interchangeably and the distinctions of the methods are beyond the scope of this discussion.

Therefore, these methods are discussed together and are referred to collectively as DIA techniques herein. DIA techniques have allowed for more information to be captured and quantified for soils specimens. For example, Alshibli and Sture (1999) utilized a uniform grid applied to the membrane of a triaxial soil specimen to measure displacements at the surface of the specimen during the development of a shear band. In another set of examples, Gudehus and Nübel (2004) and Rechenmacher and Finno (2004) both studied the evolution of shear bands in sands during biaxial tests using digital image analysis. In yet another pair of examples, Ören et al. (2006) and Önal et al. (2008) used digital image correlation to determine the volume of soil specimens during shrinkage tests.

Another class of digital image analysis is PIV; PIV was developed by Adrian (1991) for experimental fluid dynamics applications. Although PIV techniques share some common traits with DIA techniques, PIV differs significantly from DIA. PIV techniques primarily utilize image texture instead of target markers to track movement in sequential images. PIV has been used to measure planar surface deformation and to analyze displacement and strain fields for various soil tests. Examples of PIV techniques that have been employed to monitor soil specimens include Guler et al. (1999), White et al. (2003), Iskander and Liu (2010), Stanier et al. (2016), and Pinyol and Alvarado (2017). Because PIV techniques have not been shown to aid in the determination of triaxial specimen volumes, these techniques are not further discussed.

The use of digital images in conjunction with DIA techniques for monitoring triaxial tests has been presented in the literature. Examples include Macari et al. (1997), Alshibli and Sture (1999), Alshibli and Al-Hamdan (2001), Gachet et al. (2007), Sachan and Penumadu (2007), Rechenmacher and Medina-Cetina (2007), Uchaipichat et al. (2011), Bhandari et al. (2012), and Hormdee et al. (2014). In each of these examples, digital images of the soil specimens were

captured during testing with photographic equipment that was located outside of the triaxial testing cell. Although the entire length of the specimen (in the axial dimension) was captured within a single image in each of the aforementioned references, various methods were used to capture the entire surface area of the specimen in the lateral dimension. For example, Alshibli and Al-Hamdan (2001) and Bhandari et al. (2012) placed multiple cameras at intervals around the outside of the cell, whereas Macari et al. (1997) and Gachet et al. (2007) utilized only a single, fixed camera and therefore did not capture the entire specimen surface. In other instances, the entire specimen surface was not captured because only the zone of shear banding was of interest (Liang et al. 1997, Alshibli and Sture 1999, Sachan and Penumadu 2007). In all cases, proper lighting conditions were critical for collecting usable photographs for obtaining high quality results with DIA techniques, as demonstrated by Gachet et al. (2007), Bhandari et al. (2012), and Hormdee et al. (2014). Examples of the camera-based measurement apparatus are presented in Figure 2.4.

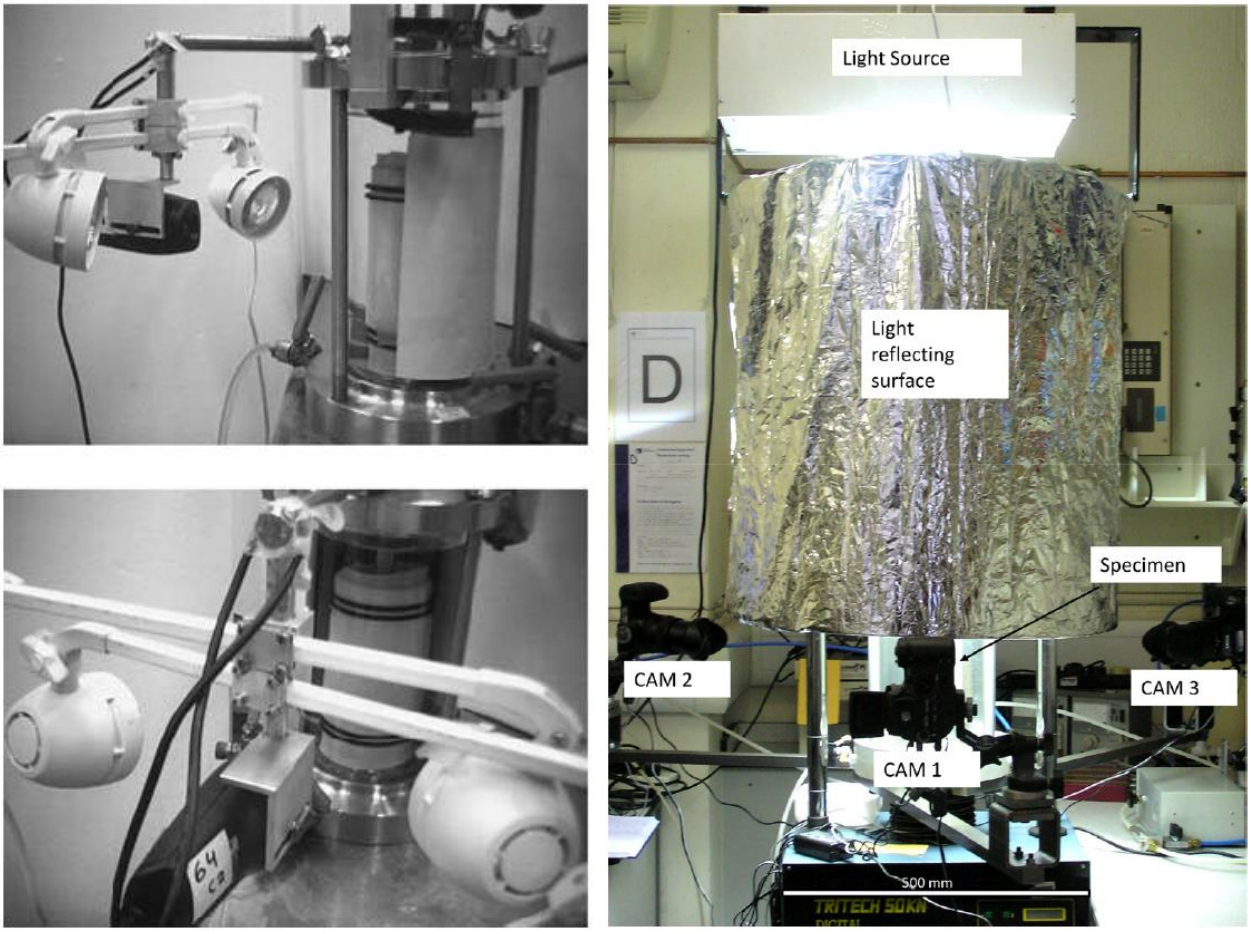

(a) **(b)**

Figure 2.4. Triaxial testing apparatus with *(a)* a single, fixed digital camera located outside of the cell (from Gachet et al. 2007), and *(b)* three, fixed digital cameras located outside of the cell (from Bhandari et al. 2012).

2.4.2. *Photogrammetric Techniques*

All of the previously discussed methods for monitoring soil specimens during triaxial tests utilized external cameras and therefore several optical challenges were encountered, as 1) described in detail by Bhandari et al. (2012) and Salazar and Coffman (2015) and 2) as illustrated in Figure 2.5. Although Kikkawa et al. (2006) first introduced a stereo photogrammetry technique for measuring local displacement and volume for specimens in triaxial compression, photogrammetric techniques for monitoring triaxial soil specimens did not

reappear in the literature until Salazar et al. (2015) and Zhang et al. (2015). The initial work by Zhang et al. (2015) was extended by the same authors in Li et al. (2016) and the Salazar et al. (2015) work was extended in Miramontes (2016) and Salazar et al. (2017a, 2017b). As stated by Zhang et al. (2015), photogrammetric techniques were needed because of the significant limitations and assumptions of other photographic methods (e.g. only local volume was obtainable, or precise control of camera location and orientation were required for accurate measurements).

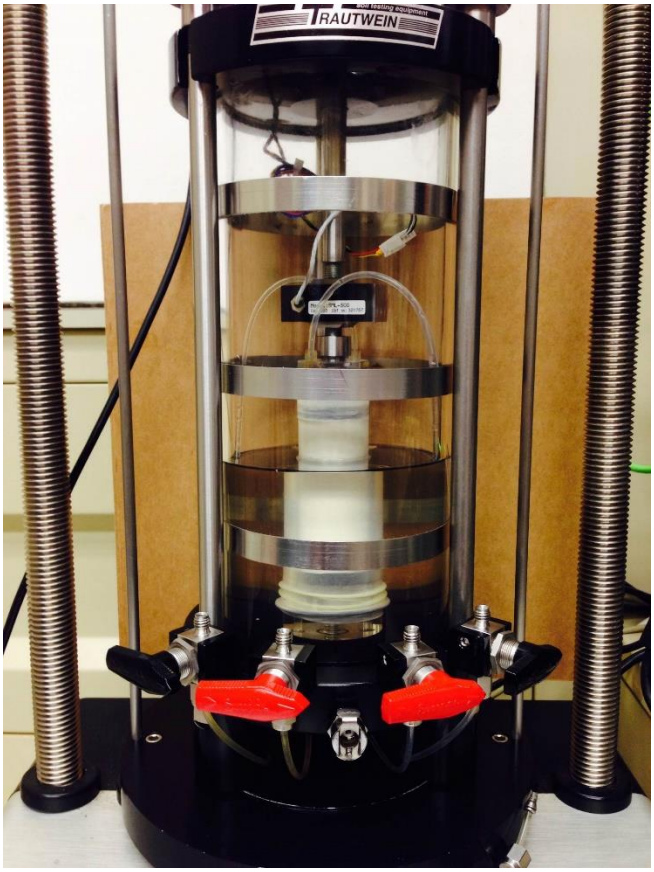

Figure 2.5. Optical magnification of soil specimen due to presence of confining fluid.

The Zhang et al. (2015) and Li et al. (2016) technique involved acquiring photographs of the specimen at various angles from outside of the cell wall using a single digital single lens reflex (DSLR) camera. The images were then used to photogrammetrically construct a three-dimensional model of the specimen, which was scaled to a real-world coordinate system to obtain the local and total volume of the specimen for a given stage of testing. The Zhang et al. (2015) and Li et al. (2016) method presented advantages of a photogrammetric approach by overcoming many of the limitations of other photograph-based methods. However, the implementation of the method introduced additional processing complexity by requiring computationally intensive corrections to account for optical distortions. Specifically, a ray tracing and least-squares optimization technique were utilized to correct for the light refraction at the confining water–cell wall and cell wall–atmosphere interfaces, for the cell wall curvature, and for the deformation of the cell wall under high confining pressures. A schematic illustrating the photogrammetric principles involved with the Zhang et al. (2015) and Li et al. (2016) technique is presented as Figure 2.6. The results obtained from the Zhang et al. (2015) and Li et al. (2016) technique are presented as Figure 2.7.

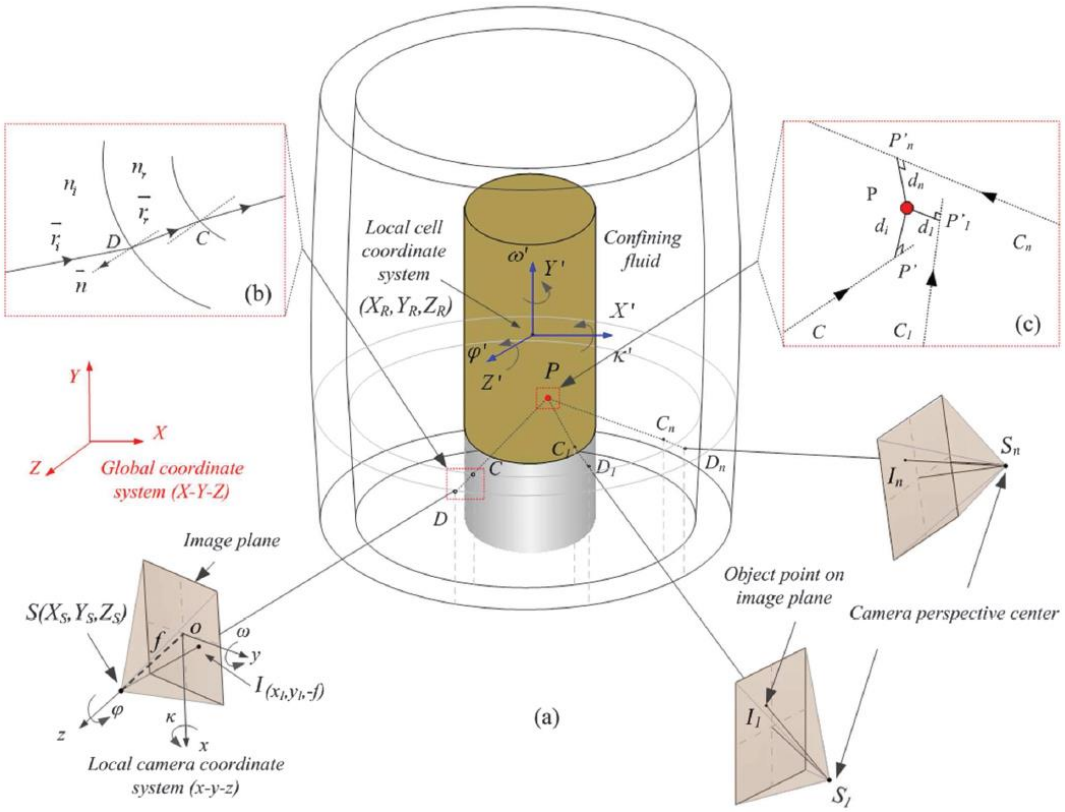

Figure 2.6. ***(a)*** **Schematic of photogrammetric principles involved in the Zhang et al. (2015) and Li et al. (2016) methodology, including** ***(b)*** **optical ray tracing, and** ***(c)*** **least-square estimation (from Li et al. 2016).**

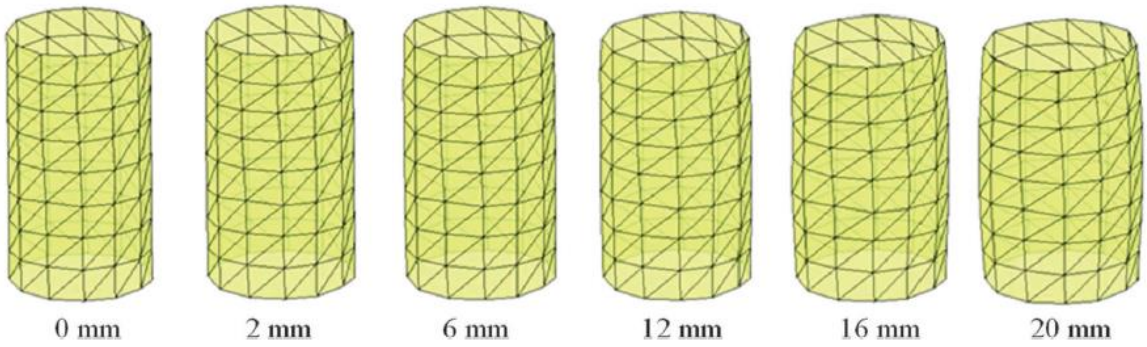

Figure 2.7. Representation of specimen deformations obtained during a triaxial test (modified from Li et al. 2016).

Salazar and Coffman (2015, 2016) introduced novel camera instrumentation for monitoring triaxial specimens during testing. A simple board camera device, modified with a pinhole aperture (BCPA), was designed and incorporated into a camera system that was placed inside of the triaxial testing cell. The camera device was designed to allow for immersion within the confining fluid of the triaxial cell (silicone oil). The full immersion of the device caused the air space behind the camera aperture to fill with the electronics-grade confining fluid, thereby overcoming the need for a pressure-resistant housing. In addition to a pressure-resistant housing being impractical for the high confining pressures reached during a triaxial test (up to 1,035 kPa), a pressure-resistant housing would have required more space than was available within the triaxial cell. Furthermore, the immersion of the camera parts, including the charge-coupled device (CCD) sensor within the fluid, allowed for direct observation of the soil specimen within the triaxial cell. Using this technique, light only traveled through one medium (the confining fluid). In tandem with the pinhole aperture, the need to account for image distortions introduced by the differences in the indices of refraction of the various materials (lens, air, oil) was eliminated. Schematics of the BCPA device and the internal camera system are presented as Figure 2.8 and Figure 2.9, respectively.

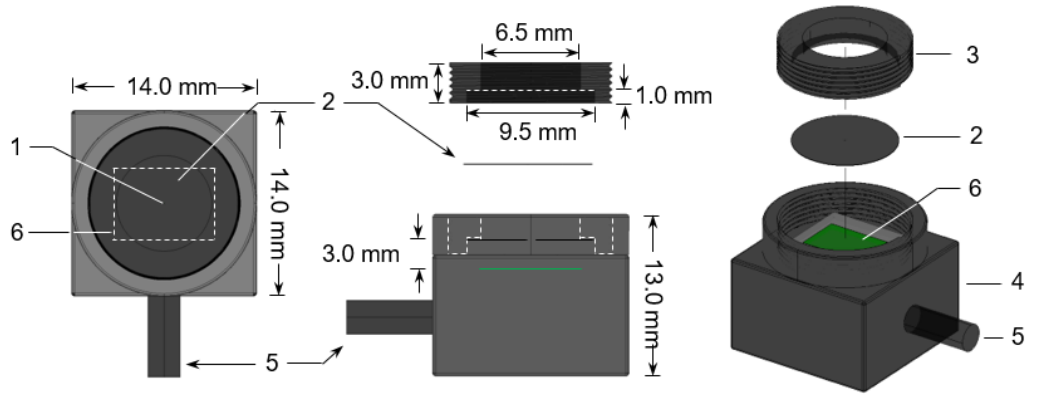

Figure 2.8. Schematic of board camera device with pinhole aperture developed at the University of Arkansas (from Salazar and Coffman 2015).

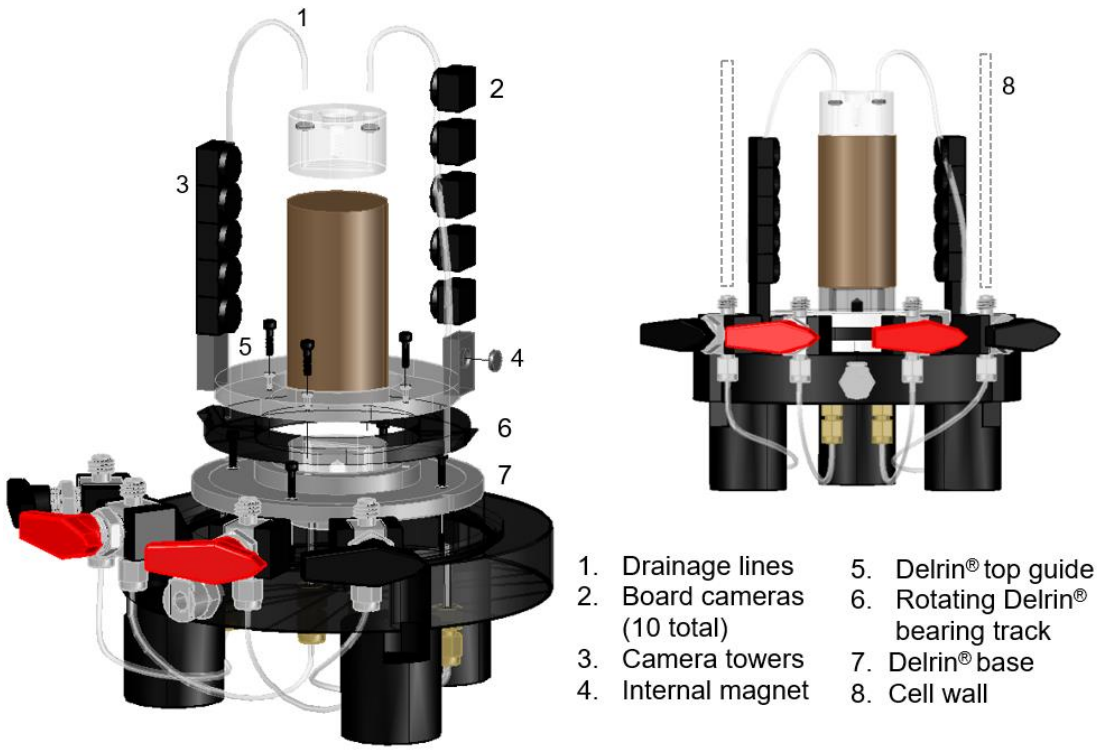

Figure 2.9. Schematic of internal camera-based photogrammetry system for triaxial testing developed at the University of Arkansas (modified from Salazar et al. 2015).

As reported in Salazar et al. (2015, 2017a, 2017b), the internal camera system was used to capture photographs of the entire specimen surface during a triaxial test by rotating the camera towers around the specimen. Just as the Zhang et al. (2015) and Li et al. (2016) photogrammetry technique relied on ringed automatically detected (RAD) targets, the Salazar et al. (2015, 2017) technique also relied on RAD targets. In Salazar et al. (2015, 2017a, 2017b), the targets were printed onto the membrane surrounding the specimen and were used to locate points on the specimen surface. A close-range photogrammetry technique was then utilized to construct a three-dimensional model of the specimen. Models that were obtained from various stages of testing were scaled to a real-world coordinate system and then compared to obtain volumetric changes. The models also allowed for virtual measurement of specimen dimensions. An example of the results obtained from the Salazar et al. (2015, 2017a, 2017b) technique is presented as Figure 2.10.

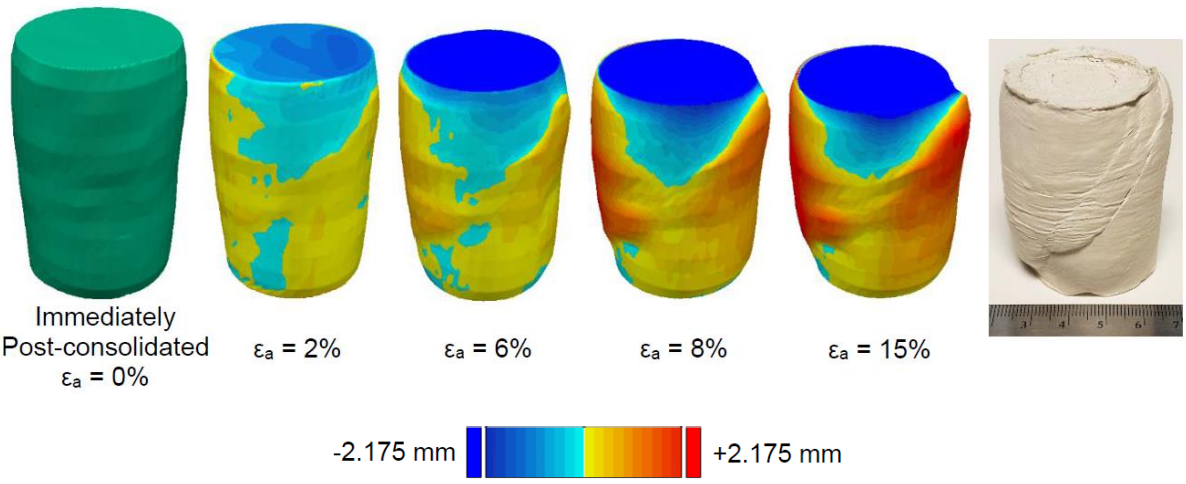

Figure 2.10. Representation of specimen deformation obtained from close-range photogrammetry during an undrained, conventional, triaxial compression test (modified from Salazar et al. 2017b).

2.5. References

Adrian, R. J., 1991, "Particle Imaging Techniques for Experimental Fluid Mechanics," *Ann. Rev. Fluid Mech.*, Vol. 23, No. 1, pp. 261-304.

Alshibli, K. A. and Sture, S., 1999, "Sand Shear Band Thickness Measurements by Digital Imaging Techniques," *J. Comput. Civ. Eng.*, Vol. 13, No. 2, pp. 103–109.

Alshibli, K. A. and Al-Hamdan, M., 2001, "Estimating Volume Change of Triaxial Soil Specimens From Planar Images," *Comput-Aid. Infrastruct. Eng.*, Vol. 16, No. 6, pp. 415–421.

ASTM D4767-11, 2011, "Standard Test Methods for Consolidated Undrained Triaxial Compression Test for Cohesive Soils," ASTM International, West Conshohocken, PA, www.astm.org. doi:10.1520/D4767-11.

Aversa, S. and Nicotera, M. V., 2002, "A Triaxial and Oedometer Apparatus for Testing Unsaturated Soils," *Geotech. Test. J.*, Vol. 25, No. 1, pp. 3-15.

Bésuelle, P. and Desrues, J., 2001, "An Internal Instrumentation for Axial and Radial Strain Measurements in Triaxial Tests," *Geotech. Test J.*, Vol. 24, No. 2, pp. 193-199.

Clayton, C. R. I. and Khatrush, S. A., 1986, "A New Device for Measuring Local Axial Strains on Triaxial Specimens," Géotechnique, Vol. 36, No. 4, pp. 593-597.

Clayton, C. R. I., Khatrush, S. A., Bica, A. V. D., and Siddique, A., 1989, "The Use of Hall Effect Semiconductors in Geotechnical Instrumentation," *Geotech. Test. J.*, Vol. 12, No. 1, pp. 69–76.

Cuccovillo, T. and Coop, M. R., 1997, "The Measurement of Local Axial Strains in Triaxial Tests Using LVDTs," *Géotechnique*, Vol. 47, No. 1, pp. 167–171.

Cui, Y.J. and Delage, P., 1996, "Yielding and Plastic Behavior of an Unsaturated Compacted Silt," *Géotechnique*, Vol. 46, No. 2, pp. 291-311.

Desrues, J., Chambon, R., Mokni, M., and Mazerolle, F., 1996, "Void Ratio Evolution Inside Shear Bands in Triaxial Sand Specimens Studied by Computed Tomography. *Géotechnique*, Vol. 46, No. 35, pp. 529-546.

Ehrgott, J. Q., 1971, "Calculation of Stress and Strain from Triaxial Test Data no Undrained Soil Specimens," Miscellaneous Paper S-71-9, U.S. Army Engineer Waterways Experiment Station, Vicksburg, Mississippi.

Gachet, P., Geiser, F., Laloui, L., and Vulliet, L., 2007, "Automated Digital Image Processing for Volume Change Measurement in Triaxial Cells," *Geotech. Test. J.*, Vol. 30, No. 2, pp. 98–103.

Gudehus, G. and Nübel, K., 2004, “Evolution of Shear Bands in Sand,” *Géotechnique*, Vol. 54, No. 3, pp. 187–201.

Guler, M., Edil, T. B., and Bosscher, P. J., 1999, Measurement of Particle Movement in Granular Soils Using Image Analysis," *J. Comput. Civ.*, Vol. 13, No. 2, pp. 116-122.

Hormdee, D., Kaikeerati, N., and Jirawattana, P., 2014, “Application of Image Processing for Volume Measurement in Multistage Triaxial Tests,” *Adv. Mat. Res.,* Vol. 931-932, pp. 501-505.

Iskander, M. and Liu, J., 2010, "Spatial Deformation Measurement Using Transparent Soil," *Geotech. Test. J.*, Vol. 33, No. 4, 8 pgs.

Jain, S., Wang, Y. H., and Fredlund, D. G., 2015, "Non-Contact Sensing System to Measure Specimen Volume During Shrinkage Test," *Geotech. Test. J.*, Vol. 38, No. 6, pp. 936-949. doi:10.1520/GTJ20140274.

Kikkawa, N., Nakata, Y., Hyodo, M., Murata, H., and Nishio, S., 2006, "Three-Dimensional Measurement of Local Strain Using Digital Stereo Photogrammetry in the Triaxial Test," *Geomechanics and Geotechnics of Particulate Media*, M. Hyodo, H. Murata, and Y. Nakata, Eds., Taylor and Francis, London, pp. 61-67.

Khan, M. H. and Hoag, D. L., 1979, “A Noncontacting Transducer for Measurement of Lateral Strains,” *Can. Geotech. J.*, Vol. 16, No. 2, pp. 409–411.

Leong, E. C., Agus, S. S., and Rahardjo, H., 2004, “Volume Change Measurement of Soil Specimen in Triaxial Test,” *Geotech. Test. J.*, Vol. 27, No. 1, pp. 47–56.

Li, L., Zhang, X., Chen, G., and Lytton, R., 2016, “Measuring Unsaturated Soil Deformations During Triaxial Testing Using a Photogrammetry-Based Method,” *Can. Geotech. J.*, Vol. 53, No. 3, pp. 472-489.

Liang, L., Saada, A., Figueroa, J. L., and Cope, C. T., 1997, “The Use of Digital Image Processing in Monitoring Shear Band Development,” *Geotech. Test. J.*, Vol. 20, No. 3, pp. 324–339.

Macari, E. J., Parker, J. K., and Costes, N. C., 1997, “Measurement of Volume Changes in Triaxial Tests Using Digital Imaging Techniques,” *Geotech. Test. J.*, Vol. 20, No. 1, pp. 103–109.

Mehdizadeh, A., Disfani, M. M., Evans, R., Arulrajah, A., and Ong, D. E. L., 2016, “Discussion of ‘Development of an Internal Camera-Based Volume Determination System for Triaxial Testing’ by S. E. Salazar, A. Barnes and R. A. Coffman (doi:10.1520/GTJ20140249).” *Geotech. Test J.*, Vol. 39, No. 1, pp. 165-168. doi:10.1520/GTJ20150153.

Messerklinger, S. and Springman, S. M., 2007, “Local Radial Displacement Measurements of Soil Specimens in a Triaxial Test Apparatus Using Laser Transducers,” *Geotech. Test. J.*, Vol. 30, No. 6, pp. 1-12.

Miramontes, L. D., 2016, "Validation of an Internal Camera Based Volume Determination System for Triaxial Testing," *Civil Engineering Undergraduate Honors Theses*. 33.

Ng, C. W. W. and Chiu, C. F., 2001, “Behaviour of a Loosely Compacted Unsaturated Volcanic Soil,” *J. Geotech. Geoenviron. Eng.*, Vol. 127, No. 12, pp. 1027–1036.

Ng, C. W. W., Zhan L. T., and Cui Y. J., 2002, “A New Simple System for Measuring Volume Changes in Unsaturated Soils,” *Can. Geotech. J.*, Vol. 39, No. 3, pp. 757-764.

Önal, O., Ören, A. H., Özden, G., and Kaya, A., 2008, “Determination of Cylindrical Soil Specimen Dimensions by Imaging With Applications to Volume Change of Bentonite–Sand Mixtures,” *Geotech. Test. J.*, Vol. 31, No. 2, pp. 124–131.

Ören, A. H., Önal, O., Özden, G., and Kaya, A., 2006, “Nondestructive Evaluation of Volumetric Shrinkage of Compacted Mixtures Using Digital Image Analysis,” *Eng. Geol.*, Vol. 85, No. 3, pp. 239–250.

Pinyol, N. M. and Alvarado, M., 2017, "Novel Analysis for Large Strains Based on Particle Image Velocimetry," *Can. Geotech. J.*, Vol. 54, No. 7, pp. 933-944. doi:10.1139/cgj-2016-0327.

Rechenmacher, A. L. and Finno, R. J., 2004, “Digital Image Correlation to Evaluate Shear Banding in Dilative Sands,” *Geotech. Test. J.*, Vol. 27, No. 1, pp. 13–22.

Rechenmacher, A. L. and Medina-Cetina, Z., 2007, “Calibration of Soil Constitutive Models with Spatially Varying Parameters,” *J. Geotech. Geoenviron.*, Vol. 133, No. 12, pp. 1567–1576.

Romero, E., Facio, J. A., Lloret, A., Gens, A., and Alonso, E. E., 1997, “A New Suction and Temperature Controlled Triaxial Apparatus,” presented at the *Fourteenth International Conference on Soil Mechanics and Foundation Engineering*, Hamburg, Germany, September 6-12, 1997, August Aimé Balkema, Amsterdam, pp. 185-188

Sachan, A. and Penumadu, D., 2007, “Strain Localization in Solid Cylindrical Clay Specimens Using Digital Image Analysis (DIA) Technique,” *Soils Found.*, Vol. 47, No. 1, pp. 67-78.

Salazar, S. E., Barnes, A., and Coffman, R. A., 2015, “Development of an Internal Camera Based Volume Determination System for Triaxial Testing,” *Geotech. Test. J.*, Vol. 38, No. 4, pp. 549-555. doi:10.1520/GTJ20140249.

Salazar, S. E., Barnes, A., and Coffman, R. A., 2017a, “Closure to “Discussion of ‘Development of an Internal Camera-Based Volume Determination System for Triaxial Testing’ S. E. Salazar, A. Barnes and R. A. Coffman” by A. Mehdizadeh, M. M. Disfani, R. Evans, A. Arulrajah and D. E. L. Ong,” *Geotech. Test. J.*, Vol. 40, No. 1, pp. 47-51. doi:10.1520/GTJ20160154.

Salazar, S. E. and Coffman, R. A., 2015a, “Consideration of Internal Board Camera Optics for Triaxial Testing Applications,” *Geotech. Test. J.*, Vol. 38, No. 1, pp. 40-49. doi:10.1520/GTJ20140163.

Salazar, S. E. and Coffman, R. A., 2016, “Pressurized Fluid-Submerged, Internal, Close-Range Photogrammetry System for Laboratory Testing,” U.S. Patent and Trademark Office. Patent 15/360,820. Filed November, 2016.

Salazar, S. E., Miramontes, L. D., Barnes, A., Bernhardt, M. L., and Coffman, R. A., 2017b, “Verification of an Internal Close-Range Photogrammetry Approach for Volume Determination During Triaxial Testing,” *Geotech. Test. J.* Submitted for Review. Manuscript Number: GTJ-2017-0125.R2.

Scholey, G. K., Frost, J. D., Lo Presti, C. F., and Jamiolkowski, M., 1995, “A Review of Instrumentation for Measuring Small Strains During Triaxial Testing of Soil Specimens,” *Geotech. Test. J.*, Vol. 18, No. 2, pp. 137–156.

Stanier, S. A., Blaber, J., Take, W. A., and White, D. J., 2016, "Improved Image-Based Deformation Measurement for Geotechnical Applications," *Can Geotech. J.*, Vol. 53, No. 5, pp. 727-739. doi:10.1139/cgj-2015-0253.

Toyota, H., Sakai, N., and Nishimura, T., 2001, "Effects of Stress History due to Unsaturation and Drainage Conditions on Shear Properties of Unsaturated Cohesive Soil," *Soils Found.*, Vol. 41, No. 1, pp. 13-24.

Uchaipichat, A., Khalili, N., and Zargarbashi, S., 2011, “A Temperature Controlled Triaxial Apparatus for Testing Unsaturated Soils,” *Geotech. Test. J.*, Vol. 34, No. 5, pp. 1-9.

Viggiani, G., Lenoir, N., Bésuelle, P., Di Michiel, M., Marello, S., Desrues, J., and Kretzschmer, M., 2004, “X-ray Microtomography for Studying Localized Deformation in Fine-Grained Geomaterials Under Triaxial Compression,” *Cr Acad Sci II B-Mec*, Vol. 332, pp. 819-826.

Wheeler, S. J., 1986, "The Stress-Strain Behaviour of Soils Containing Gas Bubbles," Ph.D. dissertation, Oxford University, Oxford, UK.

White, D., Take, W., and Bolton, M., 2003, "Soil Deformation Measurement Using Particle Image Velocimetry (PIV) and Photogrammetry," Géotechnique, Vol. 53, No. 7, pp. 619-631.

Zhang, X., Li, L., Chen, G., and Lytton, R., 2015, “A Photogrammetry-Based Method to Measure Total and Local Volume Changes of Unsaturated Soils During Triaxial Testing,” *Acta Geotechnica,* Vol. 10, No. 1, pp. 55-82. doi:10.1007/s11440-014-0346-8.

CHAPTER 3: CONSIDERATION OF INTERNAL BOARD CAMERA OPTICS FOR TRIAXIAL TESTING APPLICATIONS

3.1. Chapter Overview

The concept of optics, internal to a triaxial testing cell, is explored in this chapter. The challenges, limitations, and advantages associated with this concept are described and a simple board camera modified with a pinhole aperture (BCPA) is introduced. The challenges of implementing this camera system included limited space within the testing cell, the presence of pressurized confining fluid within the cell, and sufficient photographic coverage of the entire surface of a soil specimen. Preliminary testing of the camera device is presented and a system that incorporated multiple devices attached to rotating fixtures within the cell are introduced.

The limitations of the included manuscript (Salazar and Coffman 2015) are discussed in Section 3.2. The full citation for this document is included in Section 3.3. The motivation and background for the manuscript are described in Sections 3.4, 3.5, and 3.6. Contained within Section 3.7 are the challenges that were involved with designing a camera system capable of acquiring images of a specimen from within the testing cell during a triaxial test. Section 3.8 contains a description of the BCPA device that overcame the presented challenges and Section 3.9 includes the testing and calibration of the BCPA device. Conclusions for this work are presented in Section 3.10.

3.2. Limitations of the Described Study

The BCPA device that was designed for implementation within the internal camera-based monitoring system suffered from relatively poor image quality, due to the nature of the pinhole aperture and the low-cost board camera sensor. Although the BCPA overcame the presented challenges, the optimization of the device required compromises in the field of view, resolution, and light entry characteristics of the device. Although the study presented the concept of the

entire internal camera-based system, the results that were presented were focused primarily on the development of the BCPA device and not on the system. Therefore, the manuscript presented the development of the optics that had the potential for determination of specimen volumes.

3.3. Consideration of Internal Board Camera Optics for Triaxial Testing Applications

Reference

Salazar, Sean E. and Coffman, Richard A., "Consideration of Internal Board Camera Optics for Triaxial Testing Applications," Geotechnical Testing Journal, Vol. 38, No. 1, 2015, pp. 40-49. doi:10.1520/GTJ20140163.

3.4. Abstract

The application of small board cameras, located within a triaxial cell to determine radial and axial strain, was investigated. Specifically, charge-coupled device (CCD) sensors were utilized in conjunction with precision pinhole apertures to capture images from within the triaxial cell. The cameras were fully immersed in electronics-grade silicone oil and were able to withstand cell pressures that are common to triaxial testing (up to 1034 kPa (150 psi)). The small size of the cameras allowed for implementation within the triaxial cell, thereby avoiding: (1) the cumbersome corrections that are required to account for refraction at the confining fluid–cell wall–air interfaces and magnification due to cell wall curvature, and (2) the amount of space required for outside-of-the-cell monitoring systems that utilize cameras. The final design of the cameras was based on an iterative testing process in which various types of small board cameras, lenses, and finally pinhole apertures were investigated. The advantages of the lensless pinhole aperture camera design included: (1) lack of optical aberrations, such as those encountered in traditional lensed camera systems, (2) practically infinite depth of field, allowing for sharp, close-up images, and (3) wide-angle field of view without the distortions that are associated with the use of wide-angle lenses. As discussed herein, the pinhole cameras were optimized for optical resolution and light entry to minimize the effect of diffraction patterns that

are commonly associated with pinhole apertures. The resolution of the cameras was determined to be sufficient for the potential application of the cameras (volume measurements). The instrumentation presented herein provides a novel alternative to the state-of-the-art outside-of-the-cell photogrammetric instrumentation that is currently employed to monitor soil specimens during triaxial tests.

Keywords: photogrammetry, refraction, triaxial testing, laboratory equipment

3.5. Introduction

The current state-of-the-art photogrammetric technique for measuring the change in volume of soil specimens located within a triaxial cell utilizes expensive digital cameras that are located outside of the triaxial cell. The use of small board cameras located within the triaxial cell, that overcome pressure and space constraints, has the potential to improve the current state-of-the-art of photogrammetric techniques for triaxial testing, at a fraction of the expense. The optical design of the board camera was of particular importance, as it was necessary to develop high quality images within a confined space, while the camera was immersed in the confining fluid. Therefore, a small open body board camera with a pinhole aperture (BCPA) was designed. Although the use of board cameras with traditional lenses was attempted, the utilization of the BCPA was proven to perform better than the lensed camera and the optical design was simpler, more feasible, and more cost effective. The disadvantages of using a BCPA include (1) the need for very precise aperture construction for acquisition of high quality imagery and (2) limited resolution (when compared to traditional, lensed, outside-of-the-cell cameras). However, the practical and economic advantages of using a BCPA far outweigh the disadvantages. The basic optical principles of pinhole apertures and the existing state-of-the-art practice of obtaining volume measurements using photogrammetry are described and the challenges encountered

during the design and fabrication of the BCPA are presented. The images obtained using the BCPA, located within the triaxial cell, are compared with images obtained from traditional lensed cameras, located within the triaxial cell, and the differences are discussed. Final remarks and a summary of the BCPA system are also provided.

3.6. Background

Historically, when photogrammetric techniques were employed to measure the amount of volume change in specimens being tested in a triaxial device, outside-of-the-cell cameras were utilized (Parker 1987, Macari et al. 1997, Alshibli and Sture 1999, Alshibli and Al-Hamdan 2001, Gachet et al. 2006, Sachan and Penumadu 2007, Bhandari et al. 2012). However, light refraction at the (1) confining fluid-cell wall interface and (2) cell wall-atmosphere interface and the curvature of the cell wall have necessitated the use of models to account for the refraction and magnification effects. Furthermore, the cameras surrounding the testing apparatus have been expensive, limited by technology, and have required an excessive amount of space to develop the required focal length and lighting conditions. Moreover, the optical elements of the camera equipment have not been addressed in detail, such as optical aberrations, inherent to the camera lenses.

3.6.1. *Lens Optics*

Lenses are typically used to capture and focus light and may be used to increase the field of view. However, errors introduced by refraction of light through lenses, including spherical aberration, coma, field curvature, astigmatism, and barrel, pincushion, and complex distortions are prevalent to varying extents in lens applications (Mahajan 1998, Roichman et al. 2006, Kingslake and Johnson 2010). Most camera lenses are therefore constructed of multiple lenses (lens array) that are stacked to correct for some aberrations. A careful balance between

mitigating one type of aberration and augmenting another type has always existed; therefore, it is never truly possible to capture an image that does not contain some type of aberration when a lens or lens array is utilized. Although most cameras use lens arrays, liquid lenses (with variable focus induced by an electrowetting process) have recently been developed for small applications (Kuiper and Hendriks 2004, Hendriks et al. 2006, Nguyen 2010) to overcome aberrations encountered with lenses and to adjust the focal length without the need for mechanical servo action; liquid lenses are commonly utilized in many smart phone cameras. The aforementioned focus (inverse of power) of a given lens may be calculated utilizing the Lensmaker's equation (Equation 3.1) for thin lenses, first developed by English physicist Thomas Young (1773–1829) and later by Kuo and Ye (2004):

$$\frac{1}{f} = \left(\frac{n_1}{n_2} - 1\right)\left(\frac{1}{r_1} - \frac{1}{r_2}\right)$$ Kuo and Ye (2004) Equation 3.1

Where f is the focal length of the lens, n_1 is the refractive index of the lens material, n_2 is the refractive index of the surrounding medium, r_1 is the radius of curvature of the front surface of the lens, and r_2 is the radius of curvature of the back surface of the lens.

3.6.2. *Pinhole Aperture*

The pinhole aperture camera is the most basic type of camera and is often overlooked in favor of a lensed camera. However, despite, and perhaps because of its simplicity, the pinhole camera may provide: (1) images free of the optical distortions that are inherent to the use of lenses, (2) images with virtually infinite depth of field, (3) wide viewing angles, and (4) a foundation for understanding the basic concepts involved in the field of optics, specifically related to the use of cameras. The primary advantage of using a lens, as opposed to a simple pinhole, is that a lens can capture and focus more light without requiring long exposure times, thereby increasing optical resolution (defined as the ability to resolve detail). When resolution is

not the most critical objective of a camera application, a simple pinhole aperture camera may provide a viable alternative to typical lensed camera. Pinholes have been used for centuries for purposes of viewing and tracing images onto drawings prior to utilizing photo-sensitive materials for photography purposes (Renner 2000). Moreover, the basic concepts of pinhole optics were instrumental to the formulation of the theory of light. The theory was supported by the earliest written observations of multiple phenomena related to light, specifically diffraction, interference, and polarization of light through pinholes (Grimaldi 1665, Newton 1730, Young 1802, Fresnel 1819). According to Renner (2000), pinholes are still commonly utilized due to the impracticality of using lenses. For example, scientific application of pinhole imaging may be found in astro and nuclear physics (such as for high-energy particle imaging of laser plasma, X-rays, the sun, black holes, and exploding stars).

The design of a pinhole aperture is relatively simple; however, certain considerations are necessary to optimize image quality. Unlike lensed cameras, pinhole cameras rely on diffraction, not refraction (Figure 3.1). The theory and equations for pinhole apertures were suggested by early researchers like Herschel (1835), Airy (1835), and Strutt (1891); attempts have also been made to refine the relationship between the optical phenomena in more recent years. However, as Young (1971) indicates, the theoretical limits should only be used as a guideline because the optimal pinhole aperture diameter is often better determined experimentally. The optimal pinhole diameter is limited by resolution (larger diameters correspond with poorer resolution), by Fresnel (near-field) and Fraunhofer (far-field) diffraction limits, and by the ability to gather light (smaller diameters correspond with higher diffraction interference and allow less light to be collected). The optimal pinhole diameter for optical applications often relates to the “Airy disk,” which is the bright, focused spot, central to a diffraction pattern through a perfectly circular aperture.

1. Viewing angle
2. Pinhole aperture diameter
3. Aperture substrate thickness
4. Image plane
5. Focal length
6. Principle axis
7. Single, thin, convex lens
8. Focal point
9. Distance from object to lens
10. Distance from lens to image plane
11. Distance from object to image plane

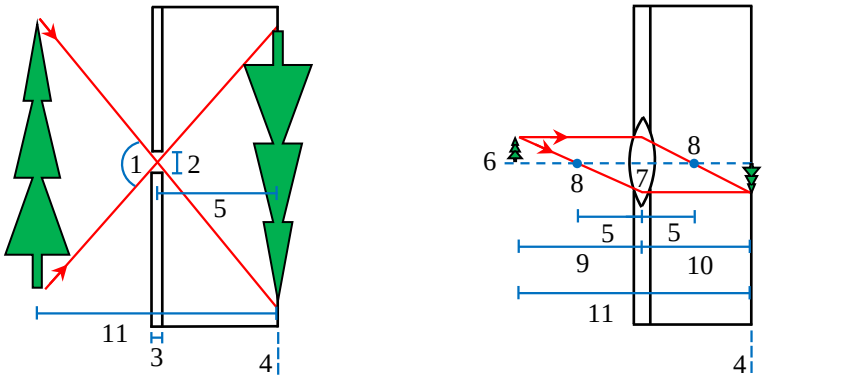

(a) (b)

Figure 3.1. Real image formation illustrated by simplified ray diagram of *(a)* diffraction of light through a pinhole aperture, and *(b)* refraction of light through a lens.

3.6.3. *Pressure Resistant Cameras*

To be able to withstand high pressures, a camera is typically sealed in pressure-resistant or, more commonly, pressure-compensating housings (Laudo et al. 1998). These housings are typically bulky, expensive, and do not allow for direct optical observation because light must first pass through a transparent thermoplastic barrier (i.e., acrylic plastic) before reaching the camera. To combat this, fluids such as silicone oil or mineral oil (Salazar and Coffman 2014), may be used in electronics applications where exposure to the fluid is unavoidable or desired. The direct contact between the electronics and fluid will not cause short-circuiting due to the inert and non-ionic properties of the oil (Mohapatra and Loikits 2005, Schmidt 2005, Lasance and Simons 2005). Furthermore, even at high pressures, the silicone oil does not crush the components of the camera even though the components are directly subjected to the fluid. This

direct immersion allows for pressure resistant design, without the need for a housing; thereby also allowing for direct optical observation.

3.7. Challenges Encountered

The design of the optical and mechanical components of a camera system that was used to monitor triaxial specimens from within a triaxial cell, submerged in confining fluid, and subjected to high pressures is presented herein. The following challenges were encountered and are addressed sequentially: (1) physical space requirements of placing multiple cameras within a standard triaxial cell, (2) direct contact between electronic components of the camera and the confining fluid, (3) space requirements for developing the appropriate focal length, (4) high cell pressures during testing, (5) sufficient coverage of entire specimen area with minimal camera deployment, and (6) analog to digital signal conversion for capturing still frames from video feeds. Discoveries were made through an initial empirical trial and error process, and through theoretical deductions to test, optimize, and fabricate new BCPA designs. The process that was followed to address each of the interrelated challenges is presented in Figure 3.2. Specifically, of most importance was the focal length, as the focal length was a function of all of the other challenges. Each of the aforementioned challenges is further discussed in the forthcoming sections.

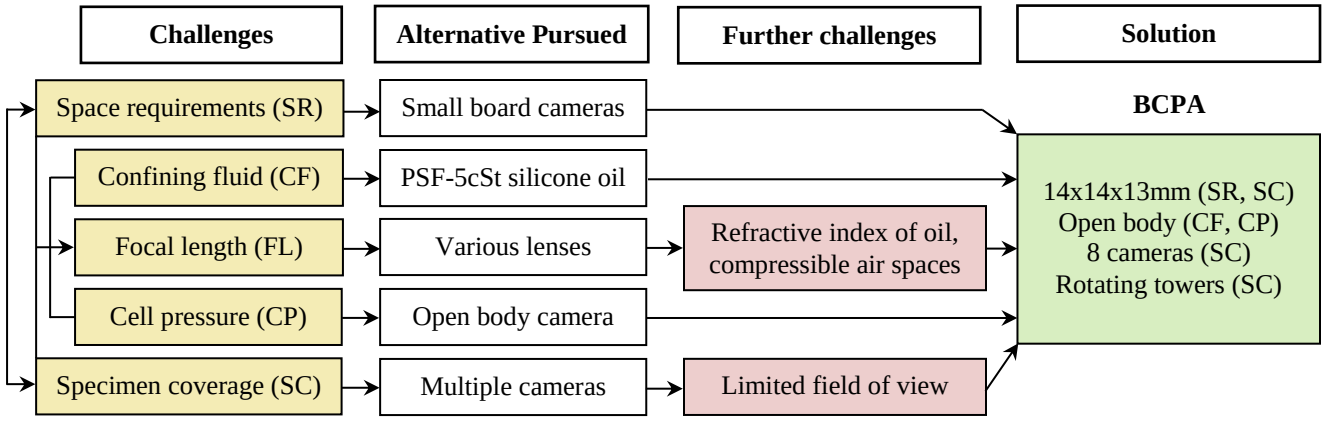

Figure 3.2. The process that was followed to address the interrelated challenges in the design of the BCPA.

3.7.1. *Space Requirements*

The first challenge was the small size of the triaxial cell (11.43 cm (4.5 in.)) inside diameter Trautwein Soil Testing Equipment Co. triaxial cell). Only 3.81 cm (1.5 in.) of space surrounded the 3.81 cm (1.5 in.) diameter specimen. To overcome this challenge, small closed circuit board cameras (with dimensions of 14mm (0.55 in.)) by 14mm (0.55 in.) by 13mm (0.51 in.)) were placed into the cell in between the cell wall and the soil specimen. Several types of cameras were investigated including various types of cameras with a 6.35mm (0.25 in.) format or 8.38mm (0.33 in.) format charge-coupled device (CCD) or complementary metal oxide semiconductor (CMOS) sensor that were mounted to a circuit board that housed composite video (yellow), audio (white), and power (red, black) wire leads and enclosed within an aperture box with a threaded lens mount assembly.

The quality and size of the images produced from the respective cameras was partially a function of the sensor size; therefore, given the available options, a 8.38mm (0.33 in.) format sensor was selected over similar 6.35mm (0.25 in.) format sensors. Each of the cameras was tested with a variety of standard lenses both in air and submerged in electronics-grade silicone

oil. Furthermore, only cameras with the highest lines of horizontal resolution (LoHR), and pixel dimensions were selected (specifications ranged from 420 LoHR to 700 LoHR and 492 by 510 to 976 by 582, respectively). The board camera that was selected for use in the triaxial cell possessed a 8.38mm (0.33 in.) format SONY CCD sensor, capable of obtaining 700 LoHR, and 976 horizontal by 582 vertical effective pixels. This camera was chosen because it had the best image quality to size ratio, thereby facilitating deployment inside of the triaxial cell. Photographs of the various types of cameras and lenses that were tested, and their respective specifications, are presented in Figure 3.3.

Given the space constraints within the triaxial cell, it was not practical to design a lens array to focus light for this application. It may have been possible to design a lens system to improve the resolution of captured images; however, given the space constraints, the design would have required using very small lenses (on the order of 2.0mm in diameter) with unusually high refractive indices (greater than 1.8) to give the appropriate focal length when immersed in the silicone oil. Specifically, the appropriate focal length that was required is discussed in the section entitled *focal length*.

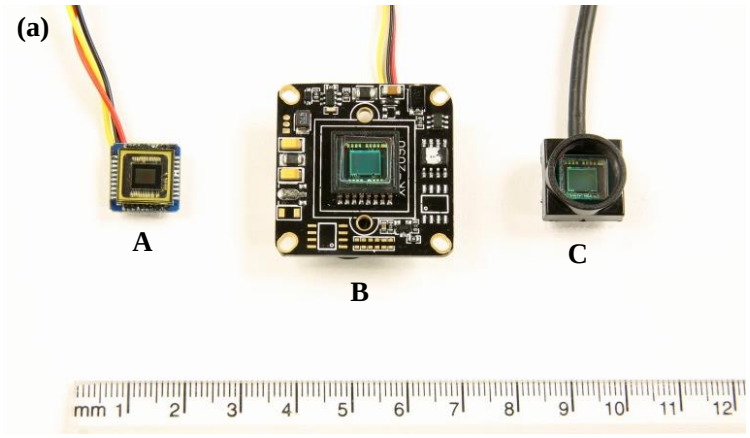

Board camera specifications:
A) 6.35mm [0.25in.] format Sharp CCD sensor, 420 LoHR, 492×510, M6.5×0.25 aperture box threading,
B) 8.38mm [0.33in.] format Sony CCD sensor, 700 LoHR, 976×494, M12×0.5 aperture box threading;
C) 8.38mm [0.33in.] format Sony CCD sensor, 700 LoHR, 976×582, M12×0.5 aperture box threading.

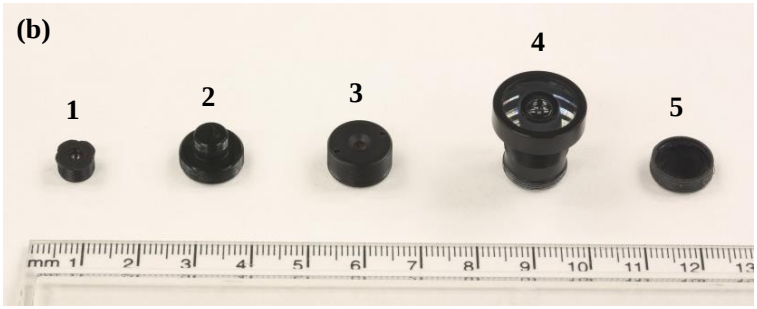

Lens specifications:
1) 3.6mm standard lens, 55° FOV;
2) 3.7mm button lens, 60° FOV;
3) 2.8mm barrel lens, 90° FOV;
4) 2.1mm wide angle lens, 170° FOV;
5) barrel-mounted pinhole aperture.
Note: All had M12×0.5 threading but Lens 1 (M6.5×0.25 thread).

Figure 3.3. ***(a)*** **Three types of board cameras that were tested, and** ***(b)*** **five different types of lenses used with the cameras.**

3.7.2. *Confining Fluid*

To avoid damage to the sensitive electronics of the cameras, while still ensuring saturation of the specimen (by utilizing pressurized fluid instead of pressurized air to prevent gas diffusion across the membrane), silicone fluid (PSF-5cSt, Trautwein Soil Testing Equipment Co.) was used to confine the specimens and surrounded the cameras. Properties of the silicone fluid include: low viscosity (5cSt), specific gravity of 0.918, dielectric constant of 2.60, dielectric strength of 375, and index of refraction of 1.397. Due to the high refractive index of the oil (relative to air), the standard lenses were not able to focus when immersed in the oil. Specifically, the index of refraction of the silicone oil (1.397) was much greater than the index of

refraction of air (1.000 in a perfect vacuum). Although unknown, it was estimated that the index of refraction of the lens material was between 1.48 and 1.60 (for crown or flint glass). The increase in the index of refraction from 1.000 to 1.397 reduced the difference in the indices of refraction between the two media (air–glass and oil–glass) and thereby increased the required focal length. This reduction in the difference in the indices of refraction provided for non-ideal light dispersion and therefore led to severely out-of focus images when the cameras containing lenses were submerged in oil. Simply put, lenses were deemed to not be a viable option (as discussed in further detail in the focal length section).

3.7.3. *Focal Length*

As discussed previously, limited space was available to deploy the cameras. This space constraint limited the maximum achievable focal length (the distance between the object and the lens, as shown in the ray diagram that was previously presented in Figure 3.1). The minimum focal length values, for the standard lenses that were included with purchase of the board cameras when tested in air, were between 4 and 6 cm (1.6 and 2.4 in.). These distances corresponded to images with the highest sharpness; therefore, focused images could not be obtained when using cameras with the standard lenses within the available confined space of 3.81 cm (1.5 in.). Furthermore, as revealed by submerging the cameras in the silicone oil, the focal length of a given lens varied, depending on the medium that surrounded the lens.

Simply put, a camera lens designed to provide focus in air, did not provide focus in the silicone oil. Although different types of lenses were tested (Figure 3.3), all of the lenses inhibited viewing of soil specimens when the lenses were immersed in silicone oil. The testing of the lenses was purely empirical, due to the unknown characteristics of the various lenses (lens shape, refractive index of lens material, and radii of curvature of the lens surfaces). The characteristics

of the lenses were unknown because the small lenses were cemented and sealed inside of a mounting assembly, making it impractical to extract the lenses or lens components for closer inspection. The Lensmaker's equation (previously presented as Equation 3.1) was employed to determine the optical properties of a lens that would enable collection of images when immersed in silicone oil. However, given the immersion medium, it was not economically, nor practically feasible to purchase or (manufacture) a lens, or lens array, with the correct refractive index (greater than 1.8) to develop the appropriate focal length (approximately 24mm (0.94 in.)) within the physical space limitations (3.81 cm (1.5 in.)). Therefore, as discussed in the section entitled Pinhole Solution, another solution was realized to enable collection of images from close distances within a fluid with a high refractive index.

3.7.4. *Cell Pressure*

To withstand the cell pressures during testing (up to 1034 kPa (150 psi)), the cameras were flooded behind the aperture, filling all of the air space with oil. It was observed, in original testing of the lensed cameras, that the focal length of the lens arrays permanently changed after being subjected to typical pressures. This was attributed to the compression of the small void spaces between the lenses when subjected to pressure, resulting in permanent deformation of the lenses and thereby altering the optical properties of the lens array. It was therefore determined that an alternative to a lens array must be developed to withstand pressure applications.

3.7.5. *Specimen Coverage*

Due to the close proximity of the board camera to the soil specimen, it was not possible to observe the entirety of the specimen with a single camera. Specifically, the field of view of an individual camera (21mm (0.83 in.)) was smaller than the height of the specimen (7.62 cm (3.0 in.)). Therefore, by using multiple cameras, individual areas of the specimen were monitored and

the photographs of the individual areas were stitched together using post-processing software. To achieve this, a camera monitoring system was designed with two arrays of four BCPA (eight total cameras). The BCPAs were mounted to towers that were rotated along a track that was attached to the base inside of the cell. The track was designed to rotate using pairs of small magnets; one magnet was mounted to the track and the other magnet was located at various positions outside of the triaxial cell wall. The use of magnets allowed for the BCPAs to capture still frames at prescribed intervals during the rotation. A schematic of the track and camera tower system is presented in Figure 3.4.

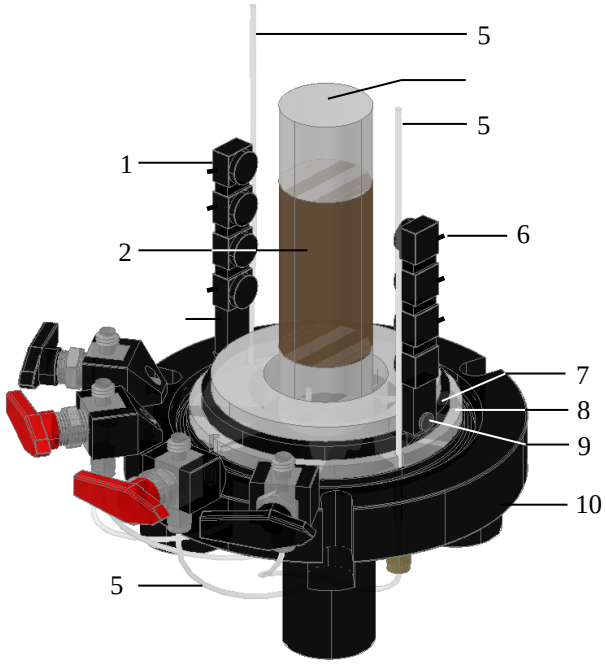

1. BCPA (typical, 8 quantity)
2. Soil sample
3. Camera tower
4. Acrylic top cap
5. Drain lines
6. Camera cable
7. Rotating Delrin® bearing track
8. Delrin® bearing base
9. Magnet
10. Triaxial apparatus base

Figure 3.4. Schematic of guided camera track system mounted on triaxial apparatus base.

In the original design of the cameras, it was hypothesized that using wide-angle lenses would be sufficient to capture large areas of the specimen and, therefore, very few cameras would be required. However, the use of this type of lens was not permitted (due to the aforementioned problems associated with lenses not enabling image collection when submerged in silicon oil, due to the physical size requirements of the lenses, and due to the distortions that were associated with wide-angle lenses (barrel, pincushion, and complex distortions)). Although these distortions are now a moot point because the wide-angle lens could not be used, these distortions are known to be difficult to correct and typically reduce the size of the image (due to cropping requirements).

3.8. Pinhole Solution

To overcome the limitations of focal length, refractive properties of the confining fluid, cell pressure, and specimen coverage, a lensless pinhole aperture was developed. The required aperture diameter was approximated, based on Equation 3.2 (Strutt 1891):

$$f = 2r^2/\lambda \qquad \text{Strutt (1891)} \qquad \text{Equation 3.2}$$

Where f is the focal length, r is the radius of the pinhole opening (or aperture), and λ is the design wavelength.

However, unlike for a lens, the f variable used in Equation 3.2 was associated with the distance between the pinhole aperture and the camera sensor plane, as previously depicted in Figure 3.1. Furthermore, as discussed previously, unlike lensed cameras, pinhole cameras have infinite depth of field; therefore, this type of aperture allowed for the entire image to be in focus. To obtain sharp images and to maximize resolution, the edges of the pinhole must be precisely cut and the diameter of the pinhole must be small. Moreover, the thickness of the substrate must be thin to allow for the widest viewing angle (as shown previously in Figure 3.1). Therefore,

various pinhole sizes 75, 100, and 150 μm (2.95×10^{-3}, 3.94×10^{-3}, and 5.91×10^{-3} in.) were laser cut into the center of a 9.5mm (0.375 in.) diameter wafer substrate (National Aperture, Part Number 1-75+ B-2, 1-100+ B-2, and 1-150+ B-2), respectively. The steel substrate (300 series stainless steel) had a thickness of 12.7 μm (5×10^{-4} in.) and both sides were blackened (+B-2) to absorb any stray light within the aperture box.

The design optical wavelength (415 nm) was selected based on the results obtained from a relative light intensity test that was conducted by examining a diffuse reflectance fluoropolymer reference material (Spectralon, Labsphere, Inc.) using a spectroradiometer (ASD FieldSpec Pro HandHeld 2 portable spectroradiometer). Although a peak value of 580nm was observed, a reduced value of 415nm was utilized because of the refractive index ratio (1.397) that was associated with silicone oil being used as the confining fluid instead of air. Furthermore, this wavelength (415 nm) was selected because the final position of the pinhole aperture was fine-tuned (in relation to the camera image plane) using a threaded barrel that screwed into the aperture box.

A recess was placed into the threaded barrel to enable the wafer substrate to be mounted to the barrel. The aforementioned three aperture diameters were tested at various distances from the camera sensor, and it was found that the 75 μm (3.94×10^{-3} in.) diameter aperture provided the best image quality when the substrate was located approximately 3.0mm away from the image plane, as assessed by visual inspection of the acquired images. Therefore, the final design components of the BCPAs are thus: (1) an 8.38mm (0.33 in.) format board camera encased in an aperture box with a M12×0.5 threaded opening; (2) a threaded barrel that was used for seating and adjusting the pinhole aperture substrate; and (3) a laser cut pinhole aperture (75 μm opening), centered at a specified focal length (3.0 mm) from the camera sensor. A schematic and

a photograph of the assembled BCPA are presented in Figures 3.5 and 3.6, respectively. As discussed in the section entitled *images collected*, the BPCA design and fabrication enabled images to be collected from inside of the triaxial cell while the cameras were immersed in silicone oil and subjected to high pressures.

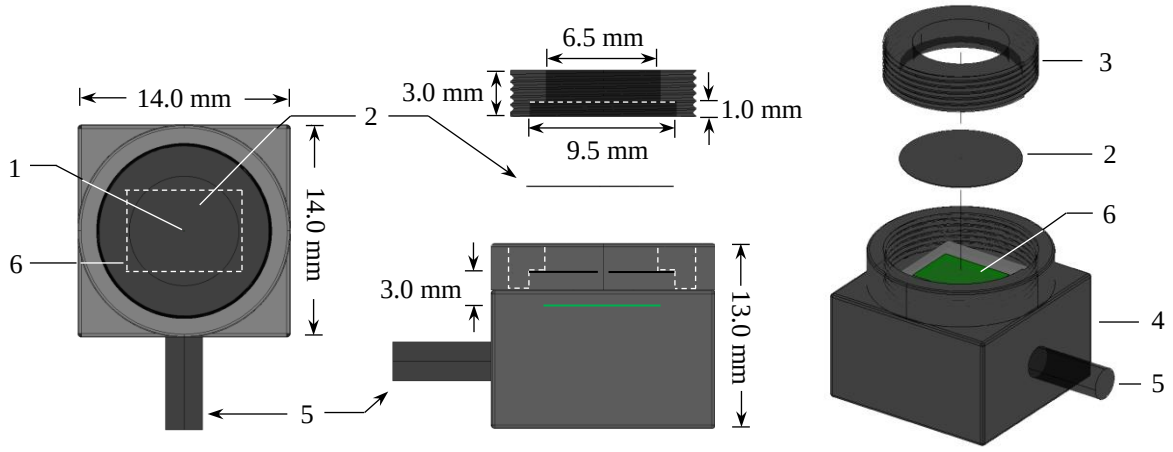

1. Pinhole aperture (75μm diameter)
2. Pinhole substrate (9.5mm diameter, 12.7μm thick)
3. Threaded barrel (M12×0.5, 6.5mm inside diameter)
4. Aperture box
5. Video signal and power supply cable
6. CCD sensor (5.0mm × 4.8mm)

Figure 3.5. Schematic of *(a)* front view, *(b)* exploded side view, and *(c)* exploded orthogonal view of the BCPA.

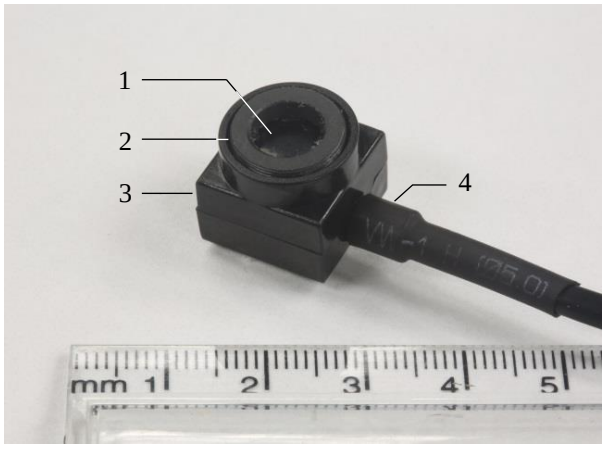

1. Substrate (9.5mm diameter) with pinhole (75μm diameter)
2. Threaded barrel (M12×0.5, 6.5mm inside diameter)
3. Aperture box
4. Video signal and power supply cable

Figure 3.6. Photograph of one of the BCPAs utilized inside of the triaxial cell.

3.8.1. *Video Signal Acquisition*

The video cables of the cameras were connected to a wire harness that was connected to a nine-pin feedthrough connector located within the top cap of the triaxial device. The feedthrough allowed for electrical signals to travel into and out of the triaxial device. The video wires that were connected to the cameras were also connected to the pins on the nine-pin feedthrough connector; the opposite sides of the pins were connected to the input channels of an eight-way video/audio switch (Maituo MT-VIKI 8 Port VGA Switch). The single video output channel from the video/audio switch was then connected to a Universal Serial Bus 2.0 Digital Video Adapter (Sabrent USB-AVCPT). Each camera was supplied with external power (DC 12V) from a common external power supply (Enercell 3-12VDC 1A AC Adapter) that provided power to all of the cameras simultaneously via the nine-pin feedthrough connector. The video feed from each of the cameras was subsequently received and displayed by switching the video/audio switch. The software that was included with the video adapter (Sabrent USB 2.0 Video Capture Creator with Audio) was utilized to capture still frames from the video feed that was obtained from each of the cameras.

3.9. Images Collected

Still frames, captured from the video feed of a board camera with a lens (located in air and immersed within PSF-5cSt silicone oil), are presented in Figures 3.7(a) and 3.7(b), respectively. Still frames, captured with the BCPA (located in air and immersed within PSF-5cSt silicone oil), are presented in Figures 3.7(c) and 5.7(d), respectively. An example of linear distortion in images captured using a lens is evident in Figure 3.7(a) and the inability of the camera to collect focused light through the lens to form a real image is displayed in Figure 3.7(b). As explained previously, because the lens was designed to work in air, the index of

refraction of the silicone oil prevented the camera that was fully immersed within oil from obtaining a focused image.

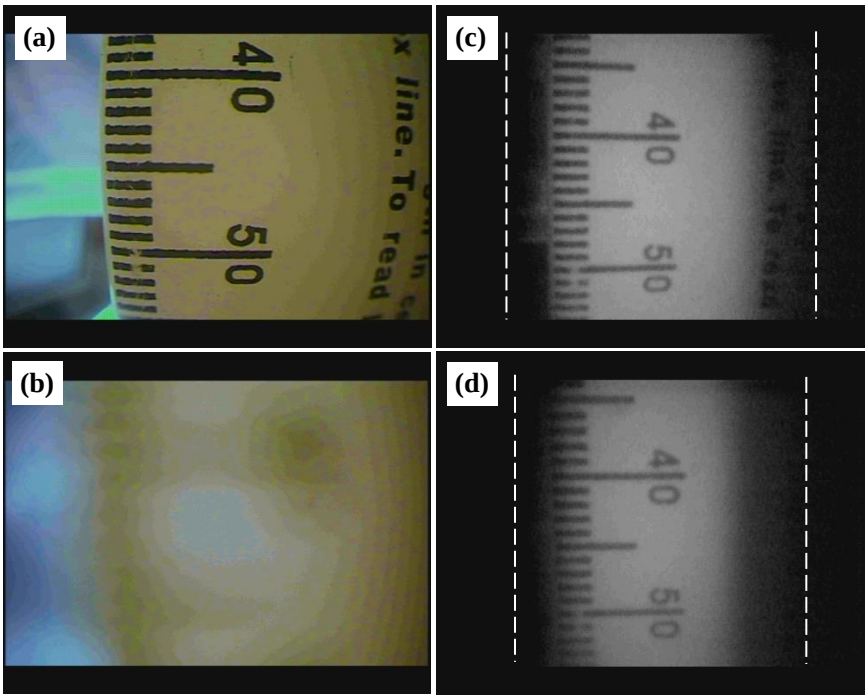

Figure 3.7. Still frames captured using a 8.38mm [0.33in.] format CCD board camera with 1) 3.7mm button lens (55° FOV, M12×0.5 thread) in *(a)* air, and within *(b)* PSF-5cSt silicone oil, and with 2) 75μm diameter pinhole aperture (attached to a M12×0.5 barrel with 6.5mm diameter opening) in *(c)* air, and within *(d)* PSF-5cSt silicone oil.

It was determined that the captured light on the far left and far right edges of the images collected using the BCPA faded abruptly and completely (as indicated by the areas to the left and right of the dashed white lines in Figures 3.7(c) and 3.7(d)). This phenomenon was attributed to a combination of physical and optical influences. The aperture barrel material blocked the edges of the CCD sensor along the longer (horizontal) side of the CCD sensor (due to the proximity of the barrel to the sensor). Thereby, light was prevented from reaching the edges of the CCD sensor that led to the black appearance. Although not required, the proximity limitation should be

overcome by enlarging the inside diameter of the threaded barrel. However, it was determined that, given the experimental equipment, the dimensions of the shorter (vertical) side of the sensor provided sufficient coverage of the object (if the camera was rotated in such a way that the camera cable exited from the camera in the horizontal plane as shown previously in Figure 3.4) and therefore an increase in the inside diameter of the barrel was not necessary. Furthermore, the "airy disk" covered the entire camera sensor so no visible diffraction patterns were present.

As observed in the comparison between images captured with a lens and those captured with a pinhole aperture, there was a significant difference in the amount of light exposure. The lens (Figures 3.7(a) and 3.7(b)) allowed for maximum light gathering. The pinhole aperture (Figures 3.7(c) and 3.7(d)) allowed for minimal light entry, due to the small size of the opening (75 μm (3.94×10^{-3} in.) diameter). In typical pinhole photography, this minimal amount of light entry is commonly overcome with longer exposure times; however, for the type of board camera that was used, it was not possible to control the exact exposure time (electronic shutter time varied between 1/60 and 1/100 000 s, as per the camera manufacturer). Furthermore, the board camera switched into "night mode" (monochromatic light gathering) when the illuminance levels dropped below a certain threshold (0.1 lux). Chromatic aberration may have been present in the captured images, but it was not possible to detect this type of aberration due to the monochromatic nature of the images. Although the lighting was not modified to collect the images presented in Figure 3.7, it is recommended that the lighting surrounding the soil sample be enhanced and controlled to aid in collection of higher quality imagery. Specifically, utilizing two 17.8 cm (7 in.) diameter dome light sources to surround the entire triaxial chamber will enhance the imagery. With the aid of the guided camera track system, multiple still frames were captured with the individual BCPAs along the length of the soil specimen, at prescribed intervals

during rotation around the circumference of the specimen. Because of the overlapping fields of view of adjacent BCPAs, in the vertical direction and in circumferential direction, common points were acquired within captured images, and the individual geopositions of the cameras were calculated, allowing for post-process stitching of the collected images. PhotoModeler (Eos Systems, Inc. 2014) was utilized to calculate the photogrammetric properties of the BCPA (Table 3.1). These properties included the focal length, format size (physical dimensions of the sensor) and principal point (intersection between principal axis and image sensor). PhotoModeler was also used to determine the geoposition of each of the individual BCPAs. Specifically, the positions of the BCPAs were determined by using unique, pre-selected targets that were adhered to a 1.5 in. (38mm) diameter by 3 in. (76mm) tall brass specimen and that were automatically recognized within the software. The PhotoModeler obtained photogrammetric properties and geopositions corresponded well with manual (caliper) measurements.

Table 3.1. Photogrammetric properties of the BCPA.

Focal length (mm)	Format size (mm)	Principal point (pixels)
3.50	5.16 width	2.62 x
	4.80 height	2.23 y

Using repeatable rotation intervals, and therefore known geopositions of each of the individual BCPAs, PhotoModeler was used to match common points within the captured images that thus enabled generation of a point cloud for any object that was viewed by the BCPAs. This point cloud was then meshed to calculate the dimensions and volume of the viewed object. By utilizing this experimental method (PhotoModeler), the volume of the brass specimen that was obtained was 91.92 cm^3. The volume obtained using manual (caliper, pi tape) measurements was 91.93 cm^3, resulting in an estimated error of 0.01 %.

3.10. Conclusions

A small board camera with a pinhole aperture was designed for deployment inside of a triaxial cell to enable measurement of the volume of soil specimens. Because the camera components were fully immersed in oil and were located very close to the soil specimen, special considerations were accounted for when designing the optical components of the photogrammetric instrumentation. To resist the high pressures that are commonly encountered within the triaxial cell during triaxial testing (up to 1034 kPa (150 psi)), the silicone oil was allowed to enter behind the camera face and to surround the CCD sensor. The relatively high refractive index of silicone oil (as compared to the refractive index of air) influenced the light entering into the traditional lenses or lens arrays yielding severely out of focus images (because the refractive index of the lens or lens array closely matched the refractive index of the lens confining fluid).

Utilizing the Lensmaker's equation, it would have only been possible to focus an image using small lenses with unusually high refractive indices. However, this option was not pursued because it was (1) limited by availability, (2) costprohibitive, and (3) required the design and fabrication of additional lens mounts and boxes. Instead, the as provided lens that was located within the aperture box of each of the board cameras was replaced with a newly created high-precision pinhole aperture. The pinhole cameras were designed, fabricated, tested, and their potential applicability inside of a triaxial cell evaluated. Specifically, high quality images were acquired using the BCPA even when the BCPA was placed inside of the triaxial cell, immersed in silicone oil, and subjected to high pressures. Furthermore, a guided track system was designed to allow for coverage of the entire soil specimen, while deploying the minimal number of BCPAs within the triaxial cell.

3.10.1. *Advantages and Limitations of a BCPA*

In summary, a careful balance existed between resolution, light entry, and field of view. To truly optimize the design of the camera, it was necessary to experiment with a variety of different pinhole diameters and focal lengths. There are many advantages to BCPAs, two of which are an infinite depth of field (including very close depths) and a lack of any of the optical aberrations associated with lenses. Other advantages of using a pinhole-type camera are as follows: the BPCA: (1) is not adversely affected by the refractive properties of the immersion fluid (silicone oil); (2) requires very little space to develop appropriate focal length and requires less space than a lens or lens array; (3) may be designed to provide very large viewing angles without the need for a lens; and (4) can withstand pressure. The disadvantages are primarily low light entry and limited resolution; however, with proper design and fabrication, these disadvantages were overcome. By utilizing a BCPA, images were obtained within a triaxial cell even though the optical design of the BCPA was simplified from that of a traditional lensed camera.

3.11. References

Airy, G. B., 1835, "On the Diffraction of an Object-Glass With Circular Aperture," *Trans. Cambr. Philos. Soc.*, Vol. 5, pp. 283–291.

Alshibli, K. A. and Sture, S., 1999, "Sand Shear Band Thickness Measurements by Digital Imaging Techniques," *J. Comput. Civ. Eng.*, Vol. 13, No. 2, pp. 103–109.

Alshibli, K. A. and Al-Hamdan, M., 2001, "Estimating Volume Change of Triaxial Soil Specimens From Planar Images," *Comput-Aid. Infrastruct. Eng.*, Vol. 16, No. 6, pp. 415–421.

Bhandari, A. R., Powrie, W., and Harkness, R. M., 2012, "A Digital Image-Based Deformation Measurement System for Triaxial Tests," *Geotech. Test. J.*, Vol. 35, No. 2, pp. 1–18.

Eos Systems Inc., 2014, PhotoModeler (Version 2014.1.1). 3D Measurements and Models Software, http://www.photomodeler.com/index.html (Last accessed 13 Oct 2014).

Fresnel, A.-J., 1819, "Memoir on the Diffraction of Light," *The Wave Theory of Light, H. Crew, Trans.*, American Book Company, New York.

Gachet, P., Geiser, F., Laloui, L., and Vulliet, L., 2006, "Automated Digital Image Processing for Volume Change Measurement in Triaxial Cells," *Geotech. Test. J.*, Vol. 30, No. 2, pp. 98–103.

Grimaldi, F. M., 1665, *Physico–mathesis de lumine, coloribus, et iride, aliisque adnexis libri duo* [A physiomathematical thesis on light, colors, the rainbow and other related topics in two books], Bologna, Italy (in Latin).

Hendriks, B. H. W., Kuiper, S., van As, M. A. J., Renders, C. A., and Tukker, T. W., 2006, "Variable Liquid Lenses for Electronic Products," *Proc. SPIE*, Vol. 6034, pp. 10–18.

Herschel, J. F. W., 1835, *Treatise on Astronomy*, 3rd ed., Carey, Lea & Blanchard, Philadelphia, PA.

Kingslake, R. and Johnson, R. B., 2010, *Lens Design Fundamentals*, 2nd ed., Academic Press, New York.

Kuiper, S. and Hendriks, B. H. W., 2004, "Variable-Focus Liquid Lens for Miniature Cameras," *Appl. Phys. Lett.*, Vol. 85, No. 7, pp. 1128–1130.

Kuo, C.-H. and Ye, Z., 2004, "Sonic Crystal Lenses that Obey the Lensmaker's Formula," *J. Phys. D.*, Vol. 37, No. 15, pp. 2155–2159.

Lasance, C. and Simons, R., 2005, "Advances in High Performance Cooling for Electronics," *Electron. Cool.*, Vol. 11, No. 4, pp. 22–39.

Laudo, J. S., Wurm, K., and Dodson, C., 1998, "Liquid-Filled Underwater Camera Lens System," *Proc. SPIE*, Vol. 3482, pp. 698–702.

Macari, E. J., Parker, J. K., and Costes, N. C., 1997, "Measurement of Volume Changes in Triaxial Tests Using Digital Imaging Techniques," *Geotech. Test. J.*, Vol. 20, No. 1, pp. 103–109.

Mahajan, V. N., 1998, *Optical Imaging and Aberrations: Part I. Ray Geometrical Optics*, SPIE, Bellingham, WA.

Mohapatra, S. C. and Loikits, D., 2005, "Advances in Liquid Coolant Technologies for Electronics Cooling," *Proceedings of the 21st IEEE Semiconductor Thermal Measurement and Management Symposium*, San Jose, CA, March 15–17, pp. 354–360.

Newton, I., 1730, *Opticks: Or a Treatise of the Reflections, Refractions, Inflections and Colours of Light*, 4th ed., William Innys, London.

Nguyen, N.-T., 2010, "Micro-Optofluidic Lenses: A Review," *Biomicrofluidics*, Vol. 4, No. 3, 031501.

Parker, J. K., 1987, "Image Processing and Analysis for the Mechanics of Granular Materials Experiment," *ASME Proceedings of the 19th SE Symposium on System Theory*, ASME, New York, pp. 536–541.

Renner, E., 2000, *Pinhole Photography: Rediscovering a Historic Technique*, 2nd ed., Butterworth–Heinemann, Boston, MA.

Roichman, Y., Waldron, A., Gardel, E., and Grier, D. G., 2006, "Optical Traps with Geometric Aberrations," *Appl. Opt.*, Vol. 45, No. 15, pp. 3425–3429.

Sachan, A. and Penumadu, D., 2007, "Strain Localization in Solid Cylindrical Clay Specimens Using Digital Image Analysis (DIA) Technique," *Soils Found.*, Vol. 47, No. 1, pp. 67–78.

Salazar, S. E. and Coffman, R. A., 2014, "Design and Fabrication of End Platens for Acquisition of Small-Strain Piezoelectric Measurements During Large-Strain Triaxial Extension and Triaxial Compression Testing," *Geotech. Test. J.*, Vol. 37, No. 6, pp. 948–958.

Schmidt, R., 2005, "Liquid Cooling is Back," Electron. Cool., Vol. 11, No. 3, pp. 34–38.

Strutt, J. W., Lord Rayleigh, 1891, "On Pin-Hole Photography," *Philos. Mag.*, Vol. 31, pp. 87–99.

Young, T., 1802, "Bakerian Lecture: On the Theory of Light and Colours," *Philos. Trans. R. Soc. Lond.*, Vol. 92, pp. 12–48.

Young, M., 1971, “Pinhole Optics,” *Appl. Opt.*, Vol. 10, No. 12, pp. 2763–2767.

CHAPTER 4: DEVELOPMENT OF AN INTERNAL CAMERA-BASED VOLUME DETERMINATION SYSTEM FOR TRIAXIAL TESTING

4.1. Chapter Overview

The development of the internal camera-based volume determination system is described in this chapter. The instrumentation presented within this manuscript provided a novel alternative to the state-of-the-art of camera-based monitoring of triaxial tests. The individual components of the system, the photogrammetric methodology, and preliminary testing of the system are detailed.

The limitations of the included manuscript (Salazar et al. 2015) are discussed in Section 4.2. The full citation for this document is included in Section 4.3. The motivation and background for the manuscript are described in Sections 4.4, 4.5, and 4.6. Contained within Section 4.7 is a detailed description of the camera system, including the mechanical and electrical components of the system (Sections 4.7.1 and 4.7.2, respectively). The photogrammetric methodology and early results are detailed in Section 4.8. Finally, conclusions for this manuscript are presented in Section 4.9.

4.2. Limitations of the Described Study

The manuscript contained within this chapter was originally published as a technical note in order to follow up the Salazar and Coffman (2015) publication that first introduced the internal camera-based volume determination system. The length of the manuscript was therefore limited. Although the preliminary testing of the system was described as a "validation process", the tests did not include any triaxial tests on soil specimens, nor were the camera-based measurements subject to immersion in confining fluid (all tests were performed in an air-filled cell only). Furthermore, the photogrammetric methodology that was utilized to determine the

volume of a dummy specimen within the testing cell was described in broad terms, but an overview of the implementation of the system was provided.

4.3. Development of an Internal Camera-Based Volume Determination System for Triaxial Testing

Reference

Salazar, Sean E., Barnes, Adam, and Coffman, Richard A., "Development of an Internal Camera-Based Volume Determination System for Triaxial Testing," Geotechnical Testing Journal, Vol. 38, No. 4, 2015, pp. 549-555. doi:10.1520/GTJ20140249.

4.4. Abstract

A triaxial testing cell was instrumented with an internal camera monitoring system. By placing the camera monitoring system inside of the triaxial cell, optical distortions due to refraction at the confining fluid–cell wall and cell wall–atmosphere interfaces and the curvature of the cell wall were eliminated. The components of the system are presented. Furthermore, the photogrammetric techniques that were utilized to analyze the photographs that were captured from within the triaxial cell are discussed. The proposed methods for acquiring and analyzing the photographs are presented and the potential for the inclusion of an internal camera–monitoring system for triaxial testing applications are discussed.

Keywords: triaxial testing, laboratory equipment, photogrammetry

4.5. Introduction

Of the unconventional testing methods (photogrammetry, other digital imaging techniques, proximity sensors, x-ray-computed tomography) used to monitor saturated and unsaturated soil specimens during triaxial testing, photograph-based measurement is a practical, cost-effective, and versatile method. Photogrammetry may be utilized to: (1) characterize the failure plane within a soil specimen during testing, (2) monitor the critical cross-sectional area of

the soil specimen (bulging or necking behavior), (3) calculate the volume of the soil specimen, and (4) calculate the volumetric strain within the soil specimen. Several drawbacks exist with current photograph-based instrumentation, namely the optical effects caused by the curvature of the cell wall, refraction at the confining fluid–cell wall and cell wall–atmosphere interfaces, and optical distortions inherent to lensed cameras. These drawbacks must be overcome and corrected using cumbersome models, further complicating the procedure of acquiring and processing images.

As described in Salazar and Coffman (2015), the optical components of internal photogrammetric instrumentation (cameras located within the cell fluid on the inside of the triaxial cell) for triaxial testing applications were designed, fabricated, and tested to overcome the aforementioned drawbacks, as well as to overcome the challenges of internal instrumentation (space, confining fluid, focal length, cell pressure, and specimen coverage). Details about the photogrammetric system that was placed within the triaxial cell to allow for direct, unobstructed observation of a specimen during triaxial testing are presented herein. The system allowed for viewing of the entire specimen surface in both the axial and radial directions. Calibration and validation of the system was attained by utilizing a photogrammetric technique to digitally reconstruct the exterior shape of a specimen with known dimensions. The methodology that was employed to reconstruct the exterior surface and the accuracy and precision of the photogrammetric measurements are presented and discussed for completeness.

4.6. Background

Specimen volume and volumetric strain measurements have historically been calculated for soil specimens, during triaxial testing, by utilizing pore fluid volume measurements (Bishop and Donald 1961, Ng et al. 2002, Leong et al. 2004). These pore fluid measurements have

typically been supplemented with data obtained from axial deformation measurements to obtain the average specimen dimensions, during or after testing, by adding or subtracting the measurements from the dimensions of the specimen that were manually measured (caliper and pi tape) prior to testing. Because the volume measurements have been attained by measuring the change in the amount of pore fluid, the measurements have been affected by temperature- and pressure-induced flexure of the cell wall and drain lines. Therefore, only estimates, not exact values, of volumetric strain have been obtained from these measurements. Likewise, conventional axial (Scholey et al. 1995, Cuccovillo and Coop 1997, Ng and Chiu 2001) and lateral or radial (Khan and Hoag 1979, Clayton et al. 1989, Bésuelle and Desrues 2001) measurements also rely on averaging methods that have not accurately accounted for irregular surfaces. Furthermore, past measurements have been limited to global volume changes that prevented the characterization of local strains during the development of shear bands, bulging bifurcation, or, in the case of extension testing, necking.

To overcome these limitations, digital imaging techniques, including digital image analysis (DIA), digital image correlation (DIC), and particle image velocimetry (PIV), have been used to monitor deformations within soil specimens by using external (cameras located outside of the triaxial cell) cameras. Specifically, these techniques have been of increasing interest as an alternative method to calculate the volumetric strain of soil specimens (Macari et al. 1997, Alshibli and Al-Hamdan 2001, Puppala et al. 2004, Rechenmacher and Finno 2004, Ören et al. 2006, Gachet et al. 2007, Sachan and Penumadu 2007, Önal et al. 2008, Bhandari et al. 2012) and to monitor the evolution of shear banding and strain localization (Alshibli and Sture 1999, Nübel and Weitbrecht 2002, Gudehus and Nübel 2004, Rechenmacher and Medina-Cetina 2007, Sachan and Penumadu 2007). Photograph-based (DIA, DIC, PIV, photogrammetry)

measurements have been shown to correlate well with conventional volume measurements of the soil specimen within the triaxial apparatus during testing (Macari et al. 1997, Alshibli and Sture 1999, Alshibli and Al-Hamdan 2001, Gachet et al. 2007, Rechenmacher and Medina-Cetina 2007, Sachan and Penumadu 2007, Bhandari et al. 2012, Zhang et al. 2015).

Video feeds and/or still frames of the soil specimens, within the triaxial device, were captured with external photographic equipment in all of the aforementioned photograph-based measurement studies. For volumetric measurements, the external instrumentation allowed for capture of the entire length of the specimen (axial dimension) within a single image; however, various methods were employed to capture the entire surface area (lateral dimension) of the specimen. These methods included the use of multiple cameras placed at intervals around the outside of the cell (Alshibli and Al-Hamdan 2001, Bhandari et al. 2012). In some instances (Macari et al. 1997, Gachet et al. 2007), the entire specimen surface was not captured and, therefore, it was not possible to capture all of the surface irregularities by assuming specimen symmetry. In other instances (Liang et al. 1997, Alshibli and Sture 1999, Sachan and Penumadu 2007), the entire specimen surface was not captured because only the zone of shear banding within soil specimens was investigated and volumetric measurements of the entire specimen were not obtained. Because all of these previous methods utilized external cameras, several optical challenges were encountered, as described in detail in Bhandari et al. (2012). Zhang et al. (2015) presented the first true photogrammetric local and total volume measurements of a triaxial specimen. As stated in Zhang et al. (2015), the need for photogrammetry was based on the significant limitations and unrealistic assumptions of other photograph-based measurement methods (i.e., only local volume was obtained; accurate and precise control of relative camera location and camera orientation were required). Although the Zhang et al. (2015) method

overcame the limitations of many other photograph-based methods, the Zhang et al. (2015) method still required computationally intensive ray tracing and least-squares optimization to correct for the curvature of the cell wall, for the deformation of the cell under cell pressure, and for light refraction at the confining fluid–cell wall and cell wall–atmosphere interfaces.

4.7. Internal Camera-Monitoring System

As described in Salazar and Coffman (2015), a small board camera with a pinhole aperture (BCPA) device was developed to acquire photographs from within the triaxial cell. The various challenges of utilizing internal photogrammetric instrumentation, namely, space requirements, confining fluid, focal length, cell pressure, and specimen coverage, were overcome by developing and utilizing the BCPAs. The optical, mechanical, and electrical components were considered in the design of the BCPA device and combined BCPA system. Specifically, the optical components were presented in Salazar and Coffman (2015), whereas the mechanical and electrical components are presented herein. A schematic of the components of the combined BCPA-monitoring system is presented in Figure 4.1.

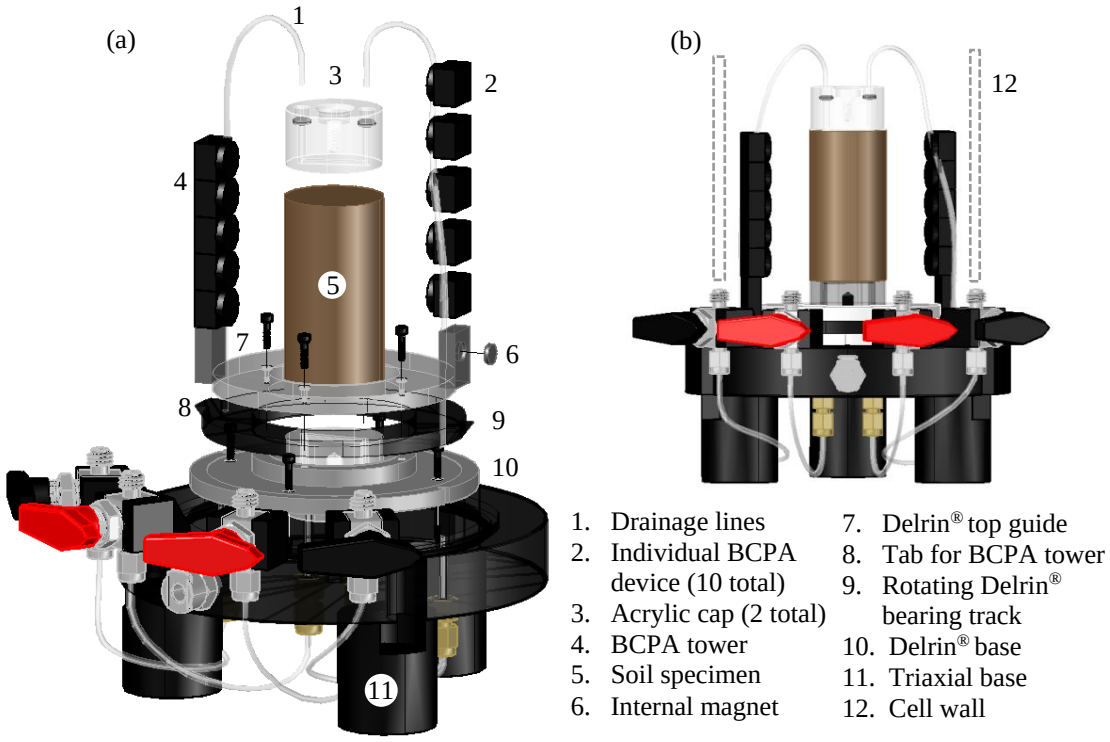

Figure 4.1. *(a)* Exploded view, and *(b)* elevation view of the internal components of the combined BCPA monitoring system.

4.7.1. *Mechanical Design*

Multiple BCPA devices were employed to enable photographic coverage of the entire surface of the specimen (during consolidation and shearing up to 15 % axial strain in triaxial compression or triaxial extension). Given the vertical viewing angle of each of the individual BCPAs (approximately 73º), the BCPA devices were stacked to allow for overlapping fields of view along the length of the specimen in the axial direction. To minimize the required number of BCPAs, a rotating platform was designed and fabricated to allow for several overlapping images at each point around the specimen in the radial direction. Because of the presence of two diametrically opposed vertical drain lines within the triaxial cell, which enable drainage from the top of the specimen through the top platen, a full 360º revolution of a single BCPA tower was not possible. Therefore, two diametrically opposed BCPA towers

were required, and the towers were rotated between the two drain lines. Each tower rotated with 155º of rotation. Given the horizontal fields of view of the individual BCPA devices and the required image overlap for photogrammetric processing, the towers were rotated around the specimen and the towers were stopped at a desired degree interval to acquire images.

To facilitate smooth and precise rotation of the two BCPA towers around the soil specimen, the rotating platform utilized a stiff, low-friction, thermoplastic material [polyoxymethylene (Delrin)], and an L-shaped slot design. A 25.4 mm x 25.4 mm x 12.7 mm [1 in. x 1 in. x 0.5 in.] neodymium magnet (52 MGOe) located on the outside of the cell was circumferentially rotated around the outside of the cell wall to pull a 6.35-mm [0.25-in.] diameter neodymium magnet, which was mounted to the base of one of the BCPA towers, causing the towers to rotate circumferentially around the vertical axis.

4.7.2. *Electrical Design*

Signals were passed into and out of the triaxial cell through the top cap of the cell by utilizing a pinned throughput connector (as previously described in Salazar and Coffman 2014). Video, power, and ground wires were connected in such a way as to reduce the required number of pin connections because of the large number of BCPA devices that were employed (ten). The video and ground wires from each of the BCPA towers were connected to common outputs, and the power wires from each BCPA were connected to a power control switchboard (Figure 4.2), which allowed for only one BCPA to be powered at a given time (thereby avoiding any video output feedback through the common grounding). Power was individually supplied to each of the BCPA devices by increasing the amount of current that was supplied to each transistor on the switchboard. Specifically, power was supplied to a given

BCPA when the amount of current matched a given transistor. The user then acquired still frames from the video feed when a desired BCPA device was powered. The power to the switchboard was supplied via an AC to DC converter (6 V; maximum 1 A). The voltage regulators on the switchboard conditioned the power to the requisite level (3.7 V) for the BCPA devices. The video feed was collected using a desktop computer via a USB interface video adapter (Sabrent USB-AVCPT). The still frames were captured and stored by utilizing video software (Ulead VideoStudio). A wiring diagram of the entire data collection system is presented in Figure 4.3.

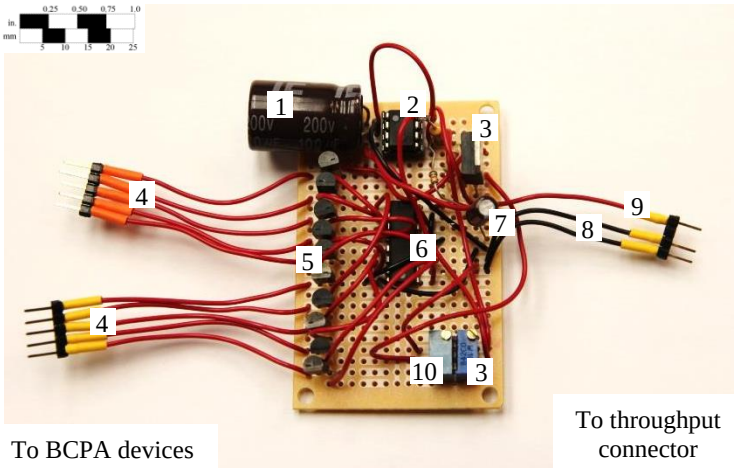

1. Capacitor (200 V, 100 µF)
2. Standard timer
3. Voltage regulator (1.2-37 V)
4. Power (BCPA devices, 3.7 V)
5. Transistors (222 A)
6. Sequencing counter (650 ns)
7. Capacitor (50 V, 10 µF)
8. Common ground
9. Power (switchboard, 6.0 V)
10. Variable resistor (timing, 10-20 sec.)

Figure 4.2. Photograph of the power switch board for the BCPA devices (power supply and timing sequence).

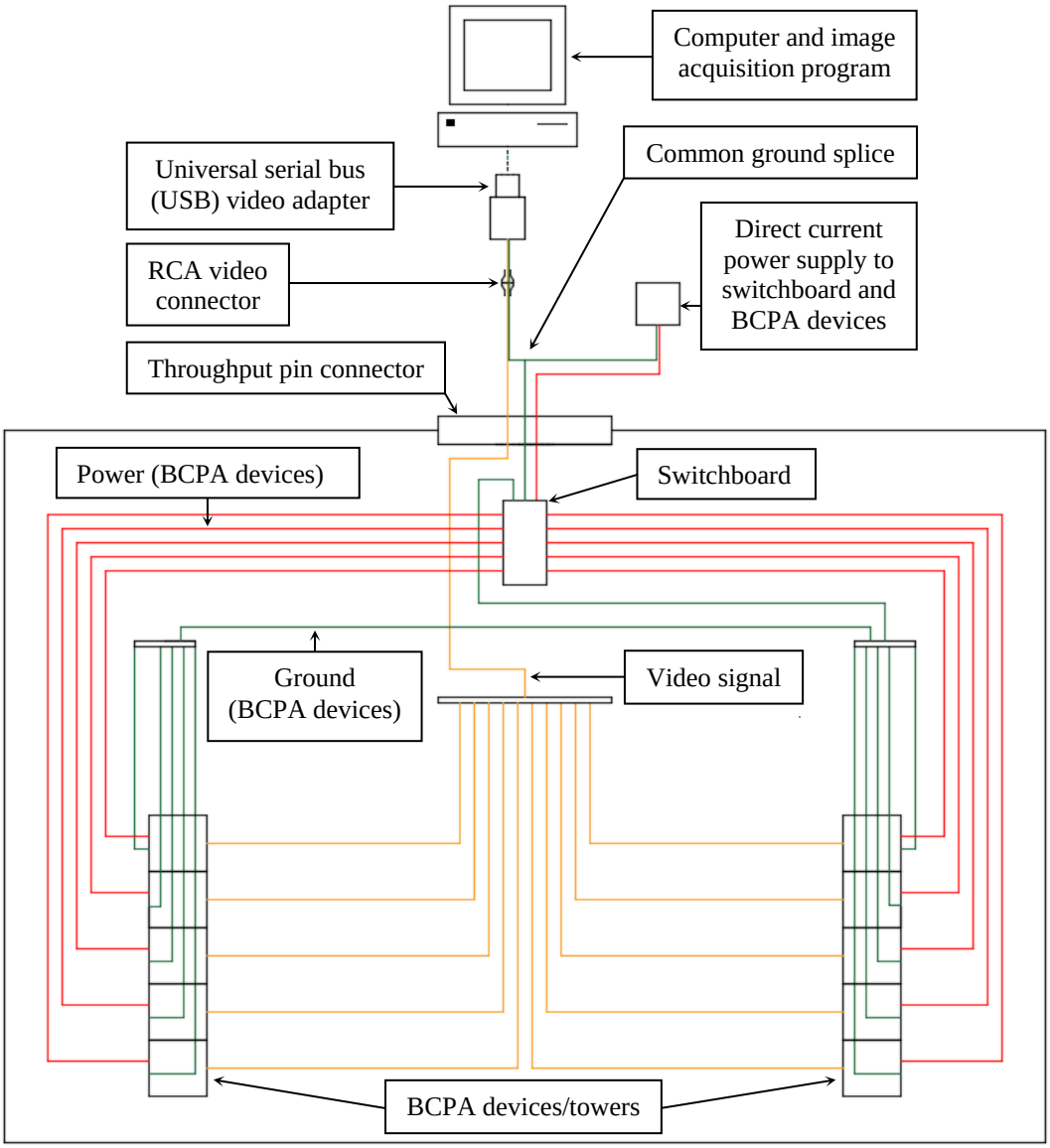

Figure 4.3. Wiring diagram of the photogrammetric instrumentation.

4.8. Photogrammetric Methods and Results

The following process (Figure 4.4) was utilized to calibrate and validate the camera monitoring system and to reconstruct a digital three-dimensional model of a brass test specimen with nominal dimensions of 3.81 cm (1.5 in.) in diameter by 7.62 cm (3.0 in.) in length. (1) Each BCPA device was calibrated by capturing a series of images of a printed PhotoModeler

calibration grid. The images of the calibration grid were subsequently analyzed using the PhotoModeler Scanner software (PhotoModeler Scanner 2015) to obtain the necessary intrinsic camera parameters (focal length, sensor format size, and principal point) of the BCPA. (2) PhotoModeler coded targets [ringed automatically detected (RAD)] were adhered to the side of the aforementioned brass specimen, and the specimen was placed on a flat surface where additional RAD targets were adhered to the surface on which the specimen rested (96 targets total). A previously calibrated digital single lens reflex (DSLR) camera (Canon 5D Mark II with fixed 28mm Nikkor lens) with known properties (aperture controlled, f/13, ISO 1250, 28mm fixed lens, and as calibrated using a PhotoModeler calibration grid) was used to capture images of all sides of the specimen. Each RAD target was captured in a minimum of four images. (3) The DSLR-acquired images were processed using the PhotoModeler software, and the center of each target was precisely surveyed to within 0.2mm (0.0079 in.). (4) The same brass specimen, with the same adhered targets, was then placed within the triaxial cell, and the target-covered surface was captured using the BCPA devices that were mounted on the two towers. Five-degree intervals were utilized to acquire a total of 320 images. As shown in Figure 4.5, adjacent images were overlapped in both the axial and radial directions. (5) The common control points within the DSLR and the BCPA images (see a_{12}, b_{21}, c_{32} in Figure 4.5) were used to photogrammetrically derive the location and orientation of each of the individual BCPA devices, at a given rotation interval, within the cell.

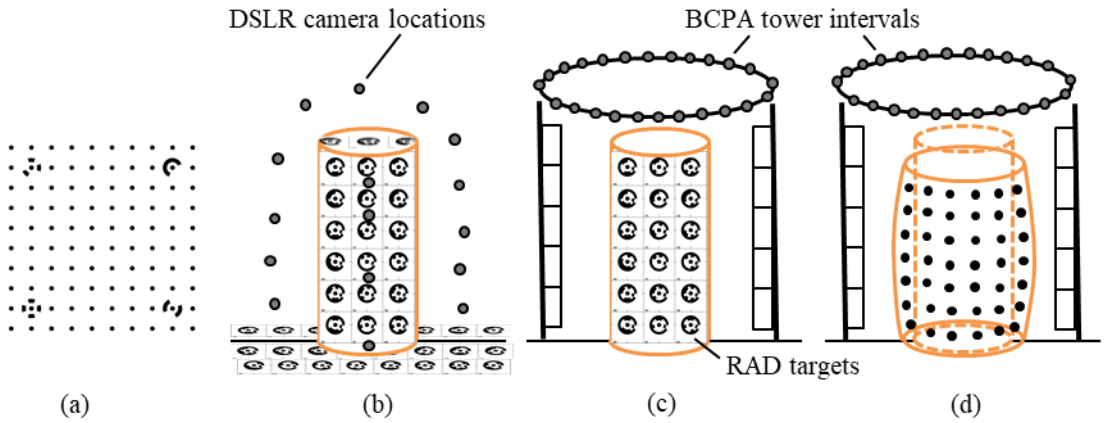

Figure 4.4. *(a)* PhotoModeler camera calibration grid, *(b)* DSLR-acquired survey images (control point identification), *(c)* BCPA-acquired calibration images (camera location and orientation identification), and *(d)* BCPA-acquired images (point cloud identification).

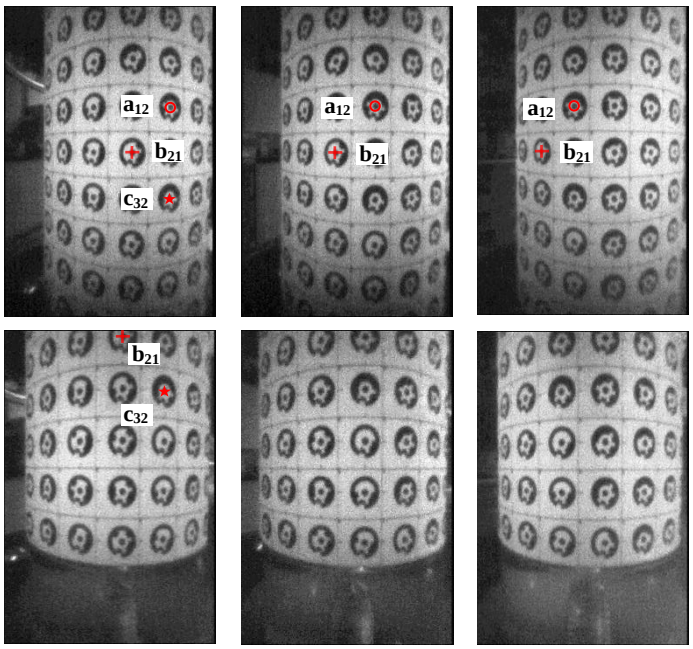

Figure 4.5. Vertically and horizontally overlapping photographs captured with two adjacent BCPA on a single tower at 15 degree rotation intervals.

To determine the practical range of rotation intervals (number of stations during rotation), specific sets of the captured images were removed from the total 320 images (as captured from the 5º rotation interval). Specifically, the locations and orientations of BCPA devices were derived by using different intervals (45º, 30º, 15º, and 5º rotation intervals). Three-dimensional recreations from the PhotoModeler software, of the calibration specimen surface (control points) and BCPA device locations and orientations within the triaxial cell, are shown in Figure 4.6. Photographic measurements obtained from the software, based on the DSLR survey, were utilized to calculate a volume for the brass test specimen. A volume of 91.58 cm^3 was obtained, which corresponded to an estimated difference of 0.34 % when compared to the volume calculations that were obtained from manual measurements (caliper and pi tape). Given repeatable positioning of the BCPA towers at a desired rotation interval, the derived location and orientation values for the individual BCPA devices were able to be used, in conjunction with PhotoModeler software, to measure points on the surface at any axial strain level, for any soil specimen that was tested within the triaxial cell. The measured points resulted in a point cloud that was then used to identify the surfaces of the given specimen. The point cloud was then exported from PhotoModeler Scanner and imported into Geomagic Design 3D software (Geomagic Design X 2015) to obtain accurate threedimensional reconstructions of any specimen.

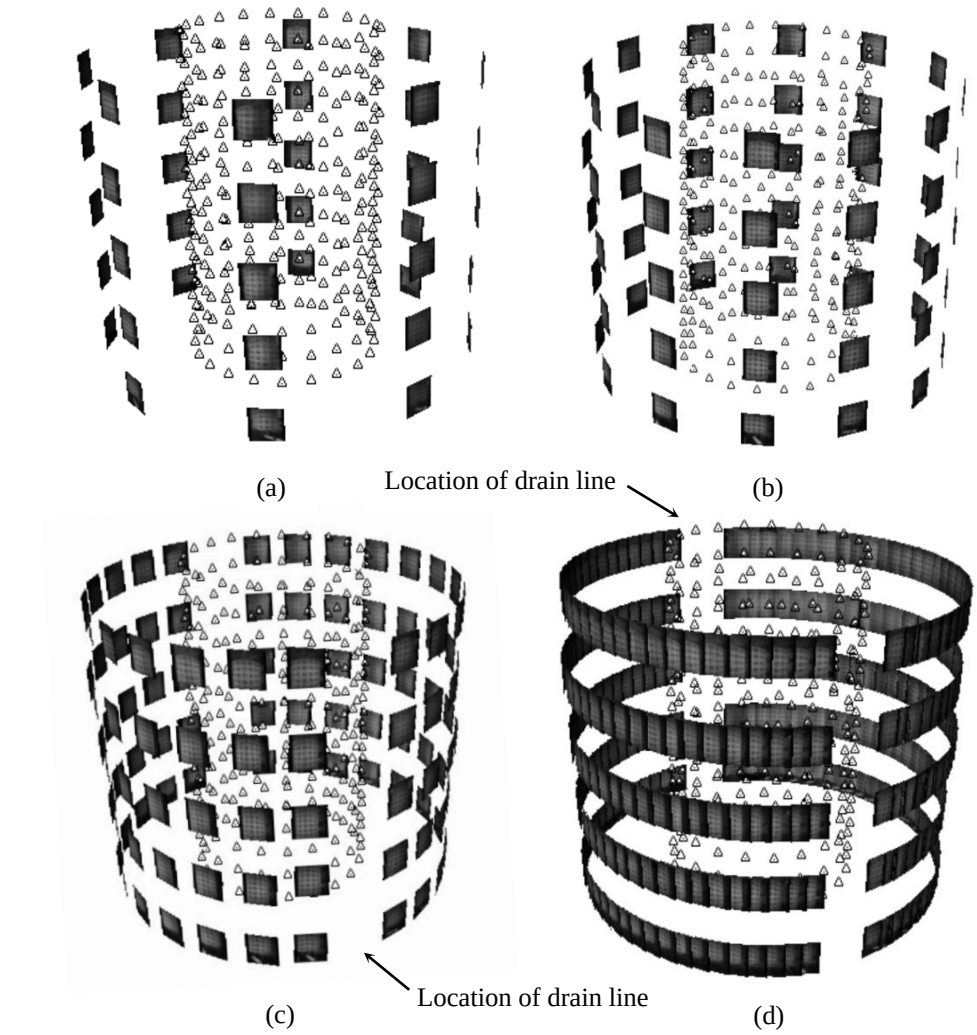

Figure 4.6. Photogrammetric reconstruction of BCPA device locations within the triaxial cell for *(a)* 45 degree, *(b)* 30 degree, *(c)* 15 degree, and *(d)* 5 degree rotation intervals.

4.9. Conclusions

Internal photogrammetric instrumentation was designed and implemented for triaxial testing applications. The mechanical and electrical components of the BCPA instrumentation were presented and the utilized photogrammetric techniques were discussed. The calibration and validation processes for the system were also described. Based on preliminary findings, use of an internal camera monitoring system is promising for future triaxial testing applications.

4.10. References

Alshibli, K. A. and Al-Hamdan, M. Z., 2001, "Estimating Volume Change of Triaxial Soil Specimens From Planar Images," *Comput.-Aided Civil Inf. Eng.*, Vol. 16, No. 6, pp. 415–421.

Alshibli, K. A. and Sture, S., 1999, "Sand Shear Band Thickness Measurements by Digital Imaging Techniques," *J. Comput. Civ. Eng.*, Vol. 13, No. 2, pp. 103–109.

Bésuelle, P. and Desrues, J., 2001, "An Internal Instrumentation for Axial and Radial Strain Measurements in Triaxial Tests," *Geotech. Test. J.*, Vol. 24, No. 2, pp. 193–199.

Bhandari, A. R., Powrie,W., and Harkness, R. M., 2012, "A Digital Image-Based Deformation Measurement System for Triaxial Tests," *Geotech. Test. J.*, Vol. 35, No. 2, pp. 209–226.

Bishop, A. W. and Donald, I. B., 1961, "The Experimental Study of Partly Saturated Soil in Triaxial Apparatus," *Proceedings of the Fifth International Conference on Soil Mechanics and Foundation Engineering*, Vols. 1/3, Paris, July 17–22, Institution of Civil Engineers, London, pp. 13–21.

Clayton, C. R. I., Khatrush, S. A., Bica, A. V. D., and Siddique, A., 1989, "The Use of Hall Effect Semiconductors in Geotechnical Instrumentation," *Geotech. Test. J.*, Vol. 12, No. 1, pp. 69–76.

Cuccovillo, T. and Coop, M. R., 1997, "The Measurement of Local Axial Strains in Triaxial Tests Using LVDTs," *Géotechnique*, Vol. 47, No. 1, pp. 167–171.

Gachet, P., Geiser, F., Laloui, L., and Vulliet, L., 2007, "Automated Digital Image Processing for Volume Change Measurement in Triaxial Cells," *Geotech. Test. J.*, Vol. 30, No. 2, pp. 98–103.

Geomagic Design X; Version 17 2015. "3D Computer-Aided Design (CAD) software," 3D Systems, Rock Hill, SC.

Gudehus, G. and Nübel, K., 2004, "Evolution of Shear Bands in Sand," *Géotechnique*, Vol. 54, No. 3, pp. 187–201.

Khan, M. H. and Hoag, D. L., 1979, "A Noncontacting Transducer for Measurement of Lateral Strains," *Can. Geotech. J.*, Vol. 16, No. 2, pp. 409–411.

Leong, E. C., Agus, S. S., and Rahardjo, H., 2004, "Volume Change Measurement of Soil Specimen in Triaxial Test," *Geotech. Test. J.*, Vol. 27, No. 1, pp. 47–56.

Liang, L., Saada, A., Figueroa, J. L., and Cope, C. T., 1997, "The Use of Digital Image Processing in Monitoring Shear Band Development," *Geotech. Test. J.*, Vol. 20, No. 3, pp. 324–339.

Macari, E. J., Parker, J. K., and Costes, N. C., 1997, "Measurement of Volume Changes in Triaxial Tests Using Digital Imaging Techniques," *Geotech. Test. J.*, Vol. 20, No. 1, pp. 103–109.

Ng, C. W. W. and Chiu, C. F., 2001, "Behaviour of a Loosely Compacted Unsaturated Volcanic Soil," *J. Geotech. Geoenviron. Eng.*, Vol. 127, No. 12, pp. 1027–1036.

Ng, C. W. W., Zhan, L. T., and Cui, Y. J., 2002, "A New Simple System for Measuring Volume Changes in Unsaturated Soils," *Can. Geotech. J.*, Vol. 39, No. 3, pp. 757–764.

Nübel, K. and Weitbrecht, V., 2002, "Visualization of Localization in Grain Skeletons With Particle Image Velocimetry," *J. Testing Eval.*, Vol. 30, No. 4, pp. 322–329.

Önal, O., Ören, A. H., Özden, G., and Kaya, A., 2008, "Determination of Cylindrical Soil Specimen Dimensions by Imaging With Applications to Volume Change of Bentonite–Sand Mixtures," *Geotech. Test. J.*, Vol. 31, No. 2, pp. 124–131.

Ören, A. H., Önal, O., Özden, G., and Kaya, A., 2006, "Nondestructive Evaluation of Volumetric Shrinkage of Compacted Mixtures Using Digital Image Analysis," *Eng. Geol.*, Vol. 85, No. 3, pp. 239–250.

PhotoModeler Scanner; Version 2015.0.0, 2015, "3D Measurements and Models Software," Eos Systems, New York.

Puppala, A. J., Katha, B., and Hoyos, L. R., 2004, "Volumetric Shrinkage Strain Measurements in Expansive Soils Using Digital Imaging Technology," *Geotech. Test. J.*, Vol. 27, No. 6, pp. 547–556.

Rechenmacher, A. L. and Finno, R. J., 2004, "Digital Image Correlation to Evaluate Shear Banding in Dilative Sands," *Geotech. Test. J.*, Vol. 27, No. 1, pp. 13–22.

Rechenmacher, A. L. and Medina-Cetina, Z., 2007, "Calibration of Soil Constitutive Models With Spatially Varying Parameters," *J. Geotech. Geoenviron. Eng.*, Vol. 133, No. 12, pp. 1567–1576.

Sachan, A. and Penumadu, D., 2007, "Strain Localization in Solid Cylindrical Clay Specimens Using Digital Image Analysis (DIA) Technique," *Soils Found.*, Vol. 47, No. 1, pp. 67–78.

Salazar, S. E. and Coffman, R. A., 2014, "Design and Fabrication of End Platens for Acquisition of Small-Strain Piezoelectric Measurements during Large-Strain Triaxial Extension and Triaxial Compression Testing," *Geotech. Test. J.*, Vol. 37, No. 6, pp. 948–958. doi:10.1520/GTJ20140057.

Salazar, S. E. and Coffman, R. A., 2015, “Consideration of Internal Board Camera Optics for Triaxial Testing Applications,” *Geotech. Test. J.*, Vol. 38, No. 1, pp. 40–49. doi:10.1520/GTJ20140163.

Scholey, G. K., Frost, J. D., Lo Presti, C. F., and Jamiolkowski, M., 1995, “A Review of Instrumentation for Measuring Small Strains During Triaxial Testing of Soil Specimens,” *Geotech. Test. J.*, Vol. 18, No. 2, pp. 137–156.

Zhang, X., Li, L., Chen, G., and Lytton, R., 2015, “A Photogrammetry-Based Method to Measure Total and Local Volume Changes of Unsaturated Soils During Triaxial Testing,” *Acta Geotech.*, Vol. 10, No. 1, pp. 55–82.

CHAPTER 5: DISCUSSION OF "A PHOTOGRAMMETRY-BASED METHOD TO MEASURE TOTAL AND LOCAL VOLUME CHANGES OF UNSATURATED SOILS DURING TRIAXIAL TESTING" BY ZHANG ET AL., 2015

5.1. Chapter Overview

The Zhang et al. (2015) publication was discussed in this chapter. The Zhang et al. (2015) manuscript contained a description of a photogrammetric method for determining total and local volume changes of soil specimens during triaxial testing. Like the other camera-based triaxial monitoring techniques found in the literature, Zhang et al. (2015) used cameras external to the testing cell and therefore had to account for refraction effects and limited visibility of test specimens through the cell wall. Despite this difference, the manuscript caught the attention of the author, because of the similarities in the photogrammetric processing of results. This manuscript echoes the Zhang et al. (2015) discussion of the limitations of non-photogrammetric methods for determining triaxial specimen volume, describes the limitations of the Zhang et al. (2015) work, and offers comparison with the methodology presented in Salazar and Coffman (2015) and Salazar et al. (2015).

The full citation for this manuscript (Salazar and Coffman 2015) is included in Section 5.2. The discussion is presented in Section 5.3, which includes discourse on the apparent improper triaxial testing techniques of the Zhang et al. (2015) publication (Section 5.3.1), a discussion of the cell wall deformation corrections and least-square optimization (Section 5.3.2), and photogrammetric methods (Section 5.3.3).

5.2. Discussion of "A Photogrammetry-based Method to Measure Total and Local Volume Changes of Unsaturated Soils During Triaxial Testing" by Zhang et al., 2015

Reference

Salazar, S. E. and Coffman, R. A., "Discussion of 'A Photogrammetry-based Method to Measure Total and Local Volume Changes of Unsaturated Soils During Triaxial Testing' by Zhang et al." Acta Geotechnica, Vol. 10, No. 5, pp. 693-696. doi:10.1007/s11440-015-0380-1.

5.3. Discussion

Zhang et al. (2015), in the paper entitled ‘‘a photogrammetry-based method to measure total and local volume changes of unsaturated soils during triaxial testing,’’ presented a method for measuring the volume and strain of saturated and unsaturated soil specimens during triaxial tests. Specifically, the presented method utilized a single, external digital camera, to capture images of a triaxial testing apparatus and of the corresponding soil specimen within the cell. Photogrammetric analyses were performed using commercially available photogrammetry software. Utilizing the Zhang et al. (2015) modeling technique, ringed automatically detected (RAD) coded targets were utilized to locate common points within each of the captured images, and then, photogrammetry techniques were employed to assign physical, three-dimensional, coordinates to each of the points.

A comprehensive and categorized review of triaxial volume measurement methods that were found in the literature was presented in the Zhang et al. (2015) article. The methods that have been previously utilized to measure the volume of saturated and unsaturated soil specimens, during triaxial testing, were presented in a clear and concise manner by citing advantages and disadvantages, accuracy, and costs associated with each method (Table 1 within Zhang et al. (2015)). Furthermore, the current state of the art of photograph-based measurements was explained. As stated in Zhang et al. (2015), the validity of other photograph-based volume measurements [digital image analysis (DIA), digital image correlation (DIC), and particle image velocimetry (PIV)] suffer from unrealistic, fundamental assumptions and limitations. Specifically, the DIA methods require accurate and precise control of the relative camera location and of the camera orientation relative to the triaxial cell soil specimen. The DIC and PIV methods typically cannot provide total volume measurements; however, Bhandari et al.

(2012) utilized the DIC method and overcame some of the difficulties associated with DIC methods to provide viable results. However, the need for true photogrammetry to accurately measure local and global volumes of saturated and unsaturated soil specimens was presented by Zhang et al. (2015). Moreover, each of the steps of the photogrammetric process was thoroughly explained. The methods presented in Zhang et al. (2015) are a valuable contribution to the literature because the methods may be used to: measure total volume, measure local volume changes (Figure 19 within Zhang et al. (2015)), and illustrate strain localization and shear banding within soil specimens during triaxial testing. However, Zhang et al. (2015) do not expound upon the limitations of the presented method. These limitations include the use of: (1) improper triaxial testing procedures and (2) photogrammetric cell wall deformation measurements combined with least-square optimization to obtain corrected ray path measurements.

5.3.1. *Improper Triaxial Testing Techniques*

An internal load cell should be utilized in triaxial testing to prevent the need for piston uplift and piston friction corrections. Silicone oil, instead of water, is commonly used within the cell, as the cell fluid, when an internal load cell is utilized. The index of refraction for silicone oil differs from the index of refraction for water, which may affect the observed results in a similar manner to that shown for difference in the indices of refraction for air and water that is presented in Figure 1 of the Zhang et al. (2015) article. Furthermore, because of the use of an external camera, the cleanliness of the acrylic cell wall (which can be compromised within a soil mechanics laboratory) may also affect the results.

Although Zhang et al. (2015) utilized an impressive back pressure saturation technique in which the sand was infused with CO2 and then subjected to 400 kPa of back pressure to obtain a

B value of 0.98, the back pressure saturation technique was for naught because the cell pressure was reduced from 435 to 100 kPa and the back pressure was reduced from 100 to 0 kPa prior to shearing. The reduction in cell pressure and back pressure most likely resulted in effervescence of the pore fluid and therefore desaturation of the sand specimen to an unknown state of suction within the soil specimen. Thereby, even though higher cell pressures (600 kPa) were utilized to determine the accuracy of the method, these pressures were not utilized for the triaxial testing of the soil specimens. This brings into question whether the Zhang et al. (2015) method will work if the cell is pressurized under high cell pressures that are commonly required to back pressure saturate and overconsolidate clay specimens (1035 kPa).

5.3.2. *Utilization of Cell Wall Deformation Combined with Least-Square Optimization*

The Zhang et al. (2015) method utilized images that were captured from outside of the cell. Therefore, ray tracing was required to correct for the refraction effects of the light (1) at the confining fluid–cell wall interface and (2) at the cell wall–air interface. Additionally, the method considered deflection of the cell wall during pressurized tests by including RAD-coded targets that were adhered to the outer surface of the cell wall and to the load frame (considered fixed control points for reference purposes). It was assumed that the cell wall deformed in a uniform, radial pattern. Furthermore, deformation of the cell wall was not considered above 600 kPa, even though typical triaxial tests may reach confining fluid pressures above 1000 kPa. It is suggested that the correction for cell wall flexure be characterized for a full range of pressures that are commonly achieved during a typical triaxial test (up to 1035 kPa for acrylic cell walls). Furthermore, it may be a useful contribution to show a sensitivity study of the photogrammetric method as applied to multiple optical media.

In Section 2.1.1, Zhang et al. (2015) identified the problems associated with the utilization of the measurement of the cell fluid for determining the volume change of a triaxial specimen. However, Zhang et al. (2015) utilized a similar method, albeit in the form of a photogrammetric correction instead of a calibration procedure, to account for the change in the ray path that is associated with the cell wall deformation during pressurization/depressurization of the cell wall deformation under a constant applied pressure (creep). Moreover, the camera that was utilized was a lensed camera. Before analysis of captured images, photogrammetric software was used by Zhang et al. (2015) to correct for lens distortions (thereby modeling the lensed camera as a pinhole camera).

Recently, as presented in Salazar and Coffman (2015a, 2015b), a triaxial insert board camera pinhole aperture (BCPA) camera system was developed by researchers at the University of Arkansas. Although utilization of eight cameras was presented in the Salazar and Coffman (2015a) article, the system was further modified to consist of ten small cameras (five cameras per tower, with the two towers being diametrically opposed), as presented in Salazar and Coffman (2015b). Two towers were required because the drainage lines for the top platen prevented a full 360º rotation of only one tower. Therefore, using the BPCA tower system, ten photographs were acquired at a given position, while each of the towers completed a 155º rotation around the specimen. The BCPA system was fully submerged in the silicone confining fluid, and the BCPA was capable of being saturated and pressurized under pressures of up to 1035 kPa. Therefore, the BCPA system enabled testing conditions that were similar to those that are commonly used instead of requiring that the cell pressure and back pressure be reduced prior to shearing. The use of the BPCA camera system: (1) reduces the complicated geometry of the camera location and orientation by utilizing photogrammetry to derive the exact camera location and orientation, (2)

does not require determination of the best fit of the shape and location of the acrylic cell, (3) does not require ray tracing or Snell's law because the photographs are acquired from within the cell fluid, and (4) provides an alternative to externally acquired photogrammetric methods.

5.3.3. *Testing Procedures and Photogrammetric Methods*

Zhang et al. (2015) performed isotropic compression tests for a stainless steel specimen to measure the accuracy for the photogrammetry method. Tests were performed on a 5.08 cm diameter by 10.16 cm tall stainless steel specimen that was tested within a 10.16 cm diameter by 20.32 cm tall acrylic cell with a 0.61 cm thick cell wall that had a refractive index of 1.491. Approximately 50 photographs were acquired for each testing condition (0 kPa in air without cell wall; 0, 200, 400, 600 kPa in water), by taking at least five photographs from different orientations for each area/point of interest to ensure ‘‘sufficient overlap between adjacent pictures.’’ Targets numbering 16, 218, and 336 were utilized to identify the load frame, acrylic cell, and stainless steel specimen, respectively.

Drained triaxial tests were also performed on a saturated sand specimen to determine the total and local volume measurements of the specimen during the triaxial tests. Unlike the triaxial cell that was utilized for the isotropic compression tests on the stainless steel cylinder, a larger triaxial cell with larger specimens and fewer targets was used for the triaxial tests conducted on the saturated sand specimens. Specifically, a 7.1 cm by 13.7 cm specimen was tested within a 16.51 cm diameter by 30.48 cm tall triaxial cell that had a cell wall thickness of 0.97 cm and a refractive index of 1.491. Also, 174 and 176 targets were utilized to identify the acrylic cell and sand specimen, respectively, within the 25 photographs that were acquired for each testing condition (at every 2–3 mm of vertical displacement…until a total displacement of 15 mm is reached). The reason for using 336 targets adhered to the specimen was never explained, nor

justified. Furthermore, it was not clear how point capture redundancy eliminates any assumptions regarding the specimen deformations. This statement requires further explanation. A parametric study of the accuracy achieved, for different numbers of points utilized, would be a useful contribution to the literature and would help other researchers make decisions on the level of refinement required to achieve a desired level of accuracy. Also, a parametric study would aid in determining the minimum number of targets required to measure the total and local volumes of specimens. Although the results presented by Zhang et al. (2015) would indicate that the method is capable of achieving high accuracy (<0.25 % error), the method is computationally intensive, due to the effects of refraction and cell wall deformation.

At the University of Arkansas, researchers performed tests on a brass specimen with nominal dimensions of 3.8 cm in diameter and 7.6 cm in height that contained 273 targets; thereby, the University of Arkansas specimen was smaller than the specimen used by Zhang et al. (2015) and contained more targets on the surface of the soil specimen. Each of the drainage lines prevented direct viewing of 25º of the specimen; however, the photos collected near the drainage lines allowed for points within these locations to be viewed in at least six photos, instead of the customary ten photos that were used for the other points. In addition to the tests on a brass specimen, at various times during triaxial tests on soil specimens [prior to confinement, during back pressure saturation, prior to consolidation, during consolidation, after consolidation, and during shearing (1, 3, 6, 9, 12, and 15 % axial strain)], photographs were obtained by rotating the towers at a desired increment ranging from a minimum of 45º increments to a maximum of 5º increments. Specifically, ranging from a minimum of 40 pictures per observation (10 pictures per increment, and 4 increments) to a maximum of 320 pictures per observation (10 pictures per increment, and 32 increments), respectively.

The same procedures that were utilized by Zhang et al. (2015) for the image analysis in air are common accuracy prediction methods, and these procedures were also utilized by Salazar and Coffman (2015b). However, the Salazar and Coffman (2015b) method offered a viable alternative to the Zhang et al. (2015) method, by placing photogrammetric equipment within the triaxial cell instead of outside of the triaxial cell. The lensless camera equipment that was devised by Salazar and Coffman (2015a) allowed for direct, unobstructed observation of a specimen during testing. Therefore, computationally intensive corrections to account for the effects of refraction through multiple types of media and deformation of the cell wall were eliminated. In a similar fashion to the Zhang et al. (2015) method, the Salazar and Coffman (2015b) method utilized the same principles of photogrammetry (using PhotoModeler Scanner software (Eos Systems, Inc. (2015)) and RAD-coded targets to create a point cloud of the specimen surface. In the Salazar and Coffman (2015b) method, the point cloud was then meshed to obtain an accurate, three-dimensional reconstruction of the specimen, whereupon the mesh was imported into Geomagic Design software (3D Systems, Inc., 2015) to calculate the volume of the specimen. The volumetric strain was then obtained by subtracting the volume of the specimen at various times from the initial volume and then dividing by the initial volume. Whereas Zhang et al. (2015) utilized a proprietary program (PhotoSoilVolume) to handle the cumbersome optical correction process through to volume calculation, the Salazar and Coffman (2015b) method required only commercially available software to calculate total specimen volumes. As described in Salazar and Coffman (2015a), the optical components of internal photogrammetric instrumentation were designed, fabricated, and tested for triaxial testing applications to overcome the aforementioned drawbacks of external methods. The cameras were

also designed to overcome the challenges of internal instrumentation (space, confining fluid, focal length, cell pressure, and specimen coverage).

In summary, the contribution produced by Zhang et al. (2015) is significant and provides an advancement of the state of knowledge of external photograph-based measurements of triaxial specimens. However, the use of internal cameras like those presented in Salazar and Coffman (2015a, 2015b), instead of an external camera, is suggested to further advance the photogrammetric technique. Specifically, the use of internal cameras will facilitate a reduction in computational demands by (1) eliminating the need for a cell deformation/position correction and by (2) eliminating the need for ray tracing and least-square optimization. Although the Salazar and Coffman (2015b) method is less computationally costly than the method presented by Zhang et al. (2015), the cost and reproducibility of required photogrammetric equipment are approximately equivalent. Therefore, it appears that the Salazar and Coffman (2015a) method is a viable alternative method for acquiring total and local volume changes of soil specimens during triaxial testing.

5.4. References

3D Systems, Inc., 2015, Geomagic Design X (Version 17). 3D Computer-Aided Design (CAD) Software. http://www.geomagic.com/en/products/design/overview

Bhandari, A. R., Powrie, W., and Harkness, R. M., 2012, "A Digital Image-Based Deformation Measurement System for Triaxial Tests," *Geotech. Test. J.*, Vol. 35, No. 2, pp. 1-18.

Eos Systems, Inc., 2015, PhotoModeler Scanner (Version 2015.0.0). 3D Measurements and Models Software. http://www.photomodeler.com/products/scanner/default.html

Salazar, S. E., Barnes, A., and Coffman, R. A., 2015b, "Development of an Internal Camera Based Volume Determination System for Triaxial Testing," *Geotech. Test. J.*, Vol. 38, No. 4, pp. 549-555. doi:10.1520/GTJ20140249.

Salazar, S. E. and Coffman, R. A., 2015a, "Consideration of Internal Board Camera Optics for Triaxial Testing Applications," *Geotech. Test. J.*, Vol. 38, No. 1, pp. 40-49. doi:10.1520/GTJ20140163.

Zhang, X., Li, L., Chen, G., and Lytton, R., 2015, "A Photogrammetry-Based Method to Measure Total and Local Volume Changes of Unsaturated Soils During Triaxial Testing," *Acta Geotech.*, Vol. 10, No. 1, pp. 55-82. doi:10.1007/s11440-014-0346-8.

CHAPTER 6: CLOSURE TO "DISCUSSION OF 'DEVELOPMENT OF AN INTERNAL CAMERA-BASED VOLUME DETERMINATION SYSTEM FOR TRIAXIAL TESTING' BY S. E. SALAZAR, A. BARNES, AND R. A. COFFMAN" BY MEHDIZADEH ET AL., 2016

6.1. Chapter Overview

A closure to the Mehdizadeh et al. (2016) discussion paper is provided in this chapter. The closure addresses queries that were raised by the discussion paper and clarifies the apparent ambiguities of the previously described Salazar et al. (2015) technique. The manuscript also provides additional testing data that shed light on the effect of pausing a triaxial test for short periods of time (at desired axial strain intervals) to capture photographs of the surface of the specimen. The full citation for this manuscript (Salazar et al. 2017) is included in Section 6.2 and the body of the closure is presented in Sections 6.3 and 6.4.

6.2. Closure to "Discussion of 'Development of an Internal Camera-Based Volume Determination System for Triaxial Testing' by S.E. Salazar, A. Barnes, and R.A. Coffman" by Mehdizadeh et al., 2016

Reference

Salazar, S. E., Barnes, A., and Coffman, R. A., "Closure to "Discussion of 'Development of an Internal Camera-Based Volume Determination System for Triaxial Testing' by S. E. Salazar, A. Barnes, and R. A. Coffman" by A. Mehdizadeh, M. M. Disfani, R. Evans, A. Arulrajah, and D. E. L. Ong," Geotechnical Testing Journal, Vol. 40, No. 1, 2017, pp. 47-51. doi:10.1520/GTJ20160154.

6.3. Abstract

The discussion paper, written by Mehdizadeh et al., provided discourse on a technical note entitled "Development of an Internal Camera-Based Volume Determination System for Triaxial Testing," which presented a novel technique of photographically monitoring soil specimens during triaxial tests by utilizing small board cameras internal to the triaxial cell. Here, a closure to the discussion paper was provided; queries raised by the

discussers were addressed, ambiguities were clarified, and additional testing data to support the closure were provided.

Keywords: triaxial testing, photogrammetry, volume measurement, local deformation

6.4. Introduction

The authors appreciate Mehdizadeh et al. (2016), herein after referred to as the discussers, for their interest in the technical note entitled "Development of an Internal Camera-Based Volume Determination System for Triaxial Testing." The authors believe that the discussers (1) primarily wished to highlight the ambiguities contained within the technical note, while also pointing to the work of Uchaipichat et al. (2011), and (2) offered a simple solution to deal with optical distortion corrections. In this closure, the authors addressed the comments put forth by the discussers, in the order in which they appeared in the discussion paper, to clarify the ambiguities within the original technical note.

The discussers mentioned that Uchaipichat et al. (2011) monitored the volumetric strain of a soil specimen during a triaxial compression test with the aid of only two cameras (external to the confining cell). However, the authors agree with Uchaipichat et al. (2011) that the digital image analysis method that was employed by Uchaipichat et al. (2011) cannot be used to reliably determine the specimen volume in the case of nonuniform deformation. The volume cannot be accurately measured using this technique because the camera setup does not capture localized strain (such as observed in shear banding) and relies heavily on averaging around the circumference of the specimen. While the Uchaipichat et al. (2011) method may be accurate enough for some applications (such as determining the total volumetric strain or approximating the radial deformation at mid-height), the technique may not be suitable for applications where it is desired to determine absolute sample volume or

to characterize the development of local deformations (by tracking individual targets on the specimen surface). Although Uchaipichat et al. (2011) showed that the averaging technique correlated well with the burette measurements for the test presented in the manuscript, the use of only one frontal view image and one side view image cannot do justice in every case, especially in the case of non-uniform deformation.

The discussers' demonstration that the need to account for the "distortion of light, cell curvature, and camera lens" could be eliminated altogether by basing all relative measurements on a point of reference is intriguing. The authors commend Uchaipichat et al. (2011) and the discussers for avoiding cumbersome corrections for optical distortions; however, this simple calibration procedure can only be used to determine changes in total specimen volume relative to an a priori volume. It is not clear how the initial volume of the specimen would be obtained with sufficient accuracy to allow for any absolute measurements before, during, or after the test. Any initial volume measurements, however meticulous, would be for naught once the specimen was placed inside of the cell and set up for testing (i.e., piston contact with specimen, filling of the cell with confining fluid). Furthermore, it is not clear how the discussers suggest to correct for cell wall deformation during tests when the confining pressure in the cell changes throughout the stages of testing (during back pressure saturation, consolidation, and shearing). As listed in Table 1 in Salazar and Coffman (2014), there are four stress paths where the cell pressure changes during the shearing stage. Moreover, Zhang et al. (2015a) and Salazar and Coffman (2015b) documented that the amount of cell wall deformation might be a significant factor when tracing rays through the media surrounding the specimen (confining fluid, cell wall, air).

The discussers noted correctly that due to the limited field of view for each of the board camera devices that were presented in Salazar et al. (2015), the size of the observed specimens was limited to nominal dimensions of 38.1-mm in diameter and 76.2-mm in height. The triaxial stress path testing performed at the University of Arkansas is primarily for stress-strain behavior to derive parameters required for constitutive modeling. The specimens that are typically tested are primarily soft soils that have been (1) trimmed from a Shelby tube sample, or (2) reconstituted in one of the 38.1-mm diameter, static weight slurry consolidometers (in a similar fashion to Zhao and Coffman (2016) and Zhao et al. (2016)) prior to K_0 reconsolidation within the triaxial cell. Furthermore, this smaller specimen size is favored because it allows for reduced consolidation time over larger specimen sizes. It should alleviate the discussers' concern to know that the internal photogrammetry system could easily be adapted to larger cells and testing of larger specimens. In fact, a larger cell would allow for more space between the specimen and camera tower, increasing the vertical and horizontal area viewed by each camera. This could also serve to reduce the number of internal board cameras required, thereby reducing the number of images captured and the amount of photogrammetric processing required.

The system presented in Salazar and Coffman (2015a, 2015b) and Salazar et al. (2015) is neither overly complicated nor costly (especially as compared to a DSLR camera and lens). However, it does require knowledge of photogrammetry for implementation. The term "photogrammetry" was misused throughout the discussion by Mehdizadeh et al. (2016); the term "photogrammetry" was interchanged with other photographic methods (including digital image analysis and digital image correlation). Salazar and Coffman (2015a, 2015b), Salazar et al. (2015), as well as Zhang et al. (2015a, 2015b), have proposed

that the application of photogrammetry (or more accurately, stereophotogrammetry) is more robust than other digital imaging techniques for determining the total- and local- radial, axial, and volumetric strains. Specifically, photogrammetry overcomes the weaknesses of other photographic methods while becoming increasingly easier to apply with the increasing availability of various commercial and open-source photogrammetry processing software packages. In addition, other photogrammetric methods, including open-source structure from motion (SfM) and multi-view stereo (MVS) applications, using more recently developed computer vision techniques, merit further investigation. Unlike the stereophotogrammetry technique that was discussed in Salazar et al. (2015,2016), no prior camera calibrations would be required using the MVS technique. Therefore, overall processing times (even for the relatively large number of images captured with the internal camera based system) would be dramatically reduced, and the reconstructed 3D model would contain more surface detail (Furukawa and Hernández 2013).

The discussers also mentioned that the use of silicone oil for the confining fluid, in place of water, would necessitate the use of specialized flow pumps that are not commonly available. In fact, the adaptation of silicone oil as confining fluid has become commonplace in research laboratories that utilize internal load cells, and there are several triaxial apparatus manufacturers that sell flow pumps for this very purpose. As an aside, the internal load cells are necessary in advanced triaxial stress path testing programs to account for the effects of piston uplift and piston friction (Race and Coffman 2011, Salazar and Coffman 2015b). The authors agree with the discussers that the choice of confining fluid has no particular impact on external photography of the triaxial specimen (as long as the fluid is not opaque and the index of refraction is taken into account). It was previously highlighted that the adaptation

of open-body internal camera equipment was made possible by the already in-place practice of using inert silicone oil as a confining fluid. The oil allows the camera devices and associated electronics to be fully saturated and fully submerged in the confining fluid without becoming damaged. Furthermore, the open-body style of the board cameras has been proven to eliminate any pressure differentials by allowing the fluid to fill the lensless cameras, including behind the pinhole aperture (as explained in Salazar and Coffman 2015a). This open body is a key design element of the camera devices, as it would be impractical (and perhaps even impossible) to design compact, waterproof camera housings capable of withstanding the pressures that are present within the confining cell during a typical triaxial test. Furthermore, due to the lack of difference in indices of refraction between the lens and the fluid, the authors' discussion of confining fluid, as related to refraction, was only provided to highlight the fact that the use of a lens submerged within the fluid does not function as intended. Specifically, the index of refraction of a typical lens is around 1.5 (depending on the material), which is too close to the index of refraction of water (around 1.33) or silicone oil (1.397, as tested). The refraction of light through a lens in air requires a larger difference (i.e. the index of refraction of air is approximately 1.0). Therefore, the use of a lensless design was necessary to function within the cell; the elimination of typical distortions associated with lenses was a fortuitous side-effect, resulting in less corrections during photogrammetric calibration and processing. The use of a lensless camera design is not without problems, due to the necessity of having good lighting to allow the camera sensors to collect data and to reduce vignetting at the edges of the image. However, proper lighting is still a key factor in collecting quality data when using external DSLR photography.

The authors commend the discussers for their approach to demonstrating a simple and practical method of monitoring a triaxial specimen from the exterior of the cell, by following the Uchaipichat et al. (2011) method. Particularly, the authors appreciate the discussers' use of stainless steel calibration specimens with known dimensions for reference, as this practice is currently missing from the available body of literature for photographic observation of triaxial specimens. In a similar fashion, the authors have performed multiple comparison tests using brass and acrylic specimens with known dimensions to validate the internal photogrammetry technique. The results of these tests were documented in Salazar et al. (2016). Furthermore, the authors have continued on to demonstrate the capabilities of the internal photogrammetry approach by monitoring soil specimens during triaxial compression and extension tests (Salazar et al. 2016). Because no universal comparison exists to assess the error for new volume measurement techniques (and often there is no comparison to an external reference at all), the authors have attempted to evaluate the difference in measured volume from a reference measurement. In Table 1 of Salazar et al. (2016), a series of volume measurements for an acrylic specimen was presented. The volume of the acrylic specimen was determined using a water displacement technique (by adapting the Proctor mold volume determination method from ASTM D698-12e2), manual measurements using a pi tape and calipers, 3D scan measurements, external DSLR photogrammetry (camera located outside of cell, in air), and internal photogrammetry (cameras located in cell filled with silicone oil confining fluid). The measured volume of the acrylic specimen, determined using the internal photogrammetry approach, fell within 0.13 % difference from the reference volume. Although the reference measurement technique for this example was the water displacement technique (because it was based on an ASTM

standard), the measured volumes of the acrylic specimen fell within 0.5 % of the reference for all five volume determination techniques.

The discussers commented that the Salazar et al. (2015) technique required rotation of the camera tower platform around the specimen to capture images of the entire surface. To ensure that there were no changes to the specimen during the image-capturing process, the test was paused at the desired intervals. The authors concede that the acquisition of the necessary images may be time-consuming; however, the short pauses during a test did not cause problems in the stress path for the test (Figures 6.1 and 6.2) and excess pore water pressure returned to the prescribed behavior after each pause during the test (Figure 6.3). Furthermore, an advantage of the technique is that the camera towers may be rotated to occupy any desired rotation interval around the specimen. Therefore, the acquisition time and subsequent processing time may be significantly reduced with a reduced number of images (i.e., greater angles between the camera intervals).

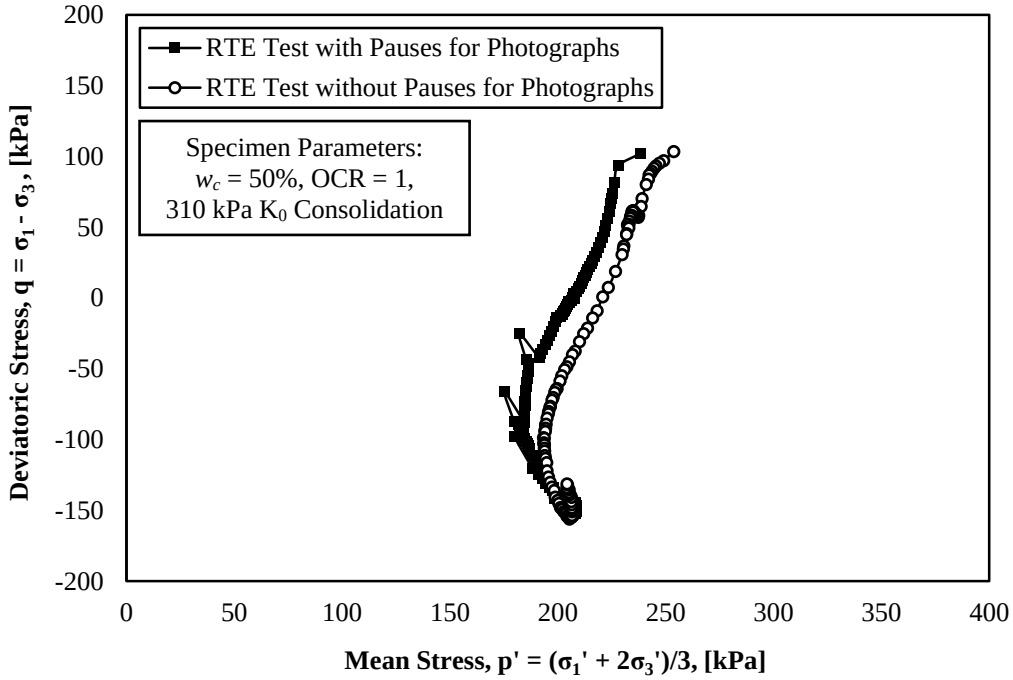

Figure 6.1. Comparison of deviatoric stress as a function of mean stress for a reduced triaxial extension test with pauses and without pauses for capturing photographs.

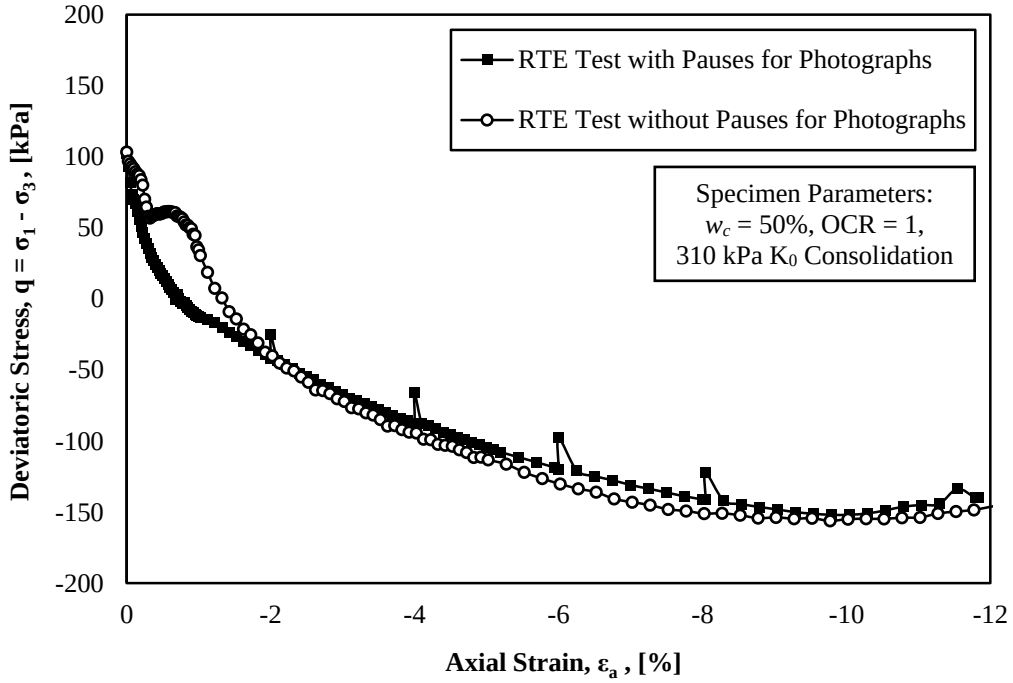

Figure 6.2. Comparison of deviatoric stress as a function of axial strain for a reduced triaxial extension test with pauses and without pauses for capturing photographs.

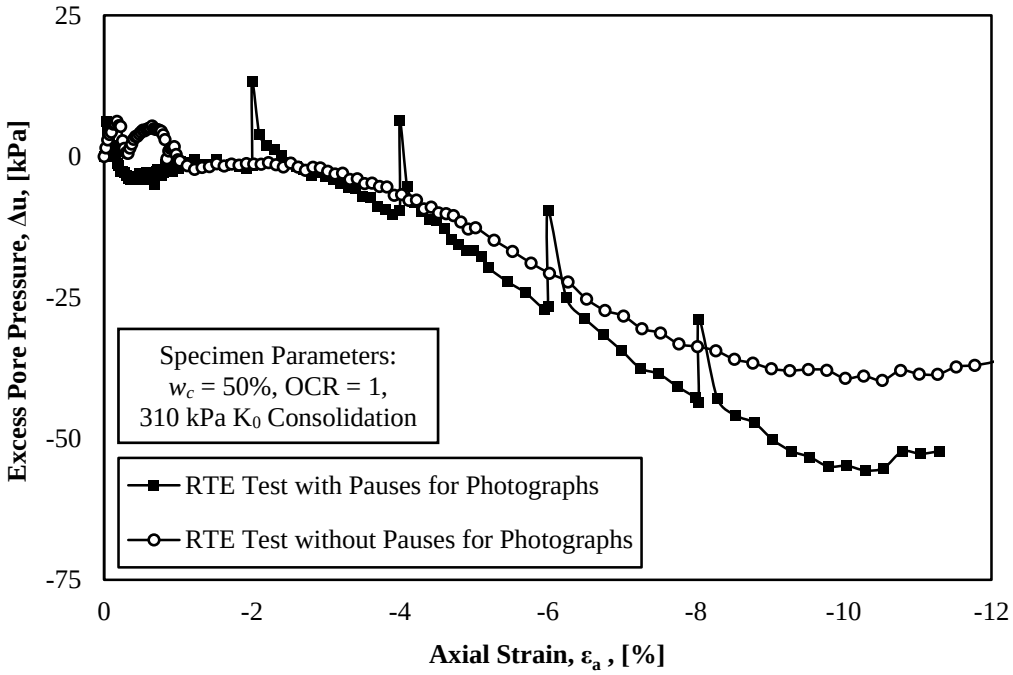

Figure 6.3. Comparison of excess pore water pressure development as a function of axial strain for a reduced triaxial extension test with pauses and without pauses for capturing photographs.

It was mentioned that during the photographic reconstruction of the stainless steel weights, the discussers experienced some difficulty establishing the specimen edges within the cell. The advantage of the photogrammetry techniques presented in Zhang et al. (2015a) and Salazar et al. (2015) is that the long edges (profile) of the specimen need never be established, because photogrammetry allows for the triangulation of individual points on the surface of the specimen in 3D space. However, similar to the discussers' experience, the authors have also had some difficulty in establishing reliable points on the ends (top and bottom) of the specimen. This difficulty was overcome by manually picking common marker points, within each photo, along the top and bottom edges of the specimen within the photogrammetry software.

As mentioned in Salazar and Coffman (2015b), the authors share the discussers' concerns that cell wall cleanliness and obstruction due to triaxial cell apparatus (frame rods, cell wall confining rings) are factors not to be overlooked when photographically monitoring specimens from the exterior of the cell. However, the discussers successfully demonstrated that the volumetric strain of a triaxial sample could be determined to a reasonable level of accuracy without having to take into account cumbersome corrections: (1) for optical distortions due to light refraction at the confining fluid-cell wall and cell wall-air interfaces, and (2) due to cell wall curvature. The authors suggest that for future applications, where only relative measurements are of interest to the discussers, more camera positions should be utilized within the Uchaipichat et al. (2011) methodology to capture more images of the specimen to increase the accuracy of non-uniform volumetric strain measurements.

6.5. References

ASTM D698-12e2, 2012, "Standard Test Methods for Laboratory Compaction Characteristics of Soil Using Standard Effort (12 400 ft-lbf/ft^3 (600 kN-m/m^3))", ASTM International, West Conshohocken, PA, www.astm.org. doi:10.1520/D0698-12E02.

Furukawa, Y. and Hernández, C., 2013, "Multi-View Stereo: A Tutorial," *Found. Trends Comput. Graphics Vis.*, Vol. 9, Nos. 1–2, pp. 1–148.

Mehdizadeh, A., Disfani, M. M., Evans, R., Arulrajah, A., and Ong, D. E. L., 2016, "Discussion of 'Development of an Internal Camera-Based Volume Determination System for Triaxial Testing' by S. E. Salazar, A. Barnes and R. A. Coffman," *Geotech. Test. J.*, Vol. 38, No. 4, 2015, pp. 549–555.

Race, M. L. and Coffman, R. A., 2011, "Effects of Piston Uplift, Piston Friction, and Machine Deflection in Reduced Triaxial Extension Testing," *ASCE Geotechnical Special Publication No. 211, Proceedings GeoFrontiers 2011: Advances in Geotechnical Engineering*, ASCE, Reston, VA, pp. 2649–2658.

Salazar, S. E., Barnes, A., and Coffman, R. A., 2015, "Development of an Internal Camera-Based Volume Determination System for Triaxial Testing," *Geotech. Test. J.*, Vol. 38, No. 4, pp. 549–555.

Salazar, S. E. and Coffman, R. A., 2014, "Design and Fabrication of End Platens for Acquisition of Small-Strain Piezoelectric Measurements During Large-Strain Triaxial Extension and Triaxial Compression Testing," *Geotech. Test. J.*, Vol. 37, No. 6, pp. 948–958. doi:10.1520/GTJ20140057.

Salazar, S. E. and Coffman, R. A., 2015a, "Consideration of Internal Board Camera Optics for Triaxial Testing Applications," *Geotech. Test. J.*, Vol. 38, No. 1, pp. 40–49. doi:10.1520/GTJ20140163

Salazar, S. E. and Coffman, R. A., 2015b, "Discussion of 'A Photogrammetry-Based Method to Measure Total and Local Volume Changes of Unsaturated Soils During Triaxial Testing' by Zhang et al.," *Acta Geotech.*, Vol. 10, No. 5, pp. 693–696.

Salazar, S. E., Miramontes, L. D., Barnes, A., Bernhardt, M. L., and Coffman, R. A., 2016, "An Internal Close-Range Photogrammetry Approach to Volume Determination for Triaxial Testing," *Acta Geotech*. (under review).

Uchaipichat, A., Khalili, N., and Zargarbashi, S., 2011, "A Temperature Controlled Triaxial Apparatus for Testing Unsaturated Soils," *Geotech. Test. J.*, Vol. 34, No. 5, pp. 424–432.

Zhang, X., Li, L., Chen, G., and Lytton, R., 2015a, "A Photogrammetry-Based Method to Measure Total and Local Volume Changes of Unsaturated Soils During Triaxial Testing," *Acta Geotech.,* Vol. 10, No. 1, pp. 55–82.

Zhang, X., Li, L., Chen, G., and Lytton, R., 2015b, "Reply to 'Discussion of "A Photogrammetry-Based Method to Measure Total and Local Volume Changes of Unsaturated Soils During Triaxial Testing" by Zhang et al.' by Salazar and Coffman," *Acta Geotech.,* Vol. 10, No. 5, pp. 697–702.

Zhao, Y. and Coffman, R. A., 2016, "Back-Pressure Saturated Constant-Rate-of-Strain Consolidation Device With Bender Elements: Verification of System Compliance," *J. Test. Eval.,* Vol. 44, No. 6, pp. 2375–2386.

Zhao, Y., Mahmood, N. S., and Coffman, R. A., 2016, "Small-Strain and Large-Strain Modulus Measurements With a Consolidation Device," *J. Test. Eval.* (under review).

CHAPTER 7: VERIFICATION OF AN INTERNAL CLOSE-RANGE PHOTOGRAMMETRY APPROACH FOR VOLUME DETERMINATION DURING TRIAXIAL TESTING

7.1. Chapter Overview

A comprehensive description of the internal camera-based photogrammetry technique for triaxial testing, that was developed at the University of Arkansas (Salazar and Coffman 2015a, 2015b, 2016; Salazar et al. 2015, 2017), is presented in this chapter. A series of sensitivity studies were performed to evaluate the accuracy, precision, and feasibility of the technique. Furthermore, the technique was implemented for two undrained triaxial tests on soil specimens. Specifically, one conventional triaxial compression (CTC) and one reduced triaxial extension (RTE) test were performed on slurry-consolidated, reconstituted kaolinite soil specimens. Results from these tests, discussion of the limitations of the technique, and anticipated improvements to the technique are presented.

The limitations of the included manuscript (Salazar et al. 2017) are discussed in Section 7.2. The full citation for this document is included in Section 7.3. The motivation and background for the manuscript are described in Sections 7.4 and 7.5. Section 7.6 presents the evaluation of the internal photogrammetry technique. Specifically, the calibration of board cameras, derivation of camera stations, determination of photograph intervals, capture of photographs within confining fluid, photogrammetric reconstruction, and volume determination are presented in Sections 7.6.1 through 7.6.6. Contained within Section 7.6.7 is a description of the method used to determine the accuracy of the internal photogrammetry technique, which included comparison of results from five different volume determination methods. Limitations and sources of error are discussed in Section 7.6.8. The methods that were used for

implementation of the technique during triaxial compression and triaxial extension tests are detailed in Section 7.7. Results from the sensitivity studies and from the triaxial tests are discussed in Section 7.8. Finally, conclusions are presented in Section 7.9.

7.2. Limitations of the Described Study

Although the manuscript contained within this chapter clarifies and further expounds on the technique that was introduced in preceding publications, there are limitations to the work. The various sensitivity studies that were completed as part of the evaluation of the technique involved primarily analog (dummy) specimens. The manuscript also described the implementation of the technique for two triaxial tests; however, these tests were undrained. It was therefore not possible to compare changes in specimen volume, as determined using the photogrammetry technique, with changes in pore fluid volume, as measured by the pore fluid pump. Furthermore, the work only describes one triaxial compression and one triaxial extension test. No repeat tests were performed to determine the precision of the technique for a given triaxial test.

7.3. Verification of an Internal Close-Range Photogrammetry Approach for Volume Determination During Triaxial Testing

Reference

Salazar, S. E., Miramontes, L. D., Bernhardt, M. L., and Coffman, R. A., "Verification of an Internal Close-Range Photogrammetry Approach for Volume Determination During Triaxial Testing," Geotechnical Testing Journal. Submitted for Review. Manuscript Number: GTJ-2017-0125.R2.

7.4. Abstract

Accurate strain and volume measurements are critical to phase relationships and strength determination for saturated and unsaturated soils. In recent years, laboratory-based photographic techniques of monitoring soil specimens have become more common. These techniques have been used to reconstruct 3D models and to determine strain and volumetric changes of triaxial

specimens. A new technique that used digital photographs of the soil specimen, captured from within a triaxial testing cell, was utilized. Photographs were processed using photogrammetric software to reconstruct 3D models of the soil specimens at various times during the triaxial test. By placing camera equipment within the cell, the technique eliminated the need to account for optical distortions due to *1)* refraction at the confining fluid-cell wall-atmosphere interface, *2)* the curvature of the cylindrical cell wall, and *3)* the pressure-induced deformation of the cell wall.

Previously unreported results from sensitivity studies and accuracy measurements for the internal photogrammetry approach are documented herein. Furthermore, through undrained triaxial compression and extension tests, the viability of determining total and local strains, volume changes, and total volume at any stage of triaxial testing was demonstrated. By comparison with other volume-determination methods that are presented herein, including DSLR camera photogrammetry, 3D scanning, manual measurements, and water displacement techniques, a relative error of the internal photogrammetry technique of 0.13 percent was assessed.

Keywords: triaxial testing, photogrammetry, volume measurements, local deformation

7.5. Introduction and Background

Researchers have employed various methods (both photograph- and non-photograph-based) for monitoring soil specimens during triaxial tests. Specifically, these measurements have enabled one or more of the following: *1)* axial and radial dimensions and deformations with time, *2)* local and/or total volume measurements, *3)* volumetric strain calculations, and *4)* shear band characterization. Examples include double-wall cell systems, differential pressure transducers, measurements of air and water volume changes (Bishop and Donald 1961, Ng et al. 2002, Leong

et al. 2004), displacement sensors (Scholey et al. 1995, Bésuelle and Desrues 2001), proximity sensors (Clayton et al. 1989), laser scanners (Romero et al. 1997, Messerklinger and Springman 2007), digital image analysis (Macari et al. 1997, Sachan and Penumadu 2007), digital image correlation (Bhandari et al. 2012), x-ray computed tomography (Desrues et al. 1996, Viggiani et al. 2004), and photogrammetry (Kikkawa et al. 2006, Zhang et al. 2015a, Li et al. 2016). In recent years, the popularity of photograph-based methods has surpassed non-photograph-based methods due to their practicality, cost-effectiveness, and versatility. The limitations of the photograph-based and non-photograph-based approaches were discussed in Salazar and Coffman (2015a, 2015b), Salazar et al. (2015), and Salazar et al. (2017); the need for the use of photogrammetry that relied upon internal cameras was presented.

Of the photograph-based triaxial monitoring examples in the literature (Macari et al. 1997, Alshibli and Sture 1999, Alshibli and Al-Hamdan 2001, Kikkawa et al. 2006, Gachet et al. 2007, Sachan and Penumadu 2007, Rechenmacher and Medina-Cetina 2007, Uchaipichat et al. 2011, Bhandari et al. 2012, Hormdee et al. 2014, Zhang et al. 2015a, Li et al. 2016, Salazar et al. 2017), only the techniques presented in Kikkawa et al. (2006), Zhang et al. (2015a) and Li et al. (2016) utilized photogrammetry to obtain total and local volume changes of triaxial soil specimens. The method presented in Zhang et al. (2015a, 2015b) and Li et al. (2016) involved acquiring digital photographs of the specimen from outside of the cell wall. The photographs were used to photogrammetrically reconstruct a digital, three-dimensional model. Due to the refracted path of light between the specimen and the camera, computationally intensive corrections were required to account for apparent distortion at the confining fluid-cell wall and cell wall-atmosphere interfaces. This approach did appear to overcome previous limitations of photograph-based measurement techniques, including Digital Image Analysis (DIA), Digital

Image Correlation (DIC), and Particle Image Velocimetry (PIV). The Zhang et al. (2015a) and Li et al. (2016) methods clearly present several advantages of a photogrammetric approach, but the implementation of the method introduces additional processing complexity to account for optical refraction and cell wall flexure (Zhang et al. 2015a, 2015b, Salazar and Coffman 2015b, Li et al. 2016).

As an alternative to the aforementioned methods, that utilized externally-acquired photographs, a photogrammetric technique that utilized photographs that were captured from within the triaxial cell was introduced (Salazar and Coffman 2015a, 2015b, 2016; Salazar et al. 2015, 2017). As described in Salazar and Coffman (2015a, 2015b, 2016) and Salazar et al. (2015, 2017), small board cameras with pinhole apertures were mounted to diametrically opposed towers that were located within the triaxial cell. The cameras were designed to withstand exposure to the confining fluid (silicone oil) and the typical high confining pressures associated with triaxial testing (up to 1,035 kPa). Despite the relatively wide field of view of each camera (~70 degrees), the confined space within the triaxial cell (11.43 cm [4.5 in.] inside diameter) required a total of ten camera devices (five devices stacked vertically on each tower) to ensure full photographic coverage of a given soil specimen. The towers were mounted on a guided track that allowed for rotation around the soil specimen as limited by the two top cap drainage lines. Each time a set of photographs was captured, the drainage lines functioned as a datum for camera stations by providing a consistent starting point for rotation. With the aid of two pairs of magnets (located on the towers and outside of the cell), the towers were manually rotated and stopped at prescribed intervals. Ten photographs were captured at each interval. Photogrammetry software (PhotoModeler Scanner 2015) was then utilized to reconstruct the surface for any soil specimen at any given stage during the triaxial testing.

The primary advantage of the internal cell photogrammetry technique presented in Salazar and Coffman (2015b, 2016) and Salazar et al. (2015, 2017) was direct observation of the soil specimen during testing. The necessity to account for the refraction of light at the confining fluid-cell wall and cell wall-atmosphere interfaces, as well as the curvature or deformation of the cell wall, was therefore eliminated. Discussion of the method presented in Salazar et al. (2015) was offered in Mehdizadeh et al. (2016), where it was claimed that yet another, simpler method (Uchaipichat et al. 2011) could be employed to eliminate some of the cumbersome refraction corrections. A closure to this discussion was provided in Salazar et al. (2017).

A comprehensive description of the steps used in the internal cell photogrammetry approach is included herein. Furthermore, an evaluation of the accuracy of the approach, is described. Three soil analog specimens were utilized for the evaluation. Specifically, an acrylic specimen was used to verify the accuracy of the photogrammetric procedures. Additionally, a brass specimen and a second acrylic specimen were used to examine the effect of the number of photographs (ranging from 40 to 320 photographs) on the photogrammetric derivation of the camera stations and on the determination of specimen volume. Undrained triaxial compression and extension tests on kaolinite soil specimens are also described. The tests were performed to demonstrate the viability of the internal photogrammetry approach to quantify total and local deformations on the surface of the soil specimens during testing.

7.6. Evaluation of the Internal Photogrammetry Technique

As discussed herein, the performance of the internal cell photogrammetry approach that was described in Salazar and Coffman (2015b, 2016) and Salazar et al. (2015, 2017) was demonstrated by conducting a series of tests using soil analog specimens (brass and acrylic specimens). Each step of the approach was evaluated prior to undrained triaxial compression and

extension testing. These steps included the *1)* calibration of each of the individual board cameras, *2)* derivation of camera locations and orientations, *3)* determination of optimal degree of rotation between photograph-capturing intervals, *4)* capture of photographs of the acrylic analog specimen, *5)* photogrammetric reconstruction of the acrylic analog specimen, *6)* determination of the volume of the acrylic analog specimen, and *7)* evaluation of the accuracy of the volume determination method. To illustrate the full evaluation process, a flow chart is presented (Figure 7.1). As a subset of Figure 7.1, the photogrammetric processes are further described in Figure 7.2.

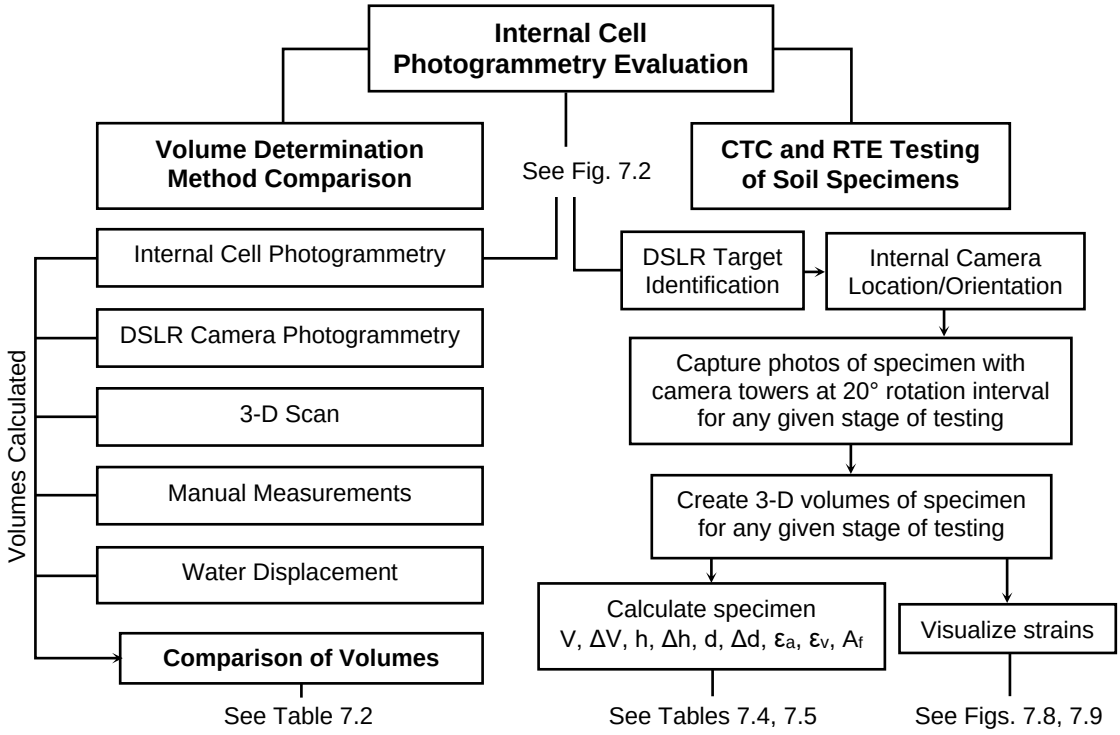

Where DSLR is digital single lens reflex (camera), CTC is conventional triaxial compression, RTE is reduced triaxial extension, V is volume, ΔV is change in volume, h is height, Δh is change in height, d is diameter, Δd is change in diameter, ε_a is axial strain, ε_v is volumetric strain, and A_f is the area of the actual failure plane.

Figure 7.1. The process used to evaluate the internal cell photogrammetry technique and to obtain test parameters.

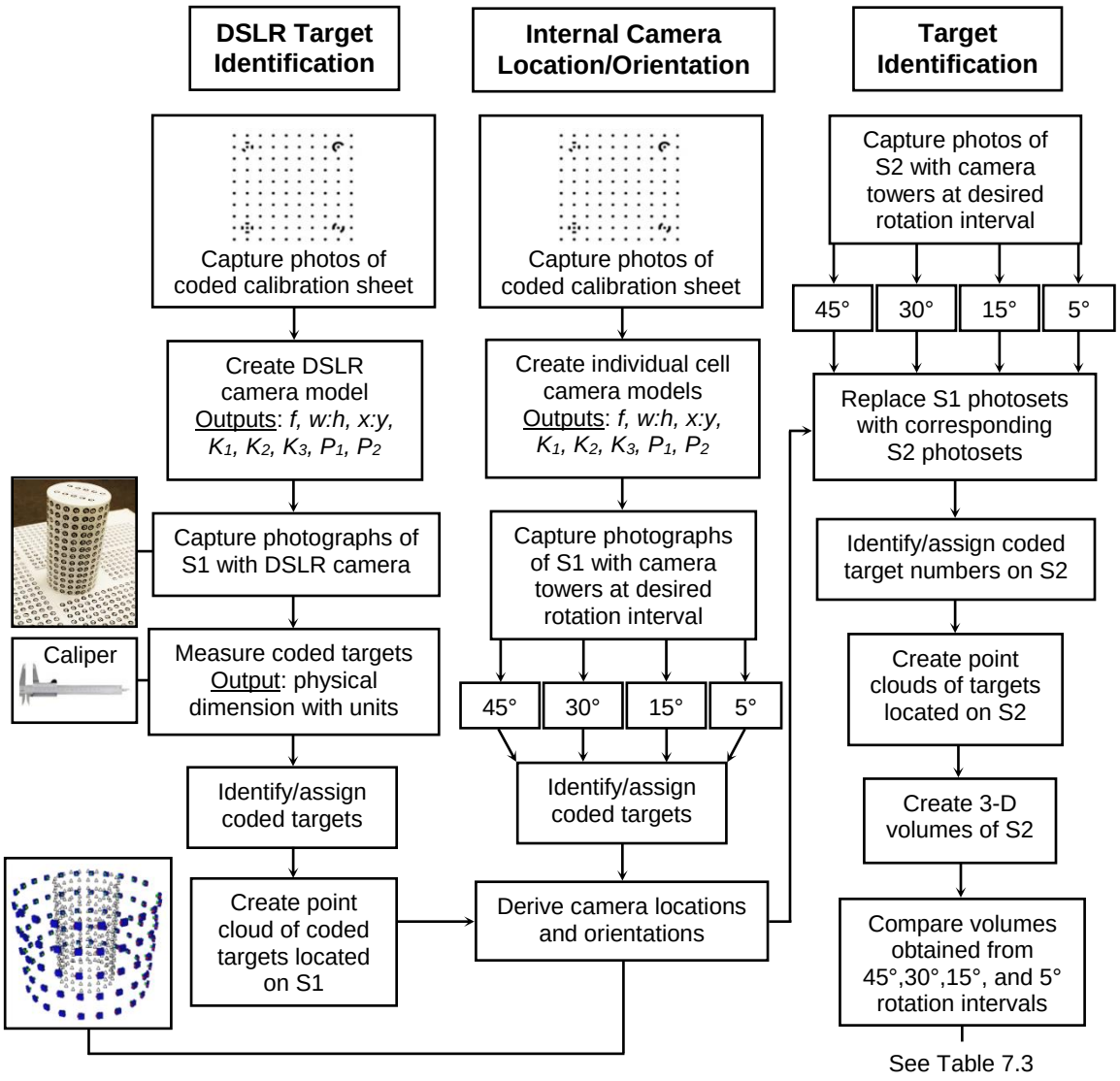

Key

S1: Analog specimen (38.1 mm [1.5 in.] diameter by 76.2 mm [3.0 in.] length, nominal) with targets used to derive location and orientation of internal cell cameras. Point cloud of targets was fixed (as obtained from DSLR camera). Camera locations/orientations were fixed (as obtained from the camera location/orientation step). *S2*: Larger analog specimen (44.5 mm [1.75 in.] diameter by 88.9 mm [3.5 in.] length, nominal) with targets used to calculate locations of targets on the specimen. *Nomenclature: f* is the focal length; *w:h* are the format size dimensions (width to height ratio); *x:y* are the principal point coordinates; and K_1, K_2, K_3, P_1, P_2 are dimensionless distortion coefficients.

Figure 7.2. The process used to determine the volume of a specimen using internal cell photogrammetry and to evaluate the sensitivity of photograph interval on the volume of the specimen.

7.6.1. *Calibration of Board Cameras*

Off-the-shelf software can be used to determine the intrinsic camera and lens parameters that describe the interior orientation of a given camera. This camera calibration process is an important step of the photogrammetric process when a high level of accuracy is desired. All cameras involved with the processes described below, even the lensless board cameras as originally described in Salazar and Coffman (2015a), were fully calibrated utilizing the single-sheet calibration procedure, as outlined by Eos Systems, Inc. (PhotoModeler Scanner 2015). Through this method, each of the ten cameras were positioned to capture convergent photographs of a calibration grid from multiple camera stations and orientations ($\pm$90 degree roll angles), with calibration targets well distributed throughout the photographs. These photographs were then processed using the photogrammetric software, resulting in a calibration data file for each camera. The data files contained intrinsic camera parameters that included the focal length (*f*), the sensor format size (w:h), the principal point (x:y), and the dimensionless distortion coefficients (K_1, K_2, K_3, P_1, P_2), as reported in Table 7.1. The intrinsic camera parameters were imported into all future photogrammetry projects that used the board camera-acquired photographs.

Table 7.1. Comparison of intrinsic camera parameters from calibration for all ten board cameras utilized for internal photogrammetry.

Calibration Parameter	Camera Tower 1				
	Camera 1	Camera 2	Camera 3	Camera 4	Camera 5
Focal Length [mm]	3.3574	3.6599	3.3390	3.5936	3.5928
Format Size [mm]	w: 5.145, h: 4.800	w: 5.149, h: 4.800	w: 5.150, h: 4.800	w: 5.152, h: 4.800	w: 5.148, h: 4.800
Princip. Point [mm]	x: 2.573, y: 2.337	x: 2.659, y: 2.419	x: 2.427, y: 2.176	x: 2.806, y: 2.459	x: 2.782, y: 2.338
K_1	3.87E-03	3.62E-03	2.37E-03	1.96E-03	2.32E-03
K_2	-5.18E-05	-2.37E-04	3.89E-05	-7.22E-06	-4.96E-05
K_3	0	0	0	0	0
P_1	-1.96E-04	2.35E-04	1.36E-04	2.59E-04	1.72E-04
P_2	2.50E-04	2.43E-04	-1.33E-04	4.49E-04	2.84E-04
Calibration Parameter	**Camera Tower 2**				
	Camera 1	Camera 2	Camera 3	Camera 4	Camera 5
Focal Length [mm]	3.4274	3.4498	3.2350	3.3464	3.5830
Format Size [mm]	w: 5.147, h: 4.800	w: 5.150, h: 4.800	w: 5.153, h: 4.800	w: 5.154, h: 4.800	w: 5.150, h: 4.800
Princip. Point [mm]	x: 2.823, y: 2.339	x: 2.608, y: 2.309	x: 2.423, y: 2.276	x: 2.397, y: 2.359	x: 2.370, y: 2.581
K_1	4.27E-03	2.19E-03	2.75E-03	8.64E-04	2.03E-03
K_2	-1.76E-04	-8.17E-05	-2.76E-05	-8.69E-05	2.05E-05
K_3	0	0	0	0	0
P_1	2.52E-04	1.14E-04	1.03E-04	9.82E-04	1.88E-05
P_2	8.78E-05	3.78E-06	6.62E-05	-3.68E-04	-4.86E-05

Note: K_1, K_2, K_3, P_1, and P_2 are dimensionless distortion coefficients.

7.6.2. *Derivation of Camera Stations within the Triaxial Cell*

With any photogrammetric project, it is necessary to obtain the exterior orientation parameters (i.e. position and orientation) for each camera station used for capturing a photograph. To derive this information for the board cameras that were internal to the triaxial cell, the following procedure was performed. A cylindrical, brass analog specimen (38.1 mm [1.5 in.] diameter by 76.2 mm [3.0 in.] length, nominal) was wrapped with a sequence of black ringed automatically detected (RAD) coded targets that were printed onto a sheet of white paper (to provide contrast). The brass specimen was then placed upright on a flat surface. Additional RAD targets were placed on the flat surface adjacent to the specimen to provide additional tie points and improve the overall geometry and accuracy of the model. A fully calibrated, digital single lens reflex (DSLR) camera with a fixed 28 mm lens were used to capture overlapping

photographs from various positions around the brass specimen (approximately 40 photographs total). A selection of these photographs were processed using the photogrammetric software, which automatically identified and measured each RAD target. Several measurements acquired using a caliper (between two distant targets) were input into the software program to define the scale. Three-dimensional coordinates for all 286 RAD target locations were then exported as a comma-delimited text file and used as control points in subsequent projects.

The same targeted brass specimen, which was used with the DSLR camera, was then placed within the instrumented triaxial cell and a set of photographs was captured by the internal board cameras at five-degree intervals. Although two 20-degree sections (40 of the total 360 degrees) were left with no directly perpendicular photographs, due to the presence of the two diametrically opposed drain lines, the entire specimen surface was observed with the internal board cameras. The set of five-degree interval photographs (total of 320) was processed using the photogrammetry software. Visible RAD targets within the newly acquired set of photographs were identified and assigned to the corresponding control point coordinates. With all control points measured and photogrammetric processing complete, the locations (X, Y, Z) and orientations (Omega, Phi, Kappa) for all 320 board camera stations were exported as a comma-delimited text file. All future photograph acquisitions were assigned to the respective photogrammetrically-derived camera locations and camera orientations listed in this file. These steps served to establish a common 3D coordinate system for future photogrammetric reconstructions.

7.6.3. *Determination of Photograph-Capturing Intervals*

Close-range photogrammetry of objects required not only full photographic coverage of all specimen surfaces, but overlapping photographs such that all points to be measured were

clearly visible in at least two but ideally three or more photographs. To meet this requirement, photographs were captured at specified intervals as the towers were manually rotated around the specimen. It was desired to minimize the number of photographs required to reconstruct the specimen, while maintaining a high degree of accuracy and precision. By increasing the base line distance (and therefore rotation angle) between camera stations, the accuracy of measurements in object space (i.e. on the specimen surface) was expected to increase. In turn, increasing the base line distance reduced *1)* the number of photographs and *2)* the available overlap between adjacent photographs. It was therefore desired to determine the optimal intervals at which photographs should be captured. A sensitivity study was performed to determine the ideal angle between adjacent sets of photographs. The study was conducted by placing a different analog specimen (acrylic, 44.5 mm [1.75 in.] diameter by 88.9 mm [3.5 in.] length, nominal) into the instrumented triaxial cell and capturing photographs of the specimen at five degree intervals (320 photographs, total). The larger specimen was selected because it represented the maximum dimensions that would be achieved during large-strain triaxial compression tests (maximum diameter) or extension tests (maximum height) on actual soil specimens. The cell remained empty (air, instead of confining fluid) for this stage of the evaluation process. The sensitivity of the camera stations to the angle between the photograph capturing intervals was evaluated for 45-, 30-, 15-, and five-degree intervals, which corresponded to 40, 60, 110, and 320 photographs, respectively. These intervals were chosen because each interval was divisible by the next, allowing for one common photoset to be used.

7.6.4. *Capture of Photographs to Determine Accuracy in Confining Fluid*

The same procedures that were utilized to *1)* derive the board camera stations using the brass analog specimen (in air) and to *2)* determine the ideal angle between photos using the

large, acrylic analog specimen (also in air) were employed to evaluate the method in confining fluid. A second, smaller acrylic analog specimen (38.1 mm [1.5 in.] diameter by 76.2 mm [3.0 in.] length, nominal) was submerged in confining fluid (silicone oil) within the triaxial cell for the procedure. RAD-coded targets were printed on a sheet of temporary tattoo adhesive paper and adhered to the surface of the acrylic specimen. The photogrammetry procedures that were previously outlined in Section 7.6.2 were repeated and final camera stations were derived for all future tests performed with the confining fluid-filled cell. This was necessary to ensure accuracy of the camera stations when the cameras were submerged in the confining fluid. The coded targets were removed and a different sequence of coded targets was adhered to the surface of subsequent specimens. The new targets were used because it distinguished them from the targets that were already identified to create the control point cloud (used to derive the camera stations). The acrylic specimen was then placed within the triaxial cell filled with confining fluid once more and photographs were captured to reconstruct the specimen. This second set of photographs of the acrylic specimen was necessary because it would not have been a fair assessment to derive the target locations on the surface of the specimen using the same photographs that were utilized to derive the camera stations.

7.6.5. *Photogrammetric Reconstruction of a Specimen*

The photographs of the two acrylic analog specimens (large specimen used to evaluate the sensitivity of the photograph-capturing interval and smaller specimen used to evaluate the accuracy of the technique when subjected to the confining fluid) that were captured from within the triaxial cell were processed within software to photogrammetrically reconstruct the specimens. The photogrammetry projects that were created during the camera location and orientation step, to establish the 3D coordinate system, were modified by replacing the

photographs within the existing projects with the newly acquired photographs of the acrylic specimens. This ensured that the already derived camera stations (location and orientation) remained constant, thereby enabling the greatest possible accuracy for the close-range photogrammetry technique. Each visible target on the surface of the acrylic specimens was then identified and measured in at least three photographs and assigned to the respective unique identification number (384 and 283 total targets for the large- and small-acrylic specimens, respectively). Once a target was measured in three or more photographs, three-dimensional coordinates for that point were computed and reported by the software. The circular centers of the targets provided a reliable means of identifying the precise locations of the targets. To aid in the reliable identification of common points on the ends of the specimen, high contrast markers were added to the porous stones on both ends of the specimen. The intersections between the markers, the porous stones, and the ends of the specimen served to identify common points along the ends of the specimen. Internal quality feedback within the software aided in identifying and reducing point measurement errors, thereby *1)* ensuring the quality of the photogrammetry projects and *2)* providing consistency among each of the projects that were processed. The quality feedback metrics included total error, residuals, and point precision values.

After all of the points on the surfaces of the specimens were identified, radial curves were drawn through the 3D points on the surface of the virtual specimens. Surface tools were utilized to create outward-facing surfaces on the specimens; these surfaces were created by using the curves as the edges of each surface, and to cap the open ends of the specimens. The virtual specimens therefore took shape using the newly created surfaces; however, the photogrammetry software did not correctly calculate the internal volumes of the virtual specimens, nor were the surfaces “watertight”. The 3D models were therefore exported in a wavefront format (.obj

extension) to allow for further analysis using a software program that was more suited to determining the accurate volume of a virtual object. A 3D computer-aided drawing (CAD) software (Geomagic Design X 2015) was utilized for this purpose.

7.6.6. *Determination of a Specimen Volume*

Each 3D model exported from the photogrammetry software consisted of a number of disconnected polygonal bands wrapped transversely around the surface of the model. Narrow gaps between these polygonal bands were sealed using the *global remesh* and *healing* tools within the software. The remesh tool worked by essentially shrink-wrapping the 3D model with a new, improved surface that was free of holes, slivers, and other topologic imperfections. The used software tools are proprietary but the results were similar to what would be expected from a Poisson surface reconstruction, like that described by Kazhdan and Hoppe (2014). The settings for this tool were adjusted so that the number of polygons that made up the output model was 100 times the number of polygons of the input model. The increase in the quantity of polygons reduced the potential for rounding that was observed along sharp edges. Moreover, the healing tool was then used to detect and remove any small clusters of free-floating polygons that were not actually part of the surface of the models. After the final watertight models were created, the calculation of the volume of each model was revealed when selecting on the properties of the model. The exact method used to calculate volume by the software was not reported by the software publishers, but the used method was likely similar to the process described by Mirtich (1996).

7.6.7. *Accuracy of Technique*

To evaluate the accuracy of the internal cell photogrammetry approach, that is presented herein, several other techniques were also employed to determine the volume of the smaller

acrylic analog specimen. The techniques included *1)* the aforementioned internal photogrammetry technique, *2)* photogrammetry using DSLR camera obtained photographs only, *3)* a 3D scanning technique, *4)* manual measurements using a caliper and pi tape, and *5)* a water-displacement technique. Each of these not previously mentioned techniques (techniques 2-5) are described in this section. Based on a review of the literature, no universal method exists to evaluate the absolute or "true" accuracy of a volume determination technique. The amount of difference relative to an external reference, often termed "error", is only meaningful when the nature of the external reference is reported. To provide a metric for comparison between the volumes of the smaller acrylic specimen, as obtained using each technique, the difference was evaluated relative to the water displacement technique. This technique was selected, because it was based on well-established procedures documented in ASTM Standard D698 (ASTM 2012) to determine the interior volume of a Proctor mold.

7.6.7.1. *DSLR Camera Photogrammetry*

For the DSLR camera survey technique, the smaller acrylic specimen was placed on a table and approximately 40 photographs were captured of the specimen from various angles. The photographs were imported into the photogrammetry software and a selection of the best photos were processed. Common points (coded targets), on the surface of the specimen, were identified and referenced to ensure that the points appeared in at least three photos. Measurements were also imported to define the scale (known distance between select points). In a similar fashion to the internal photogrammetry technique, surfaces were created on the virtual specimen and the model was exported for processing and analyzed within the 3D CAD software.

7.6.7.2. *3D Scanning*

By definition, 3D scanning is the use of a specialized instrument to rapidly record the 3D information of an object or environment. A close-range 3D digitizing system (Breuckmann SmartScan3D HE) that utilized fringe projection, or structured white light technology, was employed to obtain the 3D data of the acrylic specimen. Specifically, a projector, two 5-Megapixel color cameras, and multiple lenses were utilized to facilitate the 3D measurements. A series of patterns (or fringes) were cast onto the specimen and the difference in the pattern from each camera was utilized to compute a series of discrete measurements or 3D points. The instrument captured approximately 150,000 points per individual scan.

The smaller acrylic specimen was scanned with a set of M-125 lenses (i.e. 125 mm diagonal field of view at the optimal working distance of one meter). The M-125 lenses, the highest resolution lenses available for this scanner, were used to achieve the highest possible spatial resolution of approximately 60 μm horizontal. To begin the process of scanning, the instrument was calibrated using *1)* the prescribed procedure that was recommended by the manufacturer, *2)* a set of calibration targets, and *3)* the companion 3D digitizing software (OPTOCAT 2013R2). The calibration procedure reported an average accuracy of object points of 15.41 μm in the X, 0.74 μm in the Y, and 26.75 μm in the Z dimension (depth from scanner). The specimen was made of an acrylic material that was partially transparent. To prevent scan errors caused by light scattering during fringe projection, a thin coat of matte white spray paint was applied to the specimen. Several spherical adhesive targets were also placed on each side of the specimen to aid in the scan-to-scan alignment procedures during data processing. The specimen was then placed at a 45-degree angle on an automated turntable (Figure 7.3) and scanned at 20-degree intervals for a total of 18 scans. Two other manually positioned scans were

collected to fill in areas not visible during the turntable rotations. All of these data (20 scans) were then processed using the digitizing software. The basic processing steps that were performed included: *1)* an iterative global best-fit alignment of all scans, *2)* overlap reduction to remove scan data collected at a high angle of incidence, *3)* merging of individual scans to create a single polygonal mesh, *4)* smoothing to remove small amounts of noise and other scan artifacts, and *5)* hole-filling using the semi-automated tools that were available. The final 3D model, as presented in Figure 7.3, was composed of approximately 685,000 polygonal faces and approximately 343,000 vertices.

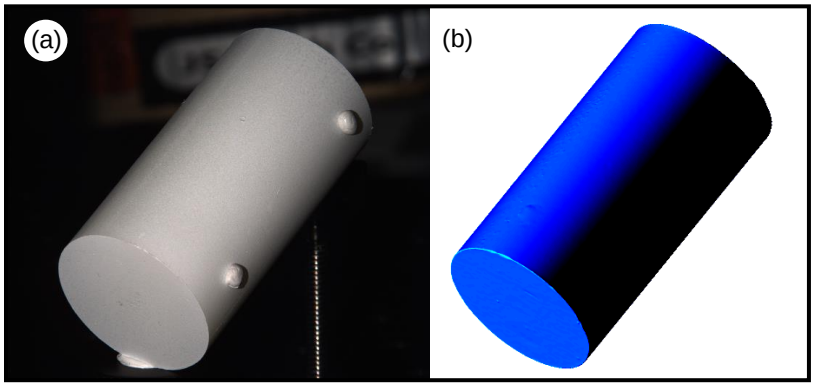

Figure 7.3. *(a)* Photograph of, and *(b)* three-dimensional, watertight model of small-acrylic analog specimen with spherical adhesive targets (removed during processing), as obtained during 3D scanning of specimen.

7.6.7.3. *Manual Measurements*

For the method that consisted of manual measurements, a linear caliper (with a resolution of 0.05 mm) was used to measure the length of the acrylic specimen (average of three measurements) and a pi tape (with a resolution of 0.01 mm) was used to measure the diameter of the specimen (average of three measurements). The volume of the specimen was then calculated based on the average measurements.

7.6.7.4. *Water Displacement*

The same procedures that are commonly utilized to measure the volume of a Proctor mold, as outlined in ASTM Standard D698 (ASTM 2012), were used to measure the volume of the specimen. Specifically, after the volume of a Proctor mold was determined using the water-filling method that is described in the Annex of the ASTM Standard, the specimen was placed into the Proctor mold and submerged in de-ionized and de-aired water to determine the amount of water that was displaced by the specimen. The mass of the acrylic specimen was determined before and after water submersion to ensure that no water was imbibed by the specimen during the testing.

7.6.8. *Limitations and Sources of Error*

The limitations of, and the identified sources of error associated with, the described photogrammetry technique are discussed herein. The identified systematic errors were mitigated during the process of collecting, processing, and evaluating data. Additionally, a schematic of the relevant qualitative factors that influence the accuracy of photogrammetry applications is presented as Figure 7.4.

Expected Accuracy	Camera Resolution	Camera Calibration Method	Angles between Photos	Photo Orientation Quality	Photo Redundancy	Targets
Lowest Accuracy	Video 640x480	No calibration	Less than 15 degrees	Few targets per photo, low coverage	Points mostly on only two photos	No targets, all user marked
Average Accuracy	5-6 Megapixel	Inverse camera Calibrated camera	Between 15 and 60 degrees	15+ targets per photo, 25- 60% coverage	All points on 3+ photos	Some naturally lit targets
Highest Accuracy	11 Megapixel	Field calibrated camera	Between 60 and 90 degrees	35+ targets per photo, 50-80% coverage	Most targets on 8 or more photos	Many good quality naturally lit Retro-reflective

Shading highlights the characteristics of the photogrammetry methodology presented in this study.

Figure 7.4. Qualitative factors affecting accuracy in photogrammetry (modified from Eos Systems, Inc. 2015).

7.6.8.1. *Precision of Repeat Interval Stops*

Measured from a fixed starting position (in contact with the drainage lines), the camera towers stopped at prescribed rotation intervals around the specimen to allow for repeat occupation (during a given photogrammetry project and between successive photogrammetry projects). The method relied upon the capture of photographs from the exact same locations with each repetition, because photographs with known (derived) camera stations were replaced with new photographs (thereby assigning the derived locations and orientations to the new photographs). Although the same locations were reoccupied for each test, any deviation from the photogrammetrically derived location could have resulted in error in the three-dimensional coordinate of an observed point within the replaced photographs.

7.6.8.2. *Model Refinement*

The number of targets that were utilized limited the mesh refinement of the surface of each specimen. Furthermore, the number of targets that were utilized was related to processing time and to the minimum size of targets. To maintain the automated target identification capability of the photogrammetry software, a target center diameter of at least 30 pixels was utilized. This resulted in the use of 286 targets that were evenly distributed (center to center spacing of 5.65 mm) across the surfaces of the 38.1 mm (1.5 in.) in diameter by 76.2 mm (3.0 in.) in length (nominal) brass and acrylic soil specimens.

7.6.8.3. *External Geometry Measurements*

To scale a photogrammetry project, one or more external reference measurements was required to be input. These reference measurements were in the form of a known distance between two measured points located within the project. The resulting overall accuracy of a project was therefore limited to the accuracy of the input measurements. To mitigate the impact of this source of error, multiple reference measurements were made for various target pairs within the project.

7.6.8.4. *Determination of Specimen Ends*

The most difficult aspect of processing the photographs of a specimen was the reliable identification of the ends of the specimen (i.e. picking points along the edges at the two ends of the specimen). Picking end points was challenging because distinct markers had to be identified subjectively in adjacent photographs without the help of target centers. This challenge has often been understated or not discussed in the literature, but should not be overlooked. To aid in the reliable identification of specimen ends, high contrast markers were applied to the porous stones on the ends of the specimens.

7.7. Implementation of the Internal Photogrammetry Technique for Soil Specimens

Two undrained triaxial tests were performed on kaolinite soil specimens to assess the viability of determining: *1)* total and local strains, *2)* total volume and volume changes at any given stage of testing, and *3)* the actual failure plane of a soil specimen. Specifically, one undrained, conventional triaxial compression (CTC) test and one undrained, reduced triaxial extension (RTE) test were conducted. The tests were performed with advanced, automated triaxial apparatus that included pore water pressure and pore water volume measurements. In a typical triaxial test, the exact total specimen volume at any given stage of testing (prior to consolidation, prior to shearing, or during shearing), must be back-calculated from testing and post-testing data using phase relationships and assumptions (most notably the right circular cylinder assumption, see ASTM D4767-11, 2011). To illustrate this concept, a schematic of the stages of a typical triaxial compression test is presented as Figure 7.5. This method of calculating specimen volume often leads to erroneous results without any means of verification. The implemented photogrammetry technique provided a means to independently determine the volume of a soil specimen, during any desired stage of testing, without the need to rely upon erroneous assumptions made during back-calculation.

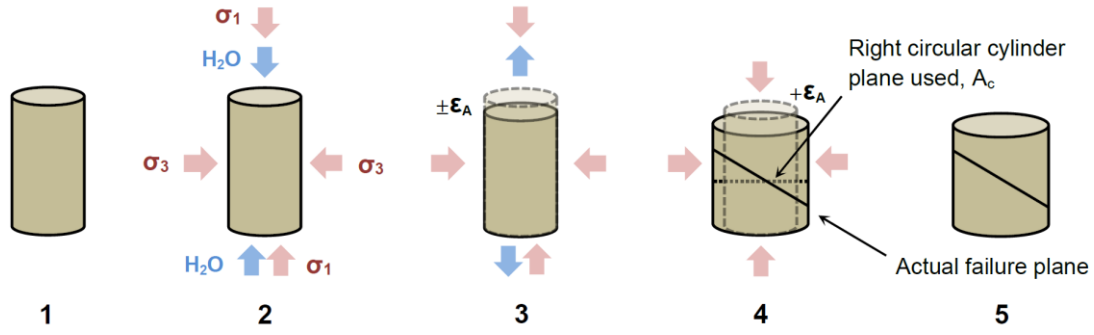

1. *Pre-test:* Mass (m) and water content (*w*), measured; Volume (V) calculated using caliper measurements.
2. *Back-pressure saturation:* Drain lines filled. Total volume change (ΔV) from pore pump measurements. This volume change includes air *1)* purged from lines, and *2)* going into suspension.
3. K_0 *Consolidation:* Sample ΔV from pore pump measurements.
4. *Shearing*: m, *w*, and V assumed to be equal to post-test m, *w*, and V (if undrained); calculated from pore pump measurements (if drained).
5. *Post-test:* m and *w*, measured. Shear strength determined based on corrected area (A_c).

Figure 7.5. Typical measurements and calculations required to determine the phase diagram of the soil specimen during a conventional triaxial compression test.

The soil specimens consisted of commercially available kaolinite soil (Kaowhite-S) obtained from the Thiele Company (Sandersonville, Georgia). The specimens were slurry-consolidated in an acrylic consolidometer under an overburden stress of 138 kPa (20 psi). Specimens with nominal dimensions of 7.62 cm in length and 3.81 cm in diameter were extracted from the consolidation apparatus and weighed. Using temporary tattoo paper, RAD-coded targets were applied to the surface of the first membrane surrounding the sample. The membrane was then placed onto the specimen, and a second membrane was applied over the first membrane (to reduce the potential for liquid transfer or gas permeation). During the specimen preparation phase, care was taken to minimize the amount of disturbance on the soil specimen. The confining cell was filled with silicone oil, the top and bottom drain lines to the specimen were flushed to remove air from the lines, and the specimen was back pressure saturated (B-check equal to 0.95 or higher) before proceeding to the consolidation phase. During each test, the specimen was consolidated under K_0-conditions to a vertical effective stress of 310 kPa (45 psi). During consolidation, the

changes in pore pump volume measurements were used to determine changes in pore water volume of the specimen. Upon completion of consolidation, the drain lines were closed and the specimen was sheared under undrained conditions (strain rate of 0.5 percent per hour). For the CTC test, the shearing was paused at intervals of 0, 2, 4, 6, 8, 11.5, and 15 percent axial strain. At each of these strain intervals, the ten board cameras were used to capture photographs of the specimen at 20-degree rotation intervals (total of 80 photographs per strain interval), as further discussed in Section 7.8.2. Similarly, for the RTE test, the shearing was paused at intervals of -0, -2, -4, -6, -8, -10, -12, -15 percent axial strain and photographs of the specimen were captured. For each strain interval, the test was paused for less than 30 minutes. For completeness, a photograph of the instrumented triaxial cell, as utilized in the RTE test, is presented (Fig. 7.6).

Processing procedures were identical to those employed to model the acrylic analog specimen. After 3D models of the soil specimens were exported to wavefront format files, the models were further analyzed within 3D CAD software. Local displacements on the surface of each soil specimen were visualized using the built-in *mesh deviation* function. The software tool likely functioned similar to the process described by Cignoni et al. (1998). Utilization of this function allowed for watertight meshes to be overlayed (with a common coordinate system) to compare the positive or negative changes between the surfaces of the two meshes. The post-consolidation mesh was selected as the reference mesh for comparisons. A color-graded scale was selected to visualize the magnitude of changes (cooler colors corresponded to negative changes while warmer colors correlated to positive changes).

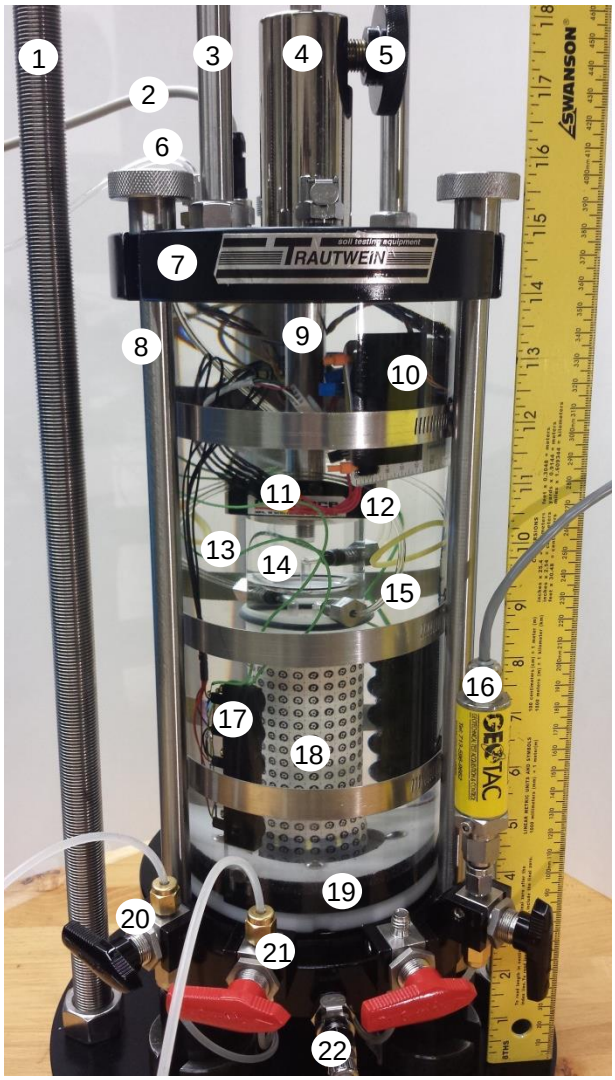

1. Load frame reaction rod (two quantity)
2. Cable with nine-pin feed-through connector (four pins for the internal load cell, two pins for the switchboard power supply, one pin for the video signal, two pins unused)
3. Uplift prevention rod (two quantity, for extension testing only)
4. Piston housing
5. Piston lock
6. Vacuum line for acrylic top cap vacuum connection
7. Top platen of cell
8. Fastening rod (three quantity)
9. Piston
10. Switchboard for camera timing (as shown in Salazar et al. [2015])
11. Electrical jumpers for individual camera power supply (red)
12. Internal load cell
13. Electrical jumpers for common grounding and video signals (green and yellow, respectively)
14. Acrylic top cap (triaxial extension vacuum cap shown)
15. Drain line (connection to top cap)
16. Pore pressure transducer
17. Camera tower (two quantity, 5 cameras each)
18. Soil specimen within membrane (RAD-coded targets adhered to membrane)
19. Rotating Delrin® bearing track
20. Top drain line and drain valve (black)
21. Bottom drain line and drain valve (red)
22. Cell pressure application line

Figure 7.6. Photograph of the kaolinite specimen within the photogrammetrically instrumented triaxial cell during the shearing stage of the extension test.

In addition to the undrained triaxial compression and triaxial extension tests, one additional unconfined compression (UC) test was performed. The purpose of the UC test was to compare *1)* the calculated volumes during a test within the triaxial cell by utilizing the internal photogrammetry technique, with *2)* the calculated volumes during a test outside of the triaxial cell utilizing the DSLR camera photogrammetry technique. The soil specimen was prepared in an identical way to those specimens that were used in the two triaxial tests. RAD-coded targets

were applied to the surface of the membrane and additional targets were placed on the loading frame around the specimen to provide tie points for photogrammetric processing. The specimen was sheared under unconfined conditions (although the specimen was wrapped in a membrane) at a strain rate of 0.5 percent per hour. During the test, the shearing was paused at intervals of 0, 2, 4, 6, 8, 11.5, and 15 percent axial strain and approximately 40 photographs of the specimen were captured at each strain interval. During the processing phase, the best 12 photos of the 40 photos that were captured for each strain interval, were selected and processed so that targets on the surface of the specimen appeared in at least three photographs. Following the same procedures as those used for the internal photogrammetry technique, 3D models were created within photogrammetry software and were exported for further analysis within the 3D CAD software.

7.8. Results and Discussion

The results from the evaluation of the internal cell photogrammetry technique are presented herein. Furthermore, a discussion of the amount of error associated with the technique and the sensitivity of the photograph-capturing interval are presented. The accuracy of the utilized photogrammetry technique is discussed and the limitations are highlighted.

7.8.1. *Volume Comparisons*

The differences between the volumes determined using the various measurement techniques (internal photogrammetry, DSLR photogrammetry, 3D scanning, manual measurements) relative to the arbitrary reference technique (water displacement) fell within one-half of one percent, as presented in Table 7.2. There was good agreement between the volumes determined from the internal photogrammetry technique and reference technique (0.13 percent difference). These difference values were expected to be greater for the techniques presented

herein than the difference values reported in the literature. This was expected because of the relatively small size of the specimen that was utilized for evaluation of the internal photogrammetry technique (nominal dimensions of 7.62 cm in length and 3.81 cm in diameter), as compared to larger size specimens contained within the literature (typically, 10.16 cm in length and 5.08 cm in diameter, or 14.22 cm in length and 7.11 cm in diameter). Despite the increased sensitivity to volume determination error for the specimen used in this study, the volume differences for all five measurement techniques were small (≤ 0.50 percent). The smaller specimen size was utilized because of the reduced drainage distance, which significantly reduced the time required for the completion of the consolidation phase of testing.

Based on a variety of tests conducted (prior to results reported in this study), the repeatability of determining the volume of an analog specimen fell within 0.011 percent for the 3D scanning technique and within 0.084 percent for the internal photogrammetry technique. Although the repeatability of the DSLR camera photogrammetry technique was not studied, it is expected to be comparable to the repeatability of the internal photogrammetry technique.

Table 7.2. Comparison of small-acrylic analog specimen volumes as obtained using five different techniques.

Volume Determination Method	Volume of Specimen [cm^3] Repetition			Mean [cm^3]	Difference from Reference [%]
	1	2	3		
Water Displacement	94.97	95.60	95.47	95.35	Reference
Manual Measurements	95.82	95.82	95.82	95.82	0.50
3-D Scan	95.64	-	-	95.64	0.31
DSLR Photogrammetry	95.62	-	-	95.62	0.29
Internal Photogrammetry	95.22	-	-	95.22	-0.13

7.8.2. *Photograph Interval*

Although it appeared that the repeatability of derived camera locations was sensitive to the photograph interval (degree of separation between sets of photographs), as indicated by convergence of camera locations in Figure 7.7, the effect was considered negligible (within 0.045 pixels for the maximum difference in camera location). The relationship between derived camera orientation and photograph interval was not directly meaningful. Therefore, the influence of the tower rotation interval on the determination of specimen volume was examined (Table 7.3). For the volume (as calculated from four photogrammetric reconstructions, using 45-, 30-, 15-, and five-degree photograph intervals), the standard deviation was equal to 0.34 cm^3, and the range was equal to 0.70 cm^3. The determination of volume was therefore not sensitive to the photograph interval. Thus, to *1)* match the 20-degree gaps surrounding the drainage lines within the triaxial cell, thereby providing consistent photograph intervals, and *2)* maintain sufficient overlap between photographs, an interval of 20 degrees was selected. This resulted in 80 photographs and approximately 240 minutes of processing time per test.

Table 7.3. Comparison of large-acrylic analog specimen volumes as determined during internal photograph interval sensitivity test.

Rotation Interval [Degrees]	Number of Photos	Computational Cost [minutes]	Specimen Volume V_T , [cm^3]	Summary Statistics	
45	40	120	135.17	Mean Volume [cm^3]	135.56
30	60	180	135.37	Standard Deviation [cm^3]	0.34
15	110	330	135.87	Standard Error [cm^3]	0.17
5	320	960	135.80	Coefficient of Variation [%]	0.25
				Range [cm^3]	0.70

Note: Photographs acquired using internal board cameras.

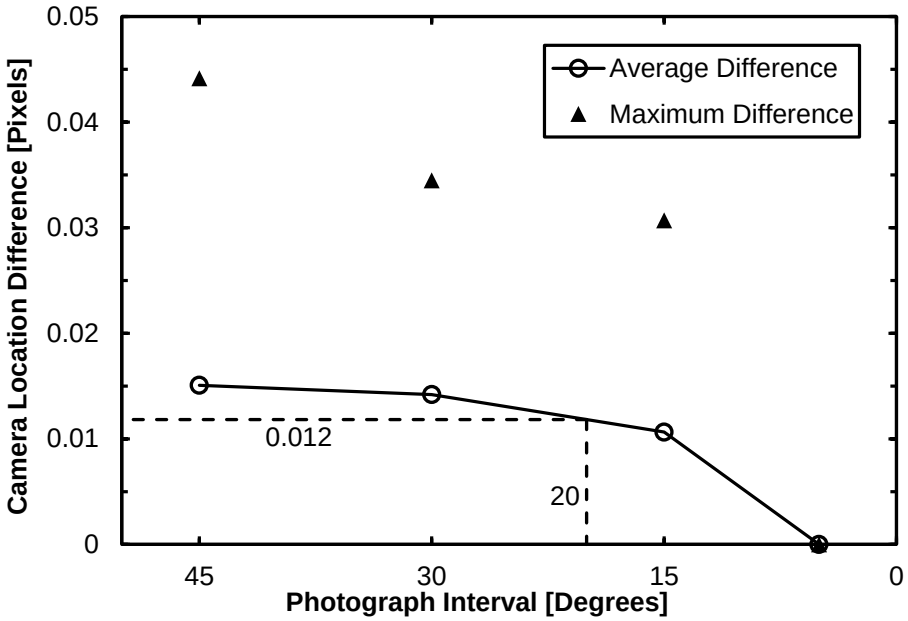

Figure 7.7. Sensitivity of derived camera location difference to interval between photographs.

7.8.3. *Testing of Internal Photogrammetry System on Soil Specimens*

The volume of the various soil specimens was determined at numerous levels of axial strain during both the CTC and RTE tests, as well as during the UC test. The CTC and RTE tests were performed in an undrained condition and therefore the total volume of the specimen was not expected to change during the shearing phase of each test. Likewise, the UC test was undrained. The volumes that were measured during each test, and the summary statistics for each test, supported this hypothesis. The results from the CTC test are presented in Table 7.4. The volume change during the consolidation phase was determined to be 6.56 cm^3, using the internal photogrammetry technique. As a comparison, the volume change determined from the pore pump measurements was equal to 6.81 cm^3 (temperature corrected) and the change calculated from the displacement transducer measurements was equal to 6.70 cm^3 (using the assumption that the cross-sectional area of the specimen remained constant during K_0 consolidation). The

internal photogrammetry approach therefore underpredicted the volume change by 3.7 percent, as compared to the pore pump measurements, and by 2.1 percent, as compared to calculations using the change in specimen height.

The results from the RTE test and the UC test are presented in Table 7.5 and Table 7.6, respectively. For the CTC, RTE, and UC tests, the small changes in total volume, during undrained shearing, were likely a result of the sensitivity to limited refinement of the 3D model surface (function of the number of targets on the membrane). As indicated by the standard deviation of total volumes calculated during the CTC test (0.37 cm^3), as compared to the standard deviation during the RTE test (0.27 cm^3), the variability was greater for the CTC test. The likely cause of the greater variability during the CTC test was that the target refinement was more sensitive to the local deformations on the surface of the specimen during compression (uneven bulging) than during extension (fairly uniform necking). Comparison with the results from the UC test (standard deviation of 0.69 cm^3) revealed that even with the high resolution DSLR camera photogrammetry technique there was variability in the volumes, further supporting the hypothesis that the model refinement (number and density of targets on surface of the specimen) affected the accurate determination of specimen volume throughout a test.

Table 7.4. Volumes of kaolinite soil specimen as determined throughout the triaxial compression test and corresponding summary statistics.

Testing Phase	Axial Strain ε_a , [%]	Volume V_T , [cm^3]	Summary Statistics	
Consolidation	Pre-consolidation	89.72	Change in Volume During Consolidation [cm^3]	6.56
	0	83.16		
Shear	2	82.92	Mean Volume During Shear [cm^3]	83.37
	4	83.28		
	6	83.27	Standard Deviation [cm^3]	0.37
	8	83.28	Standard Error [cm^3]	0.14
	11.5	84.10	Coefficient of Variation [%]	0.45
	15	83.55	Range [cm^3]	1.18

Note: Photographs acquired using internal board cameras.

Table 7.5. Volumes of kaolinite soil specimen as determined throughout the triaxial extension test and corresponding summary statistics.

Testing Phase	Axial Strain ε_a , [%]	Volume V_T , [cm^3]	Summary Statistics	
Shear	0	79.88	Mean Volume During Shear [cm^3]	80.30
	8	80.40		
	10	80.32	Standard Deviation [cm^3]	0.27
	12	80.28	Standard Error [cm^3]	0.12
	15	80.64	Coefficient of Variation [%]	0.34
			Range [cm^3]	0.76

Note: Photographs acquired using internal board cameras.

Table 7.6. Volumes of kaolinite soil specimen as determined throughout the unconfined compression test and corresponding summary statistics.

Testing Phase	Axial Strain ε_a , [%]	Volume V_T , [cm^3]	Summary Statistics	
Shear	0	91.01	Mean Volume During Shear [cm^3]	91.35
	2	91.46		
	4	90.99	Standard Deviation [cm^3]	0.69
	6	90.90	Standard Error [cm^3]	0.26
	8	90.75	Coefficient of Variation [%]	0.75
	11.5	91.57	Range [cm^3]	2.00
	15	92.75		

Note: Photographs acquired using DSLR camera.

The localized displacements of each specimen were visualized qualitatively for the CTC and RTE tests. Specifically, the displacements were visualized for the consolidation phase of testing, as presented in Figure 7.8, and for the shearing phase, as presented in Figure 7.9. During the consolidation phase, the small strains in the radial direction of the specimen were somewhat unexpected, as the triaxial testing apparatus was programmed for K_0-consolidation by which the diameter of the specimen should have remained constant throughout the consolidation phase of the test. In the CTC test (Figure 7.9a), the actual failure plane of the soil specimen was evident from the shear banding behavior at larger strains (greater than eight percent axial strain). Conversely, necking behavior was observed for the specimen in the RTE test (Figure 7.9b). Additional test data, including stress-strain and excess pore pressure relationships, were reported in Salazar et al. (2017).

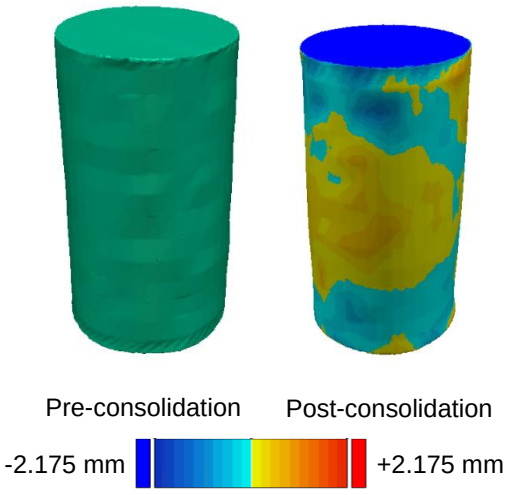

Figure 7.8. Visualization of photogrammetry-obtained, three-dimensional models of kaolinite specimen during K_0-consolidation phase of triaxial test (warm colors indicate positive deformation and cool colors indicate negative deformation).

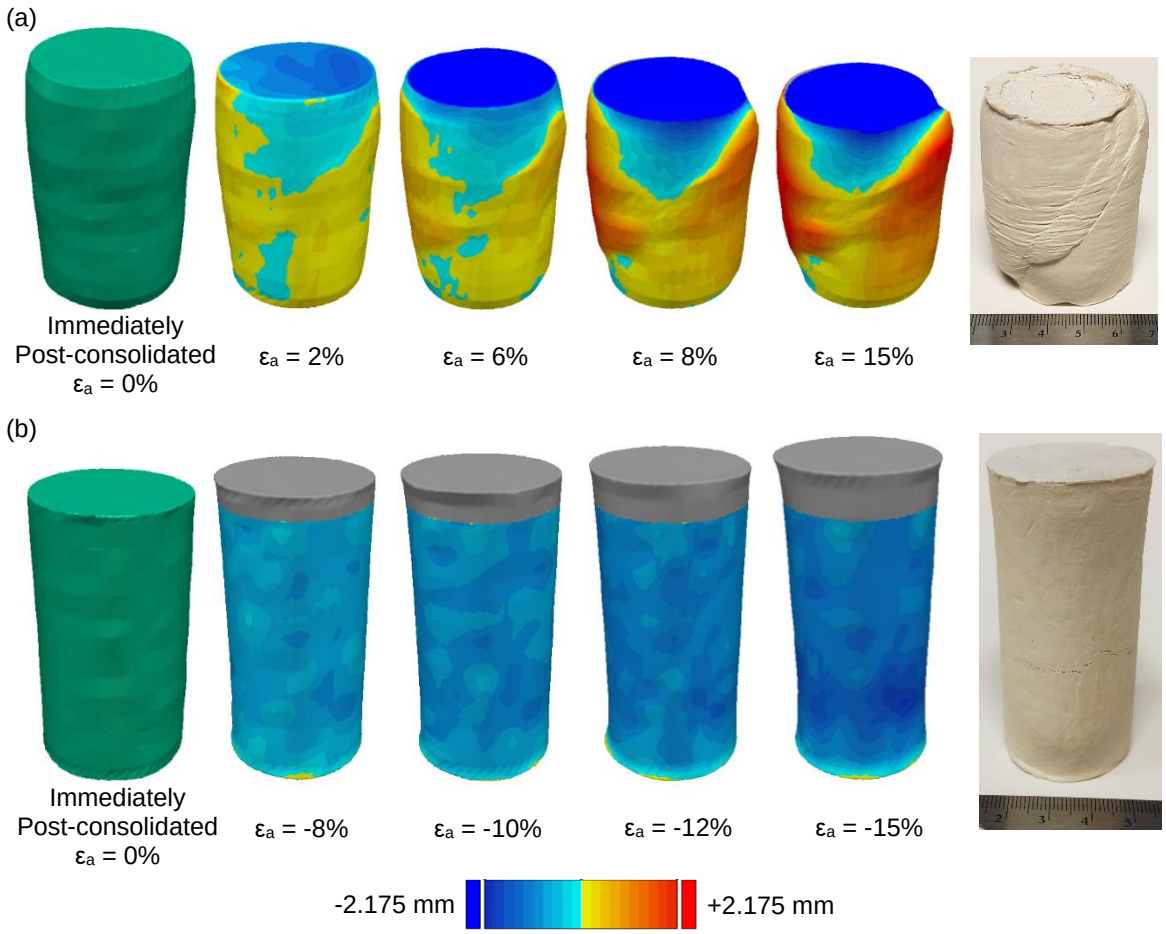

Note: Photographs on the right are of post-test, oven-dried specimens.

Figure 7.9. Visualization of photogrammetry-obtained, three-dimensional models of kaolinite test specimen during *(a)* conventional triaxial compression, and *(b)* reduced triaxial extension tests up to 15 percent axial strain during shearing (warm colors indicate positive deformation and cool colors indicate negative deformation).

Although the application of the internal photogrammetry technique required modifications to a standard triaxial testing cell, the components of the system that were presented were inexpensive, especially when compared with the cost of the triaxial testing equipment. Furthermore, the technology associated with the modifications was not complex (Salazar and Coffman 2015a, 2016 and Salazar et al. 2015). With the reduced computational cost of using less photographs to reconstruct a given test specimen, the added data collection and processing time was insignificant (hours) when compared with the total time (sample preparation, setup, testing,

and data reduction) for a typical triaxial test (weeks). Furthermore, the technique was no more computationally costly than other photogrammetry methods found in the literature.

7.9. Conclusions

The internal cell photogrammetry technique was utilized to determine the volume of soil specimens during all stages of undrained triaxial compression (CTC) and triaxial extension (RTE) tests. The camera instrumentation, internal to the triaxial cell wall, allowed for direct observation of the entire surface of the soil specimens throughout the triaxial tests and avoided the need to correct for refraction and cell wall flexure involved with other methods in the literature. The principles of close-range photogrammetry were utilized to enable accurate 3D reconstructions of the soil specimens. Prior to triaxial testing, a variety of outside-of-cell volume determination techniques, including DSLR camera photogrammetry, 3D scanning, manual measurements, and water displacement techniques were employed to provide comparisons with the volume of an acrylic analog specimen as determined utilizing the internal cell photogrammetry technique. Results from the internal photogrammetry technique fell within 0.13 percent of the reference technique (water displacement) and results from all comparison techniques fell within 0.50 percent. To minimize processing time to approximately 240 minutes, a balance was struck between the number of photographs utilized (80 photographs total, 10 photographs captured at each 20 degree interval around a specimen) and the reliability in photogrammetric measurements. 3D models were produced using commercially available software and localized displacements that developed during the triaxial testing were visualized and reported.

7.9.1. *Potential Applications and Future Improvements*

There are several potential applications for using the internal photogrammetry technique. The approach may be utilized to provide verification of axial and radial strain measurements at any point on the surface of the specimen or at the end cap connections. Furthermore, the strain-based approach could be used in conjunction with 3D finite element analysis techniques to predict the stress distribution throughout the specimen. This inverse solution will aid in developing understanding into the constitutive models used to predict soil behavior.

Although other techniques may be used to measure total pore volume changes during consolidation (i.e. pumps), these techniques may not necessarily be used to measure total volume changes during shearing, nor will localized volume changes be captured. The technique presented in this work may therefore be employed to monitor both total and local volume changes during drained and undrained triaxial tests.

Future improvements to the internal photogrammetry system may facilitate increased accuracy of the results. A higher degree of precision in the reoccupation of photograph interval stops around the specimen would reduce error arising from the predetermined camera stations. Therefore, a mechanized rotating track base is recommended for future applications. Furthermore, future projects may also incorporate a geometric constraint that allows some small amount of deviation from the known camera positions, but only along a modeled arc representing the circular path of the camera track.

To increase the level of refinement on the surface of a specimen, a greater number of targets may be required. However, the size of (and therefore the number of) the targets that were utilized was limited, due to the resolution of the modified board camera devices. To reduce the approximations between targets, improved camera resolution will allow for denser target

coverage on the specimen surface. Furthermore, improvements in automatic target identification algorithms will result in reduced time required for processing.

7.10. Acknowledgements

This material is based upon work supported by the National Science Foundation Graduate Research Fellowship under Grant No. DGE-1450079, as awarded to S.E. Salazar. The authors would also like to acknowledge *1)* support from the University of Arkansas Provost Collaborative Research Grant awarded to R.A. Coffman (PI), M.L. Bernhardt (Co-PI) and A. Barnes (Co-PI) and *2)* undergraduate student support from the United States Department of Transportation (USDOT) Office of the Assistant Secretary for Research and Technology (OST-R) under Research and Innovation Technology Administration (RITA) Cooperative Agreement Award No. OASRTRS-14-H-UARK awarded to R.A. Coffman (PI) and T. Oommen (Co-PI). The views, opinions, findings, and conclusions reflected in this manuscript are the responsibility of the authors only and do not represent the official policy or position of the USDOT/OST-R, or any state or other entity.

7.11. References

Alshibli, K. A. and Sture, S., 1999, “Sand Shear Band Thickness Measurements by Digital Imaging Techniques,” *J. Comput. Civil. Eng.*, Vol. 13, No. 2, pp. 103-109.

Alshibli, K. A. and Al-Hamdan, M. Z., 2001, “Estimating Volume Change of Triaxial Soil Specimens from Planar Images,” *Comput-Aided. Civ. Inf.*, Vol. 16, No. 6, pp. 415–421.

ASTM D698-12e2, 2012, "Standard Test Methods for Laboratory Compaction Characteristics of Soil Using Standard Effort (12 400 ft-lbf/ft^3 (600 kN-m/m^3))", ASTM International, West Conshohocken, PA, www.astm.org. doi:10.1520/D0698-12E02.

ASTM D4767-11, 2011, "Standard Test Methods for Consolidated Undrained Triaxial Compression Test for Cohesive Soils," ASTM International, West Conshohocken, PA, www.astm.org. doi:10.1520/D4767-11.

Bésuelle, P. and Desrues, J., 2001, “An Internal Instrumentation for Axial and Radial Strain Measurements in Triaxial Tests,” *Geotech. Test J.*, Vol. 24, No. 2, pp. 193-199.

Bhandari, A. R., Powrie, W., and Harkness, R. M., 2012, “A Digital Image-Based Deformation Measurement System for Triaxial Tests,” *Geotech. Test. J.*, Vol. 35, No. 2, pp. 1-18.

Bishop, A. W. and Donald, I. B., 1961, “The Experimental Study of Partly Saturated Soil in Triaxial Apparatus,” presented at the *Fifth International Conference on Soil Mechanics and Found Engineering*, Paris, France, July 17-22, 1961, Dunod, Paris, pp. 13-21.

Cignoni, P., Rocchini, C., and Scopigno, R., 1998, “Metro: Measuring Error on Simplified Surfaces,” *Comp. Graph. Forum*, Vol. 17, No. 2, pp. 167-174.

Clayton, C. R. I., Khatrush, S. A., Adriano, V. D. B., and Siddique, A., 1989, “The Use of Hall Effect Semiconductors in Geotechnical Instrumentation,” *Geotech. Test. J.*, Vol. 12, No. 1, pp. 69-76.

Desrues, J., Chambon, R., Mokni, M., and Mazerolle, F., 1996, “Void Ratio Evolution Inside Shear Bands in Triaxial Sand Specimens Studied by Computed Tomography. *Géotechnique*, Vol. 46, No. 35, pp. 529-546.

Gachet, P., Geiser, F., Laloui, L., and Vulliet, L., 2007, “Automated Digital Image Processing for Volume Change Measurement in Triaxial Cells,” *Geotech. Test. J.*, Vol. 30, No. 2, pp. 98-103.

Geomagic Design X; Version 17, 2015, “3D Computer-Aided Design (CAD) software,” 3D Systems, Rock Hill, SC.

Hormdee, D., Kaikeerati, N., and Jirawattana, P., 2014, “Application of Image Processing for Volume Measurement in Multistage Triaxial Tests,” *Adv. Mat. Res.,* Vol. 931-932, pp. 501-505.

Kazhdan, M. and Hoppe, H., 2013, “Screened Poisson Surface Reconstruction,” *ACM Trans. Graph.,* Vol. 32, No. 3, pp. 1-13.

Kikkawa, N., Nakata, Y., Hyodo, M., Murata, H., and Nishio, S., 2006, "Three-Dimensional Measurement of Local Strain Using Digital Stereo Photogrammetry in the Triaxial Test," *Geomechanics and Geotechnics of Particulate Media*, M. Hyodo, H. Murata, and Y. Nakata, Eds., Taylor and Francis, London, pp. 61-67.

Leong, E.C., Agus, S.S., and Rahardjo, H., 2004, “Volume Change Measurement of Soil Specimen in Triaxial Test,” *Geotech. Test. J.,* Vol. 27, No. 1, pp. 1-10.

Li, L., Zhang, X., Chen, G., and Lytton, R., 2016, “Measuring Unsaturated Soil Deformations During Triaxial Testing Using a Photogrammetry-Based Method,” *Can. Geotech. J.,* Vol. 53, No. 3, pp. 472-489.

Macari, E. J., Parker, J. K., and Costes, N. C., 1997, “Measurement of Volume Changes in Triaxial Tests Using Digital Imaging Techniques,” *Geotech. Test. J.,* Vol. 20, No. 1, pp. 103–109.

Mehdizadeh, A., Disfani, M. M., Evans, R., Arulrajah, A., and Ong, D. E. L., 2016, “Discussion of ‘Development of an Internal Camera-Based Volume Determination System for Triaxial Testing’ by S. E. Salazar, A. Barnes and R. A. Coffman (doi:10.1520/GTJ20140249).” *Geotech. Test J.,* Vol. 39, No. 1, pp. 165-168. doi:10.1520/GTJ20150153.

Messerklinger, S. and Springman, S. M., 2007, “Local Radial Displacement Measurements of Soil Specimens in a Triaxial Test Apparatus Using Laser Transducers,” *Geotech. Test. J.,* Vol. 30, No. 6, pp. 1-12.

Mirtich, B., 1996, “Fast and Accurate Computation of Polyhedral Mass Properties,” *J. Graph. Tools,* Vol. 1, No. 2, pp. 31-50.

Ng, C. W. W., Zhan L. T., and Cui Y. J., 2002, “A New Simple System for Measuring Volume Changes in Unsaturated Soils,” *Can. Geotech. J.,* Vol. 39, No. 3, pp. 757-764.

PhotoModeler Scanner; Version 2015.0.0, 2015, “3D Measurements and Models Software,” Eos Systems, Vancouver, BC, Canada.

Rechenmacher, A. L. and Medina-Cetina, Z., 2007, “Calibration of Soil Constitutive Models with Spatially Varying Parameters,” *J. Geotech. Geoenviron.,* Vol. 133, No. 12, pp. 1567–1576.

Romero, E., Facio, J. A., Lloret, A., Gens, A., and Alonso, E. E., 1997, "A New Suction and Temperature Controlled Triaxial Apparatus," presented at the *Fourteenth International Conference on Soil Mechanics and Foundation Engineering*, Hamburg, Germany, September 6-12, 1997, August Aimé Balkema, Amsterdam, pp. 185-188.

Sachan, A. and Penumadu, D., 2007, "Strain Localization in Solid Cylindrical Clay Specimens Using Digital Image Analysis (DIA) Technique," *Soils Found.*, Vol. 47, No. 1, pp. 67-78.

Salazar, S. E., Barnes, A., and Coffman, R. A., 2015, "Development of an Internal Camera Based Volume Determination System for Triaxial Testing," *Geotech. Test. J.*, Vol. 38, No. 4, pp. 549-555. doi:10.1520/GTJ20140249.

Salazar, S. E., Barnes, A., and Coffman, R. A., 2017, "Closure to "Discussion of 'Development of an Internal Camera-Based Volume Determination System for Triaxial Testing' S. E. Salazar, A. Barnes and R. A. Coffman" by A. Mehdizadeh, M. M. Disfani, R. Evans, A. Arulrajah and D. E. L. Ong," *Geotech. Test. J.*, Vol. 40, No. 1, pp. 47-51. doi:10.1520/GTJ20160154.

Salazar, S. E. and Coffman, R. A., 2015a, "Consideration of Internal Board Camera Optics for Triaxial Testing Applications," *Geotech. Test. J.*, Vol. 38, No. 1, pp. 40-49. doi:10.1520/GTJ20140163.

Salazar, S. E. and Coffman, R. A., 2015b, "Discussion of "A Photogrammetry-Based Method to Measure Total and Local Volume Changes of Unsaturated Soils During Triaxial Testing" by Zhang et al. (doi:10.1007/s11440-014-0346-8)" *Acta Geotechnica*, Vol. 10, No. 5, pp. 693-696. doi:10.1007/s11440-015-0380-1.

Salazar, S. E. and Coffman, R. A., 2016, "Pressurized Fluid-Submerged, Internal, Close-Range Photogrammetry System for Laboratory Testing," U.S. Patent and Trademark Office. Patent 15/360,820. Filed November, 2016.

Scholey, G. K., Frost, J. D., Lo Presti, C. F., and Jamiolkowski, M., 1995, "A Review of Instrumentation for Measuring Small Strains During Triaxial Testing of Soil Specimens," *Geotech. Test. J.*, Vol. 18, No. 2, pp. 137–156.

Uchaipichat, A., Khalili, N., and Zargarbashi, S., 2011, "A Temperature Controlled Triaxial Apparatus for Testing Unsaturated Soils," *Geotech. Test. J.*, Vol. 34, No. 5, pp. 1-9.

Viggiani, G., Lenoir, N., Bésuelle, P., Di Michiel, M., Marello, S., Desrues, J., and Kretzschmer, M., 2004, "X-ray Microtomography for Studying Localized Deformation in Fine-Grained Geomaterials Under Triaxial Compression," *Cr Acad Sci II B-Mec*, Vol. 332, pp. 819-826.

Zhang, X., Li, L., Chen, G., and Lytton, R., 2015a, "A Photogrammetry-Based Method to Measure Total and Local Volume Changes of Unsaturated Soils During Triaxial Testing," *Acta Geotechnica*, Vol. 10, No. 1, pp. 55-82. doi:10.1007/s11440-014-0346-8.

Zhang, X., Li, L., Chen, G., and Lytton, R., 2015b, “Reply to “Discussion of ‘A Photogrammetry-Based Method to Measure Total and Local Volume Changes of Unsaturated Soils During Triaxial Testing’ by Zhang et al. (doi 10.1007/s11440-014-0346-8)” by Salazar and Coffman (doi 10.1007/s11440-015-0380-1),” *Acta Geotechnica*, Vol. 10, No. 5, pp. 697-702. doi: 10.1007/s11440-015-0384-x.

CHAPTER 8: CONCLUSIONS

8.1. Chapter Overview

Conclusions that were drawn from this work are contained in this chapter. Highlights from the work are summarized in Section 8.2. The limitations of the work are outlined in Section 8.3. Finally, recommendations for future work are put forth in Section 8.4.

8.2. *Highlights*

The internal-cell photogrammetry technique that was developed in this work was successfully applied to the monitoring of soil specimens during triaxial compression and triaxial extension tests. Three-dimensional models with watertight meshes were derived from photogrammetric processing. Measurements of total volume were obtained from each model. The models developed for the specimen, when the specimen had been subjected to different levels of axial stress, were differenced to quantify the development of axial, radial, and localized deformations on the specimen surface during testing. Each set of measurements that were used to derive a specimen volume was collected and processed independently. Therefore, the obtained volume did not rely on assumptions of specimen dimensions or the deformation behavior during the testing. This measurement technique reduced the source of systematic error in the determination of specimen volume.

Volume measurements were made for a rigid reference (dummy) specimen, using five independent techniques, to evaluate the internal-cell photogrammetry technique. Results for the internal-cell photogrammetry technique fell within 0.13 percent of the reference technique and within 0.50 percent of all other techniques. A sensitivity study was performed to examine the effect that the number of photographs used in processing had on the total volume of the specimen. The study revealed that a reduced number of photographs (from 320 to 80

photographs) was suitable for accurately reconstructing a specimen. Accordingly, this reduction in photographs resulted in reduced processing time.

8.3. *Limitations*

Chapter 7 contained a detailed discussion of the limitations of the internal cell photogrammetry technique and the sources of error that were identified. For reference, these limitations included:

- the precision of repeat interval stops (Section 7.6.8.1);
- the refinement of specimen models (Section 7.6.8.2);
- the accuracy of external geometry measurements (Section 7.6.8.3); and
- the determination of specimen ends (Section 7.6.8.4).

In addition to the limitations discussed in Chapter 7, the following limitations of the work were identified:

- the lack of drained triaxial tests performed as part of this work;
- the lack of repeat tests performed as part of this work;
- the inability of the photogrammetry software to automatically identify all targets;
- the amount of time required for photogrammetric processing of results;
- the low resolution of the board camera devices; and
- the poor performance of the board camera devices in low light conditions.

8.4. *Recommendations*

In accordance with the limitations that were identified in the previous section, the following recommendations are made for future work.

- The precision of the camera towers during repeat occupation should be improved with a mechanized, rotating track (e.g. with a small stepper motor). This mechanization could

also foreseeably decrease the amount of time that the triaxial test is paused for during acquisition of photographs.

- The number/density of targets on the surface of the specimen should be increased. The increase in density will increase the number of surveyed points and therefore also increase the resolution of the three-dimensional model.
- Although a comparison with other photogrammetric methods in the literature indicated that the technique presented in this work was no more computationally costly, a reduction in processing time is still desirable. It is therefore recommended that an alternative (preferably) open-source software package be implemented for photogrammetric processing that would allow for improved automatic target and texture detection.
- Incorporating an improved board camera design in future iterations of the system could foreseeably improve image resolution and sensor performance in low light conditions, thereby improving the quality of the image data.
- The strain measurements collected with this technique should be used in conjunction with finite element analysis to predict the stress distribution throughout the soil specimen. Such an inverse solution will help to develop a better understanding of the constitutive behavior of the soil.

CHAPTER 9: WORKS CITED

3D Systems, Inc., 2015, Geomagic Design X (Version 17). 3D Computer-Aided Design (CAD) Software. http://www.geomagic.com/en/products/design/overview

Adrian, R. J., 1991, "Particle Imaging Techniques for Experimental Fluid Mechanics," *Ann. Rev. Fluid Mech.*, Vol. 23, No. 1, pp. 261-304.

Airy, G. B., 1835, "On the Diffraction of an Object-Glass With Circular Aperture," *Trans. Cambr. Philos. Soc.*, Vol. 5, pp. 283–291.

Alshibli, K. A. and Sture, S., 1999, "Sand Shear Band Thickness Measurements by Digital Imaging Techniques," *J. Comput. Civil. Eng.*, Vol. 13, No. 2, pp. 103-109.

Alshibli, K. A. and Al-Hamdan, M. Z., 2001, "Estimating Volume Change of Triaxial Soil Specimens from Planar Images," *Comput-Aided. Civ. Inf.*, Vol. 16, No. 6, pp. 415–421.

ASTM D698-12e2, 2012, "Standard Test Methods for Laboratory Compaction Characteristics of Soil Using Standard Effort (12 400 ft-lbf/ft^3 (600 kN-m/m^3))", ASTM International, West Conshohocken, PA, www.astm.org. doi:10.1520/D0698-12E02.

ASTM D4767-11, 2011, "Standard Test Methods for Consolidated Undrained Triaxial Compression Test for Cohesive Soils," ASTM International, West Conshohocken, PA, www.astm.org. doi:10.1520/D4767-11.

Aversa, S. and Nicotera, M. V., 2002, "A Triaxial and Oedometer Apparatus for Testing Unsaturated Soils," *Geotech. Test. J.*, Vol. 25, No. 1, pp. 3-15.

Bésuelle, P. and Desrues, J., 2001, "An Internal Instrumentation for Axial and Radial Strain Measurements in Triaxial Tests," *Geotech. Test J.*, Vol. 24, No. 2, pp. 193-199.

Bhandari, A. R., Powrie, W., and Harkness, R. M., 2012, "A Digital Image-Based Deformation Measurement System for Triaxial Tests," *Geotech. Test. J.*, Vol. 35, No. 2, pp. 1-18.

Bishop, A. W. and Donald, I. B., 1961, "The Experimental Study of Partly Saturated Soil in Triaxial Apparatus," presented at the *Fifth International Conference on Soil Mechanics and Found Engineering*, Paris, France, July 17-22, 1961, Dunod, Paris, pp. 13-21.

Cignoni, P., Rocchini, C., and Scopigno, R., 1998, "Metro: Measuring Error on Simplified Surfaces," *Comp. Graph. Forum*, Vol. 17, No. 2, pp. 167-174.

Clayton, C. R. I. and Khatrush, S. A., 1986, "A New Device for Measuring Local Axial Strains on Triaxial Specimens," Géotechnique, Vol. 36, No. 4, pp. 593-597.

Clayton, C. R. I., Khatrush, S. A., Adriano, V. D. B., and Siddique, A., 1989, "The Use of Hall Effect Semiconductors in Geotechnical Instrumentation," *Geotech. Test. J.*, Vol. 12, No. 1, pp. 69-76.

Cuccovillo, T. and Coop, M. R., 1997, "The Measurement of Local Axial Strains in Triaxial Tests Using LVDTs," *Géotechnique*, Vol. 47, No. 1, pp. 167–171.

Cui, Y.J. and Delage, P., 1996, "Yielding and Plastic Behavior of an Unsaturated Compacted Silt," *Géotechnique*, Vol. 46, No. 2, pp. 291-311.

Desrues, J., Chambon, R., Mokni, M., and Mazerolle, F., 1996, "Void Ratio Evolution Inside Shear Bands in Triaxial Sand Specimens Studied by Computed Tomography. *Géotechnique*, Vol. 46, No. 35, pp. 529-546.

Ehrgott, J. Q., 1971, "Calculation of Stress and Strain from Triaxial Test Data no Undrained Soil Specimens," Miscellaneous Paper S-71-9, U.S. Army Engineer Waterways Experiment Station, Vicksburg, Mississippi.

Eos Systems Inc., 2014, PhotoModeler (Version 2014.1.1). 3D Measurements and Models Software. http://www.photomodeler.com/index.html (Last accessed 13 Oct 2014).

Eos Systems, Inc., 2015, PhotoModeler Scanner (Version 2015.0.0). 3D Measurements and Models Software. http://www.photomodeler.com/products/scanner/default.html

Fresnel, A.-J., 1819, "Memoir on the Diffraction of Light," *The Wave Theory of Light, H. Crew, Trans.*, American Book Company, New York.

Furukawa, Y. and Hernández, C., 2013, "Multi-View Stereo: A Tutorial," *Found. Trends Comput. Graphics Vis.*, Vol. 9, Nos. 1–2, pp. 1–148.

Gachet, P., Geiser, F., Laloui, L., and Vulliet, L., 2007, "Automated Digital Image Processing for Volume Change Measurement in Triaxial Cells," *Geotech. Test. J.*, Vol. 30, No. 2, pp. 98-103.

Geomagic Design X; Version 17, 2015, "3D Computer-Aided Design (CAD) software," 3D Systems, Rock Hill, SC.

Grimaldi, F. M., 1665, *Physico–mathesis de lumine, coloribus, et iride, aliisque adnexis libri duo* [A physiomathematical thesis on light, colors, the rainbow and other related topics in two books], Bologna, Italy (in Latin).

Gudehus, G. and Nübel, K., 2004, "Evolution of Shear Bands in Sand," *Géotechnique*, Vol. 54, No. 3, pp. 187–201.

Guler, M., Edil, T. B., and Bosscher, P. J., 1999, Measurement of Particle Movement in Granular Soils Using Image Analysis," *J. Comput. Civ.*, Vol. 13, No. 2, pp. 116-122.

Hendriks, B. H. W., Kuiper, S., van As, M. A. J., Renders, C. A., and Tukker, T. W., 2006, "Variable Liquid Lenses for Electronic Products," *Proc. SPIE,* Vol. 6034, pp. 10–18.

Herschel, J. F. W., 1835, *Treatise on Astronomy*, 3rd ed., Carey, Lea & Blanchard, Philadelphia, PA.

Hormdee, D., Kaikeerati, N., and Jirawattana, P., 2014, "Application of Image Processing for Volume Measurement in Multistage Triaxial Tests," *Adv. Mat. Res.,* Vol. 931-932, pp. 501-505.

Iskander, M. and Liu, J., 2010, "Spatial Deformation Measurement Using Transparent Soil," *Geotech. Test. J.*, Vol. 33, No. 4, 8 pgs.

Jain, S., Wang, Y. H., and Fredlund, D. G., 2015, "Non-Contact Sensing System to Measure Specimen Volume During Shrinkage Test," *Geotech. Test. J.*, Vol. 38, No. 6, pp. 936-949. doi:10.1520/GTJ20140274.

Kazhdan, M. and Hoppe, H., 2013, "Screened Poisson Surface Reconstruction," *ACM Trans. Graph.*, Vol. 32, No. 3, pp. 1-13.

Khan, M. H. and Hoag, D. L., 1979, "A Noncontacting Transducer for Measurement of Lateral Strains," *Can. Geotech. J.*, Vol. 16, No. 2, pp. 409–411.

Kikkawa, N., Nakata, Y., Hyodo, M., Murata, H., and Nishio, S., 2006, "Three-Dimensional Measurement of Local Strain Using Digital Stereo Photogrammetry in the Triaxial Test," *Geomechanics and Geotechnics of Particulate Media*, M. Hyodo, H. Murata, and Y. Nakata, Eds., Taylor and Francis, London, pp. 61-67.

Kingslake, R. and Johnson, R. B., 2010, *Lens Design Fundamentals*, 2nd ed., Academic Press, New York.

Kuiper, S. and Hendriks, B. H. W., 2004, "Variable-Focus Liquid Lens for Miniature Cameras," *Appl. Phys. Lett.*, Vol. 85, No. 7, pp. 1128–1130.

Kuo, C.-H. and Ye, Z., 2004, "Sonic Crystal Lenses that Obey the Lensmaker's Formula," *J. Phys. D.*, Vol. 37, No. 15, pp. 2155–2159.

Lasance, C. and Simons, R., 2005, "Advances in High Performance Cooling for Electronics," *Electron. Cool.*, Vol. 11, No. 4, pp. 22–39.

Laudo, J. S., Wurm, K., and Dodson, C., 1998, "Liquid-Filled Underwater Camera Lens System," *Proc. SPIE*, Vol. 3482, pp. 698–702.

Leong, E.C., Agus, S.S., and Rahardjo, H., 2004, "Volume Change Measurement of Soil Specimen in Triaxial Test," *Geotech. Test. J.*, Vol. 27, No. 1, pp. 47-56.

Li, L., Zhang, X., Chen, G., and Lytton, R., 2016, “Measuring Unsaturated Soil Deformations During Triaxial Testing Using a Photogrammetry-Based Method,” *Can. Geotech. J.*, Vol. 53, No. 3, pp. 472-489.

Liang, L., Saada, A., Figueroa, J. L., and Cope, C. T., 1997, “The Use of Digital Image Processing in Monitoring Shear Band Development,” *Geotech. Test. J.*, Vol. 20, No. 3, pp. 324–339.

Macari, E. J., Parker, J. K., and Costes, N. C., 1997, “Measurement of Volume Changes in Triaxial Tests Using Digital Imaging Techniques,” *Geotech. Test. J.*, Vol. 20, No. 1, pp. 103–109.

Mahajan, V. N., 1998, *Optical Imaging and Aberrations: Part I. Ray Geometrical Optics*, SPIE, Bellingham, WA.

Miramontes, L. D., 2016, "Validation of an Internal Camera Based Volume Determination System for Triaxial Testing," *Civil Engineering Undergraduate Honors Theses*. 33.

Mohapatra, S. C. and Loikits, D., 2005, “Advances in Liquid Coolant Technologies for Electronics Cooling,” *Proceedings of the 21st IEEE Semiconductor Thermal Measurement and Management Symposium*, San Jose, CA, March 15–17, pp. 354–360.

Mehdizadeh, A., Disfani, M. M., Evans, R., Arulrajah, A., and Ong, D. E. L., 2016, “Discussion of ‘Development of an Internal Camera-Based Volume Determination System for Triaxial Testing’ by S. E. Salazar, A. Barnes and R. A. Coffman (doi:10.1520/GTJ20140249).” *Geotech. Test J.*, Vol. 39, No. 1, pp. 165-168. doi:10.1520/GTJ20150153.

Messerklinger, S. and Springman, S. M., 2007, “Local Radial Displacement Measurements of Soil Specimens in a Triaxial Test Apparatus Using Laser Transducers,” *Geotech. Test. J.*, Vol. 30, No. 6, pp. 1-12.

Mirtich, B., 1996, “Fast and Accurate Computation of Polyhedral Mass Properties,” *J. Graph. Tools*, Vol. 1, No. 2, pp. 31-50.

Newton, I., 1730, *Opticks: Or a Treatise of the Reflections, Refractions, Inflections and Colours of Light*, 4th ed., William Innys, London.

Nguyen, N.-T., 2010, “Micro-Optofluidic Lenses: A Review,” *Biomicrofluidics*, Vol. 4, No. 3, 031501.

Ng, C. W. W. and Chiu, C. F., 2001, “Behaviour of a Loosely Compacted Unsaturated Volcanic Soil,” *J. Geotech. Geoenviron. Eng.*, Vol. 127, No. 12, pp. 1027–1036.

Ng, C. W. W., Zhan L. T., and Cui Y. J., 2002, “A New Simple System for Measuring Volume Changes in Unsaturated Soils,” *Can. Geotech. J.*, Vol. 39, No. 3, pp. 757-764.

Nübel, K. and Weitbrecht, V., 2002, "Visualization of Localization in Grain Skeletons With Particle Image Velocimetry," *J. Testing Eval.*, Vol. 30, No. 4, pp. 322–329.

Önal, O., Ören, A. H., Özden, G., and Kaya, A., 2008, "Determination of Cylindrical Soil Specimen Dimensions by Imaging With Applications to Volume Change of Bentonite–Sand Mixtures," *Geotech. Test. J.*, Vol. 31, No. 2, pp. 124–131.

Ören, A. H., Önal, O., Özden, G., and Kaya, A., 2006, "Nondestructive Evaluation of Volumetric Shrinkage of Compacted Mixtures Using Digital Image Analysis," *Eng. Geol.*, Vol. 85, No. 3, pp. 239–250.

Parker, J. K., 1987, "Image Processing and Analysis for the Mechanics of Granular Materials Experiment," *ASME Proceedings of the 19th SE Symposium on System Theory*, ASME, New York, pp. 536–541.

Pinyol, N. M. and Alvarado, M., 2017, "Novel Analysis for Large Strains Based on Particle Image Velocimetry," *Can. Geotech. J.*, Vol. 54, No. 7, pp. 933-944. doi:10.1139/cgj-2016-0327.

Renner, E., 2000, *Pinhole Photography: Rediscovering a Historic Technique*, 2nd ed., Butterworth–Heinemann, Boston, MA.

Roichman, Y., Waldron, A., Gardel, E., and Grier, D. G., 2006, "Optical Traps with Geometric Aberrations," *Appl. Opt.*, Vol. 45, No. 15, pp. 3425–3429.

PhotoModeler Scanner; Version 2015.0.0, 2015, "3D Measurements and Models Software," Eos Systems, Vancouver, BC, Canada.

Puppala, A. J., Katha, B., and Hoyos, L. R., 2004, "Volumetric Shrinkage Strain Measurements in Expansive Soils Using Digital Imaging Technology," *Geotech. Test. J.*, Vol. 27, No. 6, pp. 547–556.

Race, M. L. and Coffman, R. A., 2011, "Effects of Piston Uplift, Piston Friction, and Machine Deflection in Reduced Triaxial Extension Testing," *ASCE Geotechnical Special Publication No. 211, Proceedings GeoFrontiers 2011: Advances in Geotechnical Engineering*, ASCE, Reston, VA, pp. 2649–2658.

Rechenmacher, A. L. and Finno, R. J., 2004, "Digital Image Correlation to Evaluate Shear Banding in Dilative Sands," *Geotech. Test. J.*, Vol. 27, No. 1, pp. 13–22.

Rechenmacher, A. L. and Medina-Cetina, Z., 2007, "Calibration of Soil Constitutive Models with Spatially Varying Parameters," *J. Geotech. Geoenviron.*, Vol. 133, No. 12, pp. 1567–1576.

Romero, E., Facio, J. A., Lloret, A., Gens, A., and Alonso, E. E., 1997, "A New Suction and Temperature Controlled Triaxial Apparatus," presented at the *Fourteenth International Conference on Soil Mechanics and Foundation Engineering*, Hamburg, Germany, September 6-12, 1997, August Aimé Balkema, Amsterdam, pp. 185-188.

Sachan, A. and Penumadu, D., 2007, "Strain Localization in Solid Cylindrical Clay Specimens Using Digital Image Analysis (DIA) Technique," *Soils Found.*, Vol. 47, No. 1, pp. 67-78.

Salazar, S. E., Barnes, A., and Coffman, R. A., 2015, "Development of an Internal Camera Based Volume Determination System for Triaxial Testing," *Geotech. Test. J.*, Vol. 38, No. 4, pp. 549-555. doi:10.1520/GTJ20140249.

Salazar, S. E., Barnes, A., and Coffman, R. A., 2017, "Closure to "Discussion of 'Development of an Internal Camera-Based Volume Determination System for Triaxial Testing' S. E. Salazar, A. Barnes and R. A. Coffman" by A. Mehdizadeh, M. M. Disfani, R. Evans, A. Arulrajah and D. E. L. Ong," *Geotech. Test. J.*, Vol. 40, No. 1, pp. 47-51. doi:10.1520/GTJ20160154.

Salazar, S. E. and Coffman, R. A., 2014, "Design and Fabrication of End Platens for Acquisition of Small-Strain Piezoelectric Measurements During Large-Strain Triaxial Extension and Triaxial Compression Testing," *Geotech. Test. J.*, Vol. 37, No. 6, pp. 948–958. doi:10.1520/GTJ20140057.

Salazar, S. E. and Coffman, R. A., 2015, "Consideration of Internal Board Camera Optics for Triaxial Testing Applications," *Geotech. Test. J.*, Vol. 38, No. 1, pp. 40-49. doi:10.1520/GTJ20140163.

Salazar, S. E. and Coffman, R. A., 2015, "Discussion of "A Photogrammetry-Based Method to Measure Total and Local Volume Changes of Unsaturated Soils During Triaxial Testing" by Zhang et al. (doi:10.1007/s11440-014-0346-8)" *Acta Geotech.*, Vol. 10, No. 5, pp. 693-696. doi:10.1007/s11440-015-0380-1.

Salazar, S. E. and Coffman, R. A., 2016, "Pressurized Fluid-Submerged, Internal, Close-Range Photogrammetry System for Laboratory Testing," U.S. Patent and Trademark Office. Patent 15/360,820. Filed November, 2016.

Salazar, S. E., Miramontes, L. D., Barnes, A., Bernhardt, M. L., and Coffman, R. A., 2017, "Verification of an Internal Close-Range Photogrammetry Approach for Volume Determination During Triaxial Testing," *Geotech. Test. J.* Submitted for Review. Manuscript Number: GTJ-2017-0125.R2.

Scholey, G. K., Frost, J. D., Lo Presti, C. F., and Jamiolkowski, M., 1995, "A Review of Instrumentation for Measuring Small Strains During Triaxial Testing of Soil Specimens," *Geotech. Test. J.*, Vol. 18, No. 2, pp. 137–156.

Schmidt, R., 2005, "Liquid Cooling is Back," Electron. Cool., Vol. 11, No. 3, pp. 34–38.

Stanier, S. A., Blaber, J., Take, W. A., and White, D. J., 2016, "Improved Image-Based Deformation Measurement for Geotechnical Applications," *Can Geotech. J.*, Vol. 53, No. 5, pp. 727-739. doi:10.1139/cgj-2015-0253.

Strutt, J. W., Lord Rayleigh, 1891, "On Pin-Hole Photography," *Philos. Mag.*, Vol. 31, pp. 87–99.

Toyota, H., Sakai, N., and Nishimura, T., 2001, "Effects of Stress History due to Unsaturation and Drainage Conditions on Shear Properties of Unsaturated Cohesive Soil," *Soils Found.*, Vol. 41, No. 1, pp. 13-24.

Uchaipichat, A., Khalili, N., and Zargarbashi, S., 2011, "A Temperature Controlled Triaxial Apparatus for Testing Unsaturated Soils," *Geotech. Test. J.*, Vol. 34, No. 5, pp. 1-9.

Viggiani, G., Lenoir, N., Bésuelle, P., Di Michiel, M., Marello, S., Desrues, J., and Kretzschmer, M., 2004, "X-ray Microtomography for Studying Localized Deformation in Fine-Grained Geomaterials Under Triaxial Compression," *Cr Acad Sci II B-Mec*, Vol. 332, pp. 819-826.

Wheeler, S. J., 1986, "The Stress-Strain Behaviour of Soils Containing Gas Bubbles," Ph.D. dissertation, Oxford University, Oxford, UK.

White, D., Take, W., and Bolton, M., 2003, "Soil Deformation Measurement Using Particle Image Velocimetry (PIV) and Photogrammetry," Géotechnique, Vol. 53, No. 7, pp. 619-631.

Young, T., 1802, "Bakerian Lecture: On the Theory of Light and Colours," *Philos. Trans. R. Soc. Lond.*, Vol. 92, pp. 12–48.

Young, M., 1971, "Pinhole Optics," *Appl. Opt.*, Vol. 10, No. 12, pp. 2763–2767.

Zhang, X., Li, L., Chen, G., and Lytton, R., 2015, "A Photogrammetry-Based Method to Measure Total and Local Volume Changes of Unsaturated Soils During Triaxial Testing," *Acta Geotechnica*, Vol. 10, No. 1, pp. 55-82. doi:10.1007/s11440-014-0346-8.

Zhang, X., Li, L., Chen, G., and Lytton, R., 2015, "Reply to "Discussion of 'A Photogrammetry-Based Method to Measure Total and Local Volume Changes of Unsaturated Soils During Triaxial Testing' by Zhang et al. (doi 10.1007/s11440-014-0346-8)" by Salazar and Coffman (doi 10.1007/s11440-015-0380-1)," *Acta Geotechnica*, Vol. 10, No. 5, pp. 697-702. doi: 10.1007/s11440-015-0384-x.

Zhao, Y. and Coffman, R. A., 2016, "Back-Pressure Saturated Constant-Rate-of-Strain Consolidation Device With Bender Elements: Verification of System Compliance," *J. Test. Eval.*, Vol. 44, No. 6, pp. 2375–2386.

Zhao, Y., Mahmood, N. S., and Coffman, R. A., 2017, "Small-Strain and Large-Strain Modulus Measurements with a Consolidation Device," *J. Test. Eval.* (In Press).